DETERMINATION OF THE THERMODYNAMIC PROPERTIES OF RARE EARTH-OXYGEN-SULFUR SYSTEMS AT HIGH TEMPERATURES

By

© RATNESH KUMAR DWIVEDI

A Thesis

Submitted to the School of Graduate Studies

in Partial Fulfilment of the Requirements

for the Degree

Doctor of Philosophy

McMaster University

July, 1982

DETERMINATION OF THE THERMODYNAMIC PROPERTIES OF RARE EARTH-OXYGEN-SULFUR SYSTEMS AT HIGH TEMPERATURES

DOCTOR OF PHILOSOPHY (1982) McMASTER UNIVERSITY
(Metallurgy) Hamilton, Ontario

TITLE: Determination of the Thermodynamic Properties of Rare Earth-Oxygen-Sulfur Systems at High Temperatures

AUTHOR: Ratnesh Kumar Dwivedi
B. Tech. (Met. Engg.)
(Indian Institute of Technology, Bombay, India)

SUPERVISOR: Professor D.A.R. Kay

NUMBER OF PAGES: xviii, 215

ABSTRACT

The thermodynamics of rare earth-oxygen-sulfur systems was studied at high temperatures using the following four types of oxygen concentration cells.

Type I Cells:

$$\text{Pt} \;\big|\; \begin{matrix} RE_2O_2S(s),\ RE_2O_2SO_4(s) \\ \text{in presence of } RE_2O_3(s) \end{matrix} \;\big|\; \text{CSZ} \;\big|\; \text{Air} \;\big|\; \text{Pt}$$

Type II Cells:

$$\text{Pt} \;\big|\; \begin{matrix} RE_2O_2S(s),\ RE_2O_2SO_4(s) \\ \text{in presence of } Ag/Ag_2S \end{matrix} \;\big|\; \text{CSZ} \;\big|\; \text{Air} \;\big|\; \text{Pt}$$

Type III Cells:

$$\text{Pt} \mid RE_2O_3(s),\ RE_2O_2SO_4(s),\ Cu(s),\ Cu_2S(s) \mid \text{CSZ} \mid \text{Air} \mid \text{Pt}$$

Type IV Cells:

$$\text{Pt} \mid RE_2O_3(s),\ RE_2O_2S(s),\ Ag(s),\ Ag_2S(s) \mid \text{CSZ} \mid \text{Air} \mid \text{Pt}$$

Type I and II cells were used to yield the standard free energy changes corresponding to the reaction

$$\frac{1}{2}\, RE_2O_2S(s) + O_2(g) = \frac{1}{2}\, RE_2O_2SO_4(s)$$

(RE = La, Pr, Nd, Sm, Eu, Gd, Tb, Dy)

at two different sulfur partial pressures. Type III cells were used to determine the standard free energy changes for the reaction.

$$\frac{2}{3}\, RE_2O_3(s) + \frac{2}{3}\, Cu_2S(s) + O_2(g) = \frac{2}{3}\, RE_2O_2SO_4(s) + \frac{4}{3}\, Cu(s)$$

(RE = La, Pr, Nd, Sm, Eu, Gd)

Type IV cells were used to determine the standard free energy changes for the reaction

$$RE_2O_3(s) + Ag_2S(s) = RE_2O_2S(s) + \frac{1}{2} O_2(g) + 2Ag(s) \qquad (RE = Ce,Y)$$

Combining the experimental results for the above three reactions with the values of ΔG_f^o for Cu_2S and Ag_2S, the standard free energies of formation of $La_2O_2SO_4$, $Pr_2O_2SO_4$, $Nd_2O_2SO_4$, $Sm_2O_2SO_4$, $Eu_2O_2SO_4$, $Gd_2O_2SO_4$, La_2O_2S, Pr_2O_2S, Nd_2O_2S, Sm_2O_2S, Eu_2O_2S, Gd_2O_2S, Y_2O_2S and Ce_2O_2S were determined at high temperatures. In addition, the standard free energy changes for oxidation of Tb_2O_2S and Dy_2O_2S to $Tb_2O_2SO_4$ and $Dy_2O_2SO_4$ were determined.

The above data were used to construct the phase stability diagrams for the rare earth-oxygen-sulfur systems at high temperatures.

ACKNOWLEDGEMENTS

I wish to express my gratitude to Dr. D.A.R. Kay for his guidance and encouragement during the course of this study. Grateful acknowledgements are also due to Dr. W.W. Smeltzer and Dr. John Greedan for their fruitful suggestions during course of this study. Thanks are also due to the staff of the Department of Metallurgy and Materials Science. The invaluable technical assistance and help from Mr. Horst Neumayer and Tom Bryner is greatly appreciated.

The author gratefully acknowledges the Department of Metallurgy and Materials Science for the financial support for this project.

TABLE OF CONTENTS

LIST OF ILLUSTRATIONS

LIST OF TABLES

CHAPTER I

INTRODUCTION

Rare earth elements and their compounds have some very interesting and useful properties and as a result are used in many industrial processes. The physico-chemical properties of rare earth elements are related to their electronic structures which are characterized by progressive filling of 4f orbitals, the outer shell structure remaining the same ($6s^2\ 5d^1$) throughout the lanthanide series. Thus, the most common valence for the rare earth elements is +3. According to Hund's Rule, a change in valence is expected at completely empty (Ce^{4+}, Pr^{4+}), half full (Eu^{2+}) and completely full (Yb^{2+}) 4f orbitals. This multivalence is illustrated in Table 1.1 along with the normal valence of rare earth elements. A combination of charge and ionic radius enables rare earth elements (denoted by RE) to form some of the most stable compounds with nonmetals. For example, rare earth oxides, sulfides and oxysulfides are among the most stable compounds formed with oxygen and sulfur.

The strong affinity of rare earth elements for oxygen and sulfur can be utilized in several industrial processes. Inclusion morphology control in steelmaking, graphite morphology control in cast irons and desulfurization of hot sulfur-bearing gases using rare earth oxides are some of the more important processes based on the ability of rare earths to form stable oxygen-sulfur compounds.

TABLE 1.1

IONS OF RARE EARTH ELEMENTS AND THE NUMBER OF 4f ELECTRONS IN THEIR RESPECTIVE GROUND STATES (Ref. 2)

Element	Ion	Number of 4f Electrons
Lanthanum	La^{3+}	0
Cerium	Ce^{3+}	1
Cerium	Ce^{4+}	0
Praseodymium	Pr^{3+}	2
Praseodymium	Pr^{4+}	1
Neodymium	Nd^{3+}	3
(Promethium)	Pm^{3+}	4
Samarium	Sm^{2+}	6
Samarium	Sm^{3+}	5
Europium	Eu^{2+}	7
Europium	Eu^{3+}	6
Gadolinium	Gd^{3+}	7
Terbium	Tb^{3+}	8
Terbium	Tb^{4+}	7
Dysprosium	Dy^{3+}	9
Holmium	Ho^{3+}	10
Erbium	Er^{3+}	11
Thulium	Tm^{3+}	12
Ytterbium	Yb^{2+}	14
Ytterbium	Yb^{3+}	13
Lutetium	Lu^{3+}	14

1.1 Inclusion Morphology Control in Steelmaking

Sulfide inclusions formed at low oxygen potentials (e.g. those prevailing in Al-killed steels) have deleterious effects on mechanical properties, formability and weldability of steel. These effects arise, primarily, from the elongation of sulfide inclusions in the rolling direction and can be minimized by adding rare earth elements to the steel to form RE-O-S type inclusions which are relatively undeformable at the temperatures of hot rolling. The formation of rare earth inclusions can be represented as:

$$2\underline{RE} + 3\underline{O} = RE_2O_3(s) \qquad (1.1)$$

and

$$2\underline{RE} + 2\underline{O} + \underline{S} = RE_2O_2S(s) \qquad (1.2)$$

1.2 Graphite Morphology Control in Cast Iron

Graphite morphology in cast iron is controlled by surface active elements such as oxygen and sulfur. Graphite spheroids, instead of flakes, are formed when the sulfur and oxygen contents of cast iron are reduced to very low levels. Rare earth elements can be conveniently used to bring about this reduction in oxygen and sulfur levels needed for spherodization of graphite in cast irons. The products formed on adding RE to an iron melt (high in carbon and silicon) are RE_2O_2S, RE_2S_3 and, sometimes, RES. Formation of these compounds may be represented by the following reactions:

$$2\underline{RE} + 2\underline{O} + \underline{S} = RE_2O_2S(s) \qquad (1.3)$$

$$2\underline{RE} + 3\underline{S} = RE_2S_3(s) \qquad (1.4)$$

$$\underline{RE} + \underline{S} = RES(s) \qquad (1.5)$$

The first two of the above reactions normally predominate.

1.3 Desulfurization of Hot Sulfur-Bearing Gases Using Rare Earth Oxides

At high temperatures, rare earth oxides can reduce sulfur in sulfur-bearing gases to very low levels. The important reactions in the desulfurization of hot gases are:

$$RE_2O_3(s) + \tfrac{1}{2}S_2(g) = RE_2O_2S(s) + \tfrac{1}{2}O_2(g) \qquad (1.6)$$

$$RE_2O_3(s) + \tfrac{1}{2}S_2(g) + \tfrac{3}{2}O_2(g) = RE_2O_2SO_4(s) \qquad (1.7)$$

$$RE_2O_2S(s) + S_2(g) = RE_2S_3(s) + O_2(g) \qquad (1.8)$$

and

$$RE_2O_2SO_4(s) + S_2(g) + 3O_2(g) = RE_2(SO_4)_3(s). \qquad (1.9)$$

The process of regeneration of rare earth oxides from the products of desulfurization can be represented by the following reactions:

$$RE_2O_2S(s) + \tfrac{1}{2}O_2(g) = RE_2O_3(s) + \tfrac{1}{2}S_2(g) \qquad (1.10)$$

$$RE_2S_3(s) + O_2(g) = RE_2O_2S(s) + S_2(g) \qquad (1.11)$$

$$RE_2S_3(s) + 6O_2(g) = RE_2(SO_4)_3(s) \quad (1.12)$$

$$RE_2O_2S(s) + 2O_2(g) = RE_2O_2SO_4(s) \quad (1.13)$$

$$RE_2(SO_4)_3(s) = RE_2O_2SO_4(s) + S_2(g) + 2O_2(g) \quad (1.14)$$

$$RE_2O_2SO_4(s) = RE_2O_3(s) + \frac{1}{2}S_2(g) + \frac{3}{2}O_2(g) \quad (1.15)$$

It is clear from the above discussion that the products in the processes of desulfurization and regeneration depend on the prevailing oxygen and sulfur partial pressures, and temperature.

1.4 The Thermodynamics of Oxygen-Sulfur Compounds of Rare Earths

Any chemical process can be understood in terms of the thermodynamics and the kinetics involved. Thermodynamic parameters give an indication regarding the formation and stability of certain phases, under a given set of conditions, out of several possible phases. Thus in order to understand a chemical process, it is imperative to have reliable thermodynamic data. The single most important thermodynamic parameter for a compound is its standard free energy of formation, denoted by ΔG_f^o. The standard free energy of formation of a compound is the driving force for a particular compound to form in its standard state from its constituent elements, each being in its chosen standard states.

Since sulfides, oxides, oxysulfides and oxysulfates of rare earth elements are important from an industrial viewpoint, a knowledge of their standard free energies of formation is essential.

The standard free energies of formation of most of the stoichiometric oxides of the rare earths are fairly well established (3). However, only a few studies (reviewed in Ref. 1) have been reported on nonstoichiometric rare earth oxides. Some rare earth sulfides have been studied (42), but for most, only estimates of their thermodynamic parameters are available. Similarly, only estimates are available of the standard free energies of formation of oxysulfides (3), except Ce_2O_2S and no worthwhile data are available on the thermodynamic properties of oxysulfates. The first work reporting the thermodynamics of decomposition of RE sulfates was done in 1913. Only $Ce_2(SO_4)_3$ has been studied thereafter. Thus, the main aim of the present study was to determine the ΔG_f^o of oxygen-sulfur compounds of rare earths, concentrating mainly on the oxysulfides and oxysulfates, at high temperatures.

1.5 Measurement of the Standard Free Energies of Formation of Rare Earth Oxysulfides and Oxysulfates

The standard free energies of formation of compounds have been measured using a variety of techniques. However, calorimetric, gas equilibration and electrochemical methods are most popular at high temperatures.

Calorimetric methods, though less accurate, are absolute since the thermodynamic data are not measured relative to any substance. The normal accuracy of calorimetric techniques is around $\pm$1-5 kcals, depending upon the temperature and the system under study.

Gas equilibration methods are relative methods. However, they are more accurate than calorimetric methods and the range of composition of a compound can be studied. The typical accuracy of a gas equilibration method is about ±1000 cals. The main disadvantage of this method lies in preparing gas mixtures with a large component ratio.

Electrochemical methods using solid electrolytes are the most accurate methods for determining ΔG_f^o of a compound with a typical accuracy of about ±1000 cals. However, their use is limited by availability of suitable electrolyte and electrode materials.

1.5.1 Solid Electrolytes and Oxygen Concentration Cells

Solid electrolytes are materials which have substantial ionic conductivity and negligible electronic conductivity at elevated temperatures. Some of the common solid electrolytes are α-AgI, calcia stabilized zirconia (CSZ), yttria doped thoria (YDT) and the β-aluminas.

Calcia stabilized zirconia, which conducts by oxygen ions, has been extensively used to study metal-oxygen systems since the pioneering work of Kiukkola and Wagner (5,6). An oxygen concentration cell can be represented by

$$\mu_{O_2}^{I} \mid CSZ \mid \mu_{O_2}^{II} \quad : \text{where} \quad \mu_{O_2}^{II} > \mu_{O_2}^{I} \qquad (1.16)$$

The oxygen potentials of two compartments are related through, E, the reversible cell emf. In a two component metal-oxygen system, the oxygen partial pressure can be fixed uniquely at a particular temperature in the presence of two condensed phases and a gas phase.

This oxygen partial pressure can be measured using a reference electrode having a known oxygen partial pressure. A typical cell of this kind can be represented as:

$$\text{Pt} \mid \text{A, AO} \mid \text{CSZ} \mid \text{B, BO} \mid \text{Pt} \qquad (1.17)$$

and the cell emf is given by:

$$E = \frac{RT}{4F} \ln\left[\frac{P_{O_2}(B/BO)}{P_{O_2}(A/AO)}\right] \qquad (1.18)$$

where A and B are metals, AO and BO their respective oxides and $P_{O_2}(A/AO)$ and $P_{O_2}(B/BO)$ are the oxygen partial pressures corresponding to the metal/oxide coexistence.

In the case of systems containing three components, such as those containing a metal, oxygen and sulfur, in presence of two condensed phases, an additional constraint needs to be imposed on the system for it to be uniquely defined at a constant temperature. The cell:

$$\text{Pt} \mid \begin{matrix}\text{MO(s), MS(s)} \\ (P_{SO_2} = 1 \text{ atm.})\end{matrix} \mid \text{CSZ} \mid \text{Air} \mid \text{Pt}$$

used by Larson and Elliott (7), illustrates this principle wherein the additional constraint is fixed by $P_{SO_2} = 1$.

1.5.2 Oxygen Concentration Cells Used in the Present Study

The following four types of oxygen concentration cell were used to study the ternary rare earth-oxygen-sulfur systems:

Type I Cells:

$$\text{Pt} \mid \begin{matrix} RE_2O_2S(s),\ RE_2O_2SO_4(s) \\ \text{in presence of } RE_2O_3(s) \end{matrix} \mid \text{CSZ} \mid \text{Air} \mid \text{Pt}$$

Type II Cells:

$$\text{Pt} \mid \begin{matrix} RE_2O_2S(s),\ RE_2O_2SO_4(s) \\ \text{in presence of } Ag/Ag_2S \end{matrix} \mid \text{CSZ} \mid \text{Air} \mid \text{Pt}$$

Type III Cells:

$$\text{Pt} \mid RE_2O_3(s),\ RE_2O_2SO_4(s),\ Cu(s),\ Cu_2S(s) \mid \text{CSZ} \mid \text{Air} \mid \text{Pt}$$

Type IV Cells:

$$\text{Pt} \mid RE_2O_3(s),\ RE_2O_2S(s),\ Ag(s),\ Ag_2S(s) \mid \text{CSZ} \mid \text{Air} \mid \text{Pt}$$

The additional constraint needed to uniquely define a ternary RE-O-S system, in the presence of two condensed phases at constant temperature, can be provided either by fixing the potential of one of the components such as sulfur by a metal/metal sulfide couple (here Ag/Ag_2S or Cu/Cu_2S) or by introducing an extra condensed phase. The former principle is utilized in cells of Type II, III and IV, while the latter is followed in cells of Type I.

The underlying assumption in construction of all of the above

cells is that the nonstoichiometry of the condensed phases is very small. In view of this assumption, cells of Type I and II yield the standard free energy of formation of the oxysulfate relative to the oxysulfide and cells of Type III and Type IV yield the standard free energy of formation of the oxysulfate and the oxysulfide, respectively, relative to the oxide. Combining data from these cells, the standard free energies of formation of rare earth oxysulfates and oxysulfides from their constituent elements, can be determined.

CHAPTER II

LITERATURE REVIEW

In this chapter, a brief discussion on the structural and thermodynamic properties of the compounds relevant to this study is presented. Several excellent review articles (1,3) are available on the thermodynamic properties of rare earth oxides. Thus, in the present study, only the highlights of RE-O systems will be presented. An attempt is made to review and document the existing data on rare earth oxygen-sulfur compounds. Some important studies of RE-S systems have also been included.

2.1 Rare Earth Oxides

As indicated in the first chapter, the most common valence of rare earth elements is +3 and valences other than +3 are expected for elements like Ce, Pr, Eu and Tb. Thus, oxides of the RE can be broadly divided into two categories according to:

1. whether the rare earth has a valence +3 (sesquioxides)
2. whether the rare earth has a valence other than +3 (higher and lower oxides of rare earths).

2.1.1 Rare Earth Sesquioxides (RE_2O_3)

Sesquioxides are the most common oxides of rare earths. They exist in several polymorphic forms. Goldschmidt et al. (8) designated

three polymorphs found below about 2000°C as A, B and C. Above this temperature, two more polymorphs designated X and H have been reported (9). Fig. 2.1, taken from the Ref. (1), shows the range of existence of the various polymorphs of rare earth oxides. Polymorphs of type A, B and C have been reported for all rare earth systems. For any polymorphic form, there is a gradual decrease in the lattice parameter across the lanthanide series, as shown in Fig. 2.2, attributed to a gradual decrease in the ionic radius of the rare earth ion. In the present study we are concerned with only the polymorphs of type A, B and C, and in subsequent discussion, the word 'polymorphs' will refer only to these forms.

The structure of various polymorphs has been extensively studied. The hexagonal A-type sesquioxides have a space group $P\bar{3}m1$ with one formula per unit cell. The metal atoms are seven-coordinated (10). B-type sesquioxides have a space group C2/m and are monoclinic. They have six formulae per unit cell in which rare earth atoms are seven- and six-coordinated (11). C-type sesquioxides have a body-centered cubic structure with a space group Ia3. The unit cell of C-type sesquioxides consists of 32 metal atoms and 48 oxygen atoms. The rare earth atoms in this structure are six-coordinated (12).

Eyring and Holmberg (13) have pointed out a useful relationship between the structures of the various polymorphs of sesquioxides and the fluorite structure. It has been proposed that A, B and C type structures can be derived from the fluorite structure by removing oxygen atoms along certain crystallographic directions. Fig. 2.3 shows the

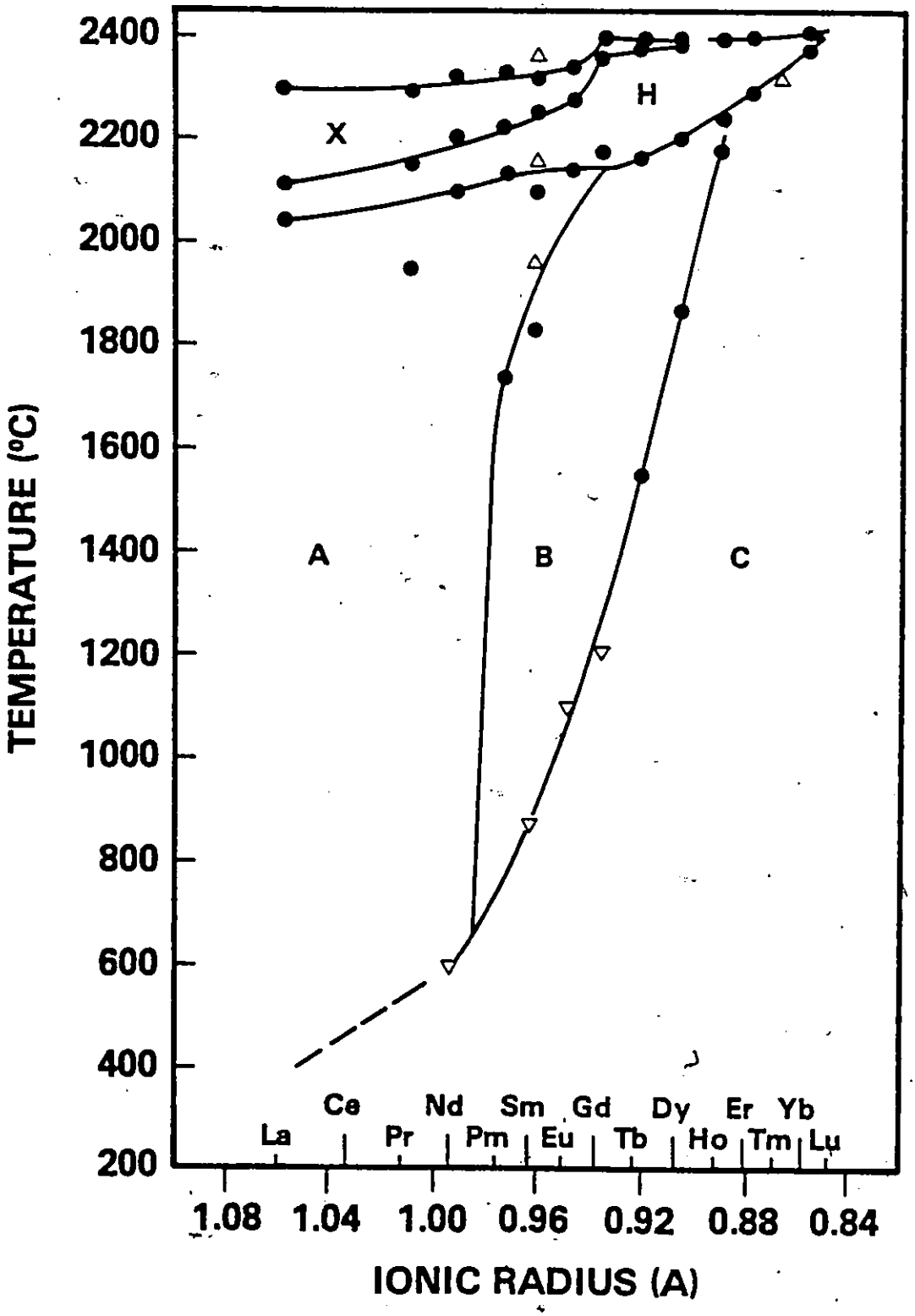

Fig. 2.1 Polymorphic forms and transition temperatures of the rare earth sesquioxides (Ref. 1).

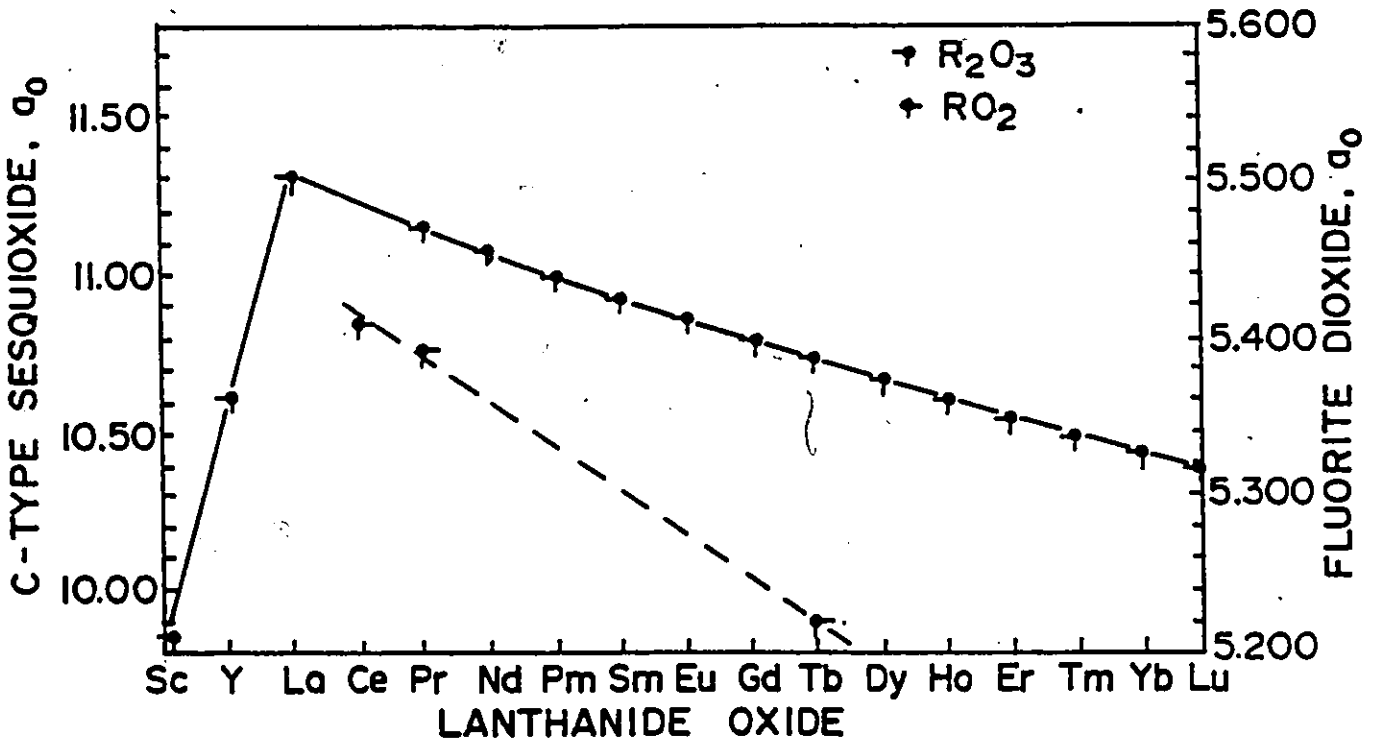

Fig. 2.2 Lattice parameter, a_o, for the cubic rare earth oxides (Ref. 1).

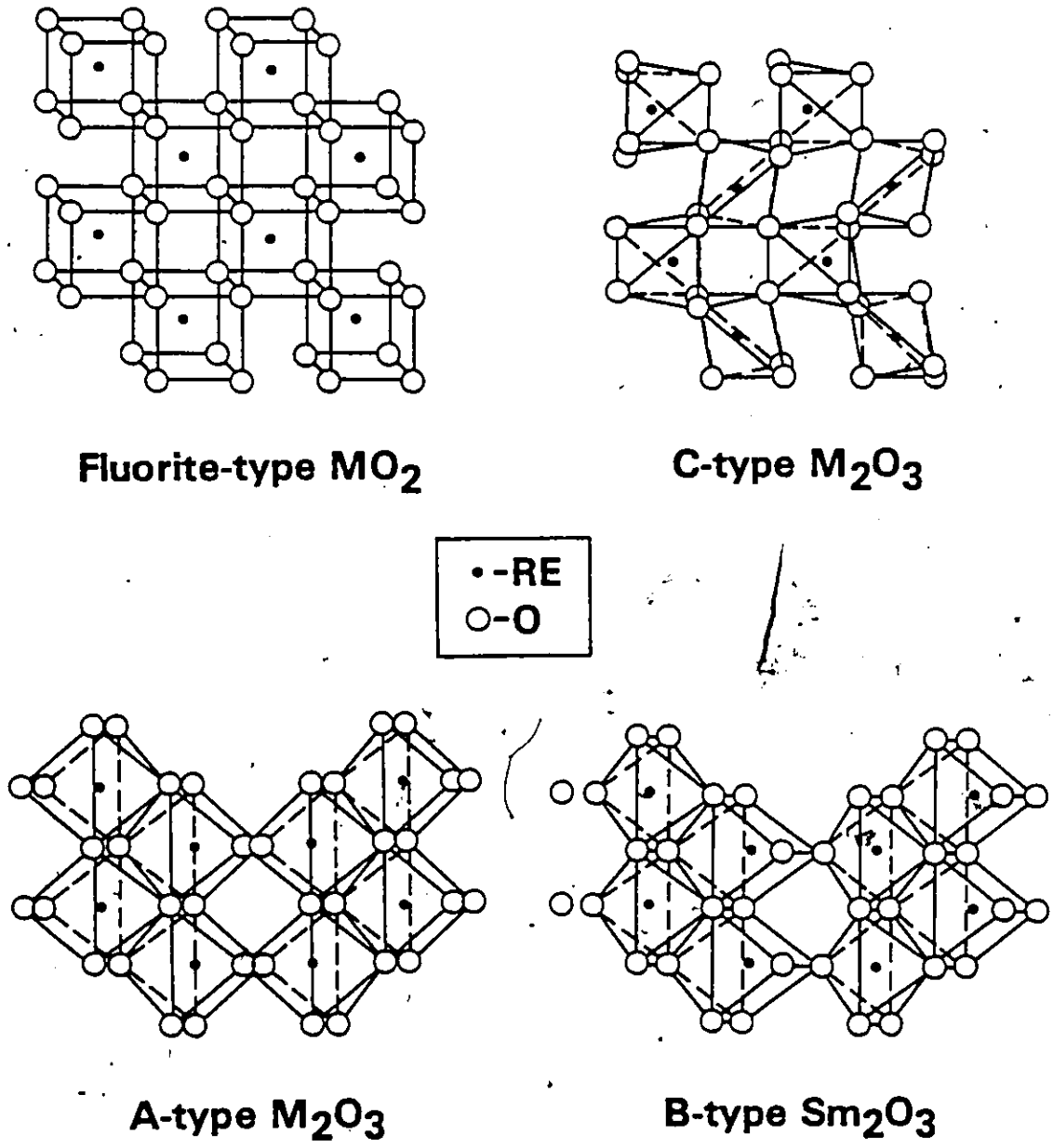

Fig. 2.3 Representation of REO_2, C-type RE_2O_3 , A-type RE_2O_3 and B-type RE_2O_3 and interrelation in their structures (Ref. 1).

relationship between the structures of A, B and C type polymorphs and the fluorite structure. This figure has been taken from Ref. 13.

The range of nonstoichiometry in sesquioxides of all rare earths, except those of cerium, praseodymium and terbium, is found to be very small. Miller and Daane (14) produced partially reduced C-type oxides by codistilling and comelting the sesquioxides with their respective metals. The compositions of $GdO_{1.495}$, $YO_{1.4991}$, $ErO_{1.489}$ and $LuO_{1.485}$ were observed by these authors. On the oxygen deficit side, the composition of the sesquioxide of Yb was determined to be $YbO_{1.495}$ by Bedford and Catalano (15). Ackermann and Rauh (16) have reported the nonstoichiometric composition of oxygen deficient La_2O_3 as $La_2O_{2.980}$ at 2400K in a tungsten effusion cell and as $La_2O_{2.998}$ at 2427K in a rhenium cell. Fairly large ranges of composition have been reported for the sesquioxides of cerium, praseodymium and terbium. A discussion on these will follow in the next section.

Thermodynamically, sesquioxides of rare earths are some of the most stable compounds. The thermodynamic properties of sesquioxides have been reviewed by Westrum (17), Holley et al. (18) and, more recently, by Gschneidner et al. (3). The last review is more exhaustive and includes most of the studies conducted up to 1973. Some new data have become available (19-23) since the review of Gschneidner et al. However, these do not affect the standard free energies of formation of the oxides listed by Gschneidner et al., in any significant way. Table 2.1 shows the values of the standard free energies of formation of the sesquioxides at two different temperatures. The single most important

TABLE 2.1

THE STANDARD FREE ENERGIES OF FORMATION AND THE STANDARD ENTHALPIES OF FORMATION OF RARE EARTH SESQUIOXIDES (Ref. 3)

Rare Earth	Freezing Point (°C)	ΔH°_{298} (cal /mole·K)	ΔG°_{f} at 298K (cal /mole·K)	ΔG°_{f} at 1100K (cal /mole·K)
La	2256	-482820	-407869	-353891
Ce	2210	-429310	-408052	-353529
Pr	2183	-435800	-414440	-360238
Nd	2233	-432110	-411072	-356927
(Pm)	2320			
Sm	2269	-435860 (B)	-414804 (B)	-359581 (B)
		-436760 (C)	-415257 (C)	-358996 (C)
Eu	2291	-394700 (B)	-371891 (B)	-314632 (B)
		-397400 (C)	-374144 (C)	-316122 (C)
Gd	2339	-433940 (B)	-413522 (B)	-359810 (B)
		-436640 (C)	-415775 (C)	-361091 (C)
Tb	2303	-445800	-424679	-371018
Dy	2228	-445320	-423948	-369701
Ho	2330	-449550	-428214	-373567
Er	2344	-453590	-432338	-377257
Tm	2341	-451406	-429581	-374130
Yb	2355	-433680	-413316	-361484
Lu	2427	-448900	-427559	-372002
Y	2376	-455450	-434266	-379255

parameter which significantly affects the values of the standard free energy of formation, ΔG_f^o, of a compound is the standard enthalpy of formation at 298K, denoted by ΔH_{298}^o. For this reason, values of ΔH_{298}^o for the sesquioxides have also been included in the Table 2.1. The data of Gschneidner et al. (3) can be fitted into linear equations, which are presented in Table 2.2.

2.1.2 Lower Oxides of the Rare Earths

Monoxides of rare earths have an NaCl structure. Of the monoxides, only EuO and YbO are well established (24, 25). Thermodynamic properties of EuO have been extensively studied. Haschke and Eick (26) and Huber and Holley (27, 28) have measured the standard enthalpy of formation of EuO at 298K. The low temperature heat capacity data for this compound was obtained by Teany and Moruzzi (29). Finally, McMasters et al. (30) have measured the heat capacity of EuO at high temperatures (up to 1725K) and calculated various thermodynamic functions at these temperatures. The values of the standard free energy of formation of EuO at high temperatures in analytical form, listed in Table 2.2, have been derived from these data.

The only other oxide of rare earths in which the valence of RE is less than +3 is Eu_3O_4. It is orthorhombic with a space group Pnam (31). The thermodynamic parameters of Eu_3O_4 have been estimated by Gschneidner et al. (3) and are listed in Table 2.2.

Finally, utilizing the available data, McCarthy (32) has calculated the regions of stability of the different oxides of

TABLE 2.2

STANDARD FREE ENERGIES OF FORMATION OF RARE EARTH OXIDES

Reaction	Temp. Range (K)	ΔG_f^o = -A + BT (cal /mole.K) A (cal /mole.K)	B (cal /mole)	Error in ΔG_f^o (cal /mole.K)
$2La(\beta) + 3/2O_2(g) = La_2O_3$(A type)	550 - 1134	426770	66.00	±2600
$2La(\gamma) + 3/2O_2(g) = La_2O_3$(A type)	1134 - 1193	427100	66.50	±2600
$2La(\ell) + 3/2O_2(g) = La_2O_3$(A type)	1103 - 2000	428800	68.00	±2600
$2Ce(\gamma) + 3/2O_2(g) = Ce_2O_3$(A type)	298 - 999	428060	68.00	±2700
$2Ce(\delta) + 3/2O_2(g) = Ce_2O_3$(A type)	999 - 1071	427420	67.13	±2700
$2Ce(\ell) + 3/2O_2(g) = Ce_2O_3$(A type)	1071 - 2000	426000	66.16	±2700
$Ce(\gamma) + O_2(g) = CeO_2(s)$	298 - 999	259620	49.23	±2300
$Ce(\delta) + O_2(g) = CeO_2(s)$	999 - 1071	259550	49.05	±2300
$Ce(\ell) + O_2(g) = CeO_2(s)$	1071 - 2000	259910	49.45	±2300
$2Pr(\alpha) + 3/2O_2(g) = Pr_2O_3$(A type)	298 - 1068	434150	67.47	±3600
$2Pr(\beta) + 3/2O_2(g) = Pr_2O_3$(A type)	1068 - 1204	433260	66.38	±3600
$2Pr(\ell) + 3/2O_2(g) = Pr_2O_3$(A type)	1204 - 2000	434750	67.73	±3600

TABLE 2.2 (CONT'D)

Reaction	Temp. Range (K)	ΔG_f^o = -A + BT (cal /mole.K) A (cal /mole.K)	B (cal /mole)	Error in ΔG_f^o (cal /mole.K)
$Pr(\alpha) + \frac{1.833}{2} O_2(g) = PrO_{1.833}$(A type)	1068 - 1204	222450	37.37	±4000
$Pr(\beta) + \frac{1.833}{2} O_2(g) = PrO_{1.833}$(A type)	1204 - 2000	219790	35.45	±4000
$2Nd(\alpha) + 3/2O_2(g) = Nd_2O_3$(A type)	298 - 1128	430780	67.28	±2200
$2Nd(\beta) + 3/2O_2(g) = Nd_2O_3$(A type)	1128 - 1289	430580	66.94	±2200
$2Nd(\ell) + 3/2O_2(g) = Nd_2O_3$(A type)	1289 - 1395	433750	69.40	±2200
$2Nd(\ell) + 3/2O_2(g) = Nd_2O_3$(C type)	1395 - 2000	433510	69.22	±2200
$2Sm(\alpha) + 3/2O_2(g) = Sm_2O_3$(α,B type)	1000 - 1190	434670	68.27	±2400
$2Sm(\beta) + 3/2O_2(g) = Sm_2O_3$(α, B type)	1190 - 1195	437210	70.40	±2400
$2Sm(\beta) + 3/2O_2(g) = Sm_2O_3$(β, B type)	1195 - 1345	435830	69.24	±2400
$2Sm(\ell) + 3/2O_2(g) = Sm_2O_3$(β, B type)	1345 - 2000	439820	72.20	±2400
$2Sm(\alpha) + 3/2O_2(g) = Sm_2O_3$(C type)	1000 - 1190	435280	69.34	±2700
$Eu(\ell) + \frac{1}{2}O_2(g) = EuO(s)$	1090 - 1800	144520	23.77	±2000
$3Eu(\ell) + 2O_2(g) = Eu_3O_4(s)$	1090 - 1800	539340	96.67	±6000
$2Eu(\ell) + 3/2O_2(g) = Eu_2O_3$(C type)	1090 - 1800	393790	70.85	±2900
$2Eu(\ell) + 3/2O_2(g) = Eu_2O_3$(B type)	1090 - 1800	392330	70.70	±2800

TABLE 2.2 (CONT'D)

Reaction	Temp. Range (K)	ΔG_f^o = -A + BT (cals/mole.K) A (cals/mole.K)	B (cals/mole)	Error in ΔG_f^o (cals/mole.K)
$2Gd(\alpha) + 3/2O_2(g) = Gd_2O_3$(B type)	1000 - 1533	431610	65.26	±2900
$2Gd(\alpha) + 3/2O_2(g) = Gd_2O_3$(C type)	1000 - 1533	433780	66.07	±2900
$2Tb(\alpha) + 3/2O_2(g) = Tb_2O_3$(C type)	1000 - 1560	441370	63.95	±2900
$2Dy(\alpha) + 3/2O_2(g) = Dy_2O_3$(C type)	1000 - 1590	440800	64.63	±2800
$2Ho(\alpha) + 3/2O_2(g) = Ho_2O_3$(C type)	1000 - 1701	445940	65.78	±3200
$2Er(\alpha) + 3/2O_2(g) = Er_2O_3$(C type)	1000 - 1795	450180	66.29	±2400
$2Tm(s) + 3/2O_2(g) = Tm_2O_3$(C type)	1000 - 1680	447020	66.17	±3400
$2Yb(\alpha) + 3/2O_2(g) = Yb_2O_3$(C type)	1000 - 1033	430610	62.82	±2500
$2Yb(\beta) + 3/2O_2(g) = Yb_2O_3$(C type	1033 - 1097	430820	63.01	±2500
$2Yb(\ell) + 3/2O_2(g) = Yb_2O_3$(C type)	1097 - 1467	434510	66.38	±2500
$2Lu(s) + 3/2O_2(g) = Lu_2O_3$(C type)	1000 - 1900	445490	66.80	±3800
$2Y(s) + 3/2O_2(g) = Y_2O_3$(C type)	900 - 1330	452790	66.83	±2500

europium. His results are summarized in Fig. 2.4.

2.1.3 Higher Oxides of the Rare Earths

Cerium, praseodymium and terbium are known to exist in valences higher than +3 in some of their oxides. These oxides can be represented by a general formula REO_x ($1.5 \leq x \leq 2.0$). The dioxides in these systems have the fluorite structure. Numerous fluorite related phases are formed due to loss of oxygen from the dioxides of Ce, Pr and Tb. The Ce-O, Pr-O and Tb-O systems are quite similar and each has a homologous series with a generic formula RE_nO_{2n-2}. However, there are some important differences between these systems mainly related to the structure and stability of certain phases. These differences are extensively discussed by Eyring (1). Because of the enormously large number, not all higher oxides of the rare earths can be discussed here. However, an attempt is made to highlight the important features of the higher oxides. The phase diagrams of the Ce-O, Pr-O and Tb-O systems, shown in the Figures 2.5, 2.6 and 2.7, respectively, give an indication of the complexity of these systems.

Bevan and Kordis (33) reported the first extensive work on the Ce-O system. In this work, the existence and stability of Ce-O phases was studied at various temperatures and oxygen partial pressures. The oxygen partial pressure was controlled using H_2/H_2O and CO/CO_2 gas mixtures. Using the information from their experiments, these authors were able to construct a Ce-O phase diagram which was subsequently modified by Height and Bevan (34) to its present form, shown in Fig.

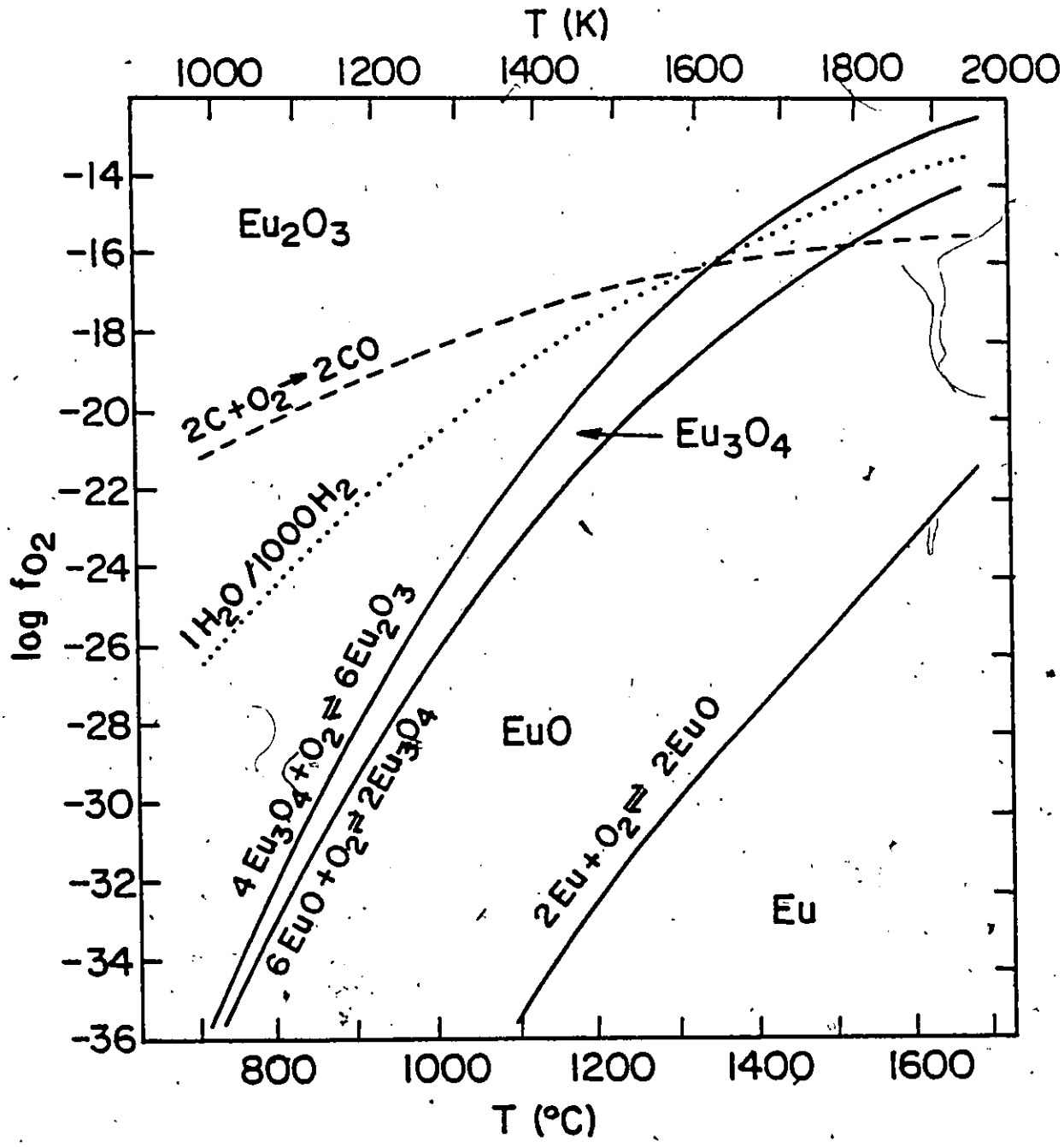

Fig. 2.4 Stability ranges of various oxides of europium. f_{O_2} denotes the fugacity of oxygen (Ref. 32).

Fig. 2.5 The Ce-O phase diagram. Ordered phases are indicated by Greek letters. s characterizes a subregion within the fluorite region having a uniform defect structure. Notation: θ-$CeO_{1.5}$; σ-$CeO_{1.65}$; ι-$CeO_{1.714}$; ζ-$CeO_{1.778}$; ε-$CeO_{1.800}$; δ-$CeO_{1.818}$; α-fluorite phase (Ref. 1).

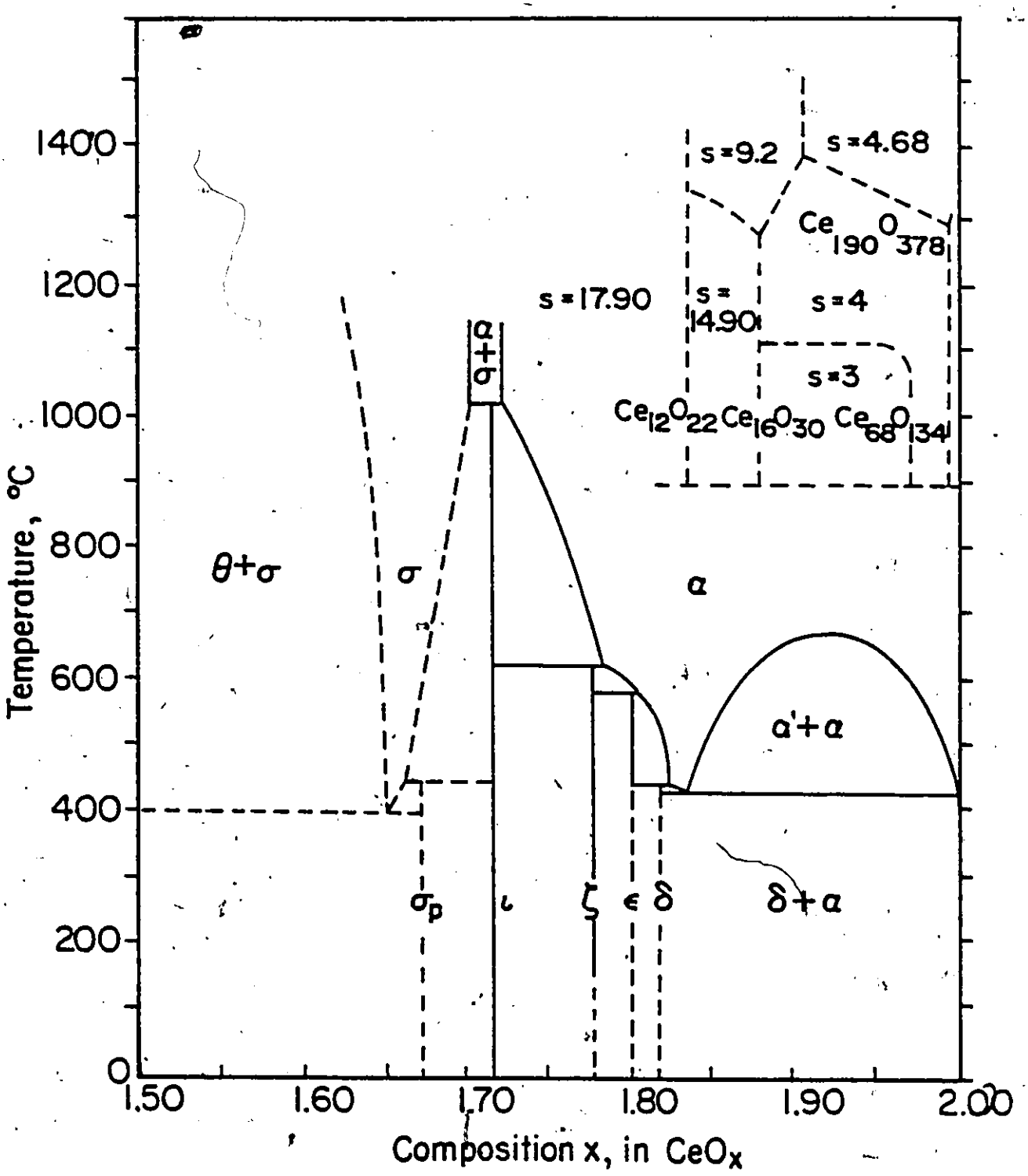
1400
1200
1000
800
600
400
200
0
Temperature, °C
1.50
1.60
1.70
1.80
1.90
2.00
Composition x, in CeOx
θ+σ
σ
α+σ
α
α'+α
δ+α
σp
ι
ζ
ϵ
δ
s=9.2
s=4.68
Ce190O378
s=17.90
s=14.90
s=4
s=3
Ce12O22
Ce16O30
Ce68O134

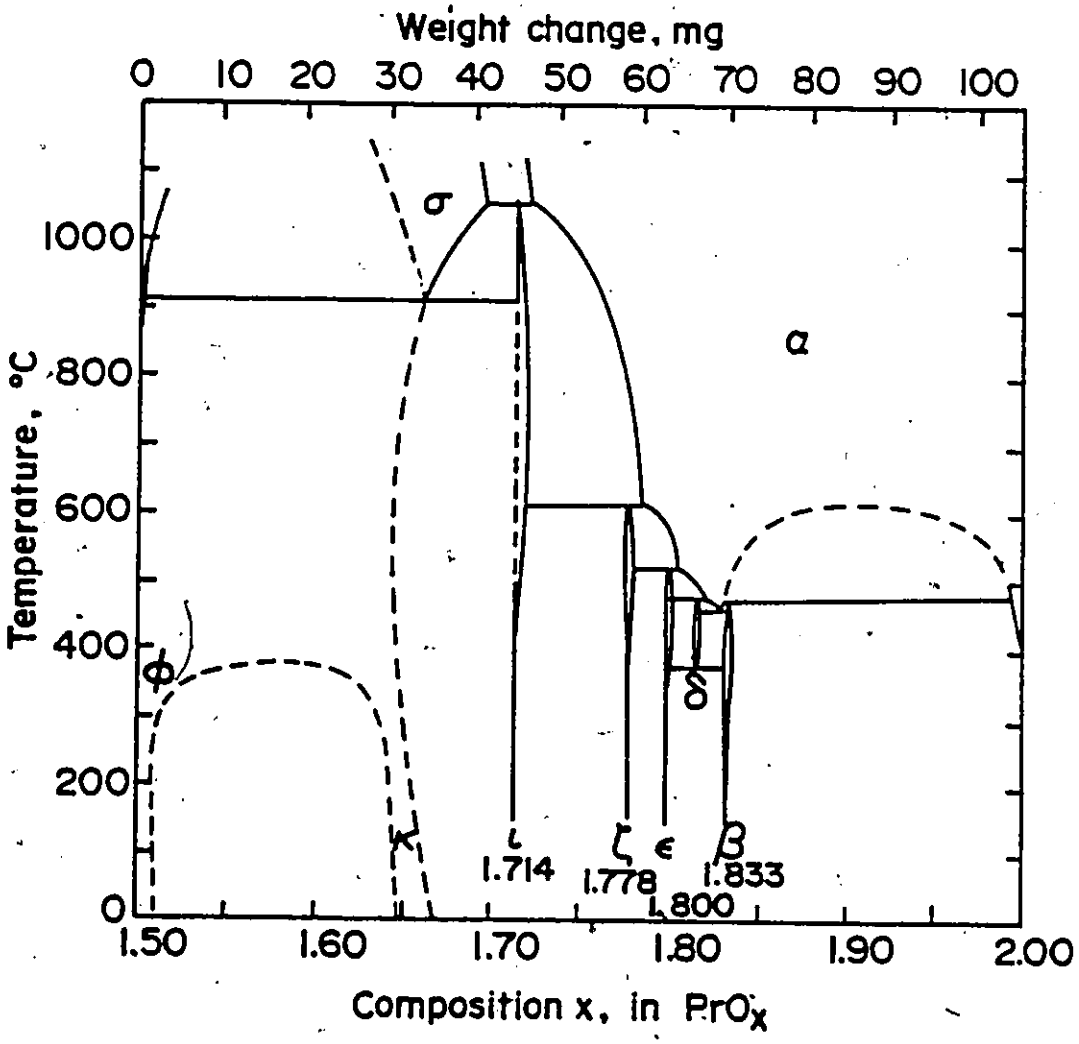

Fig. 2.6 The Pr-O phase diagram. Metastable or assumed boundaries are dashed. Notation: ϕ-$PrO_{1.5}$; σ-$PrO_{1.65}$; ι-$CeO_{1.714}$; ζ-$PrO_{1.778}$; ε-$PrO_{1.800}$; δ-$PrO_{1.818}$; β-$PrO_{1.833}$; α-fluorite phase (Ref. 1).

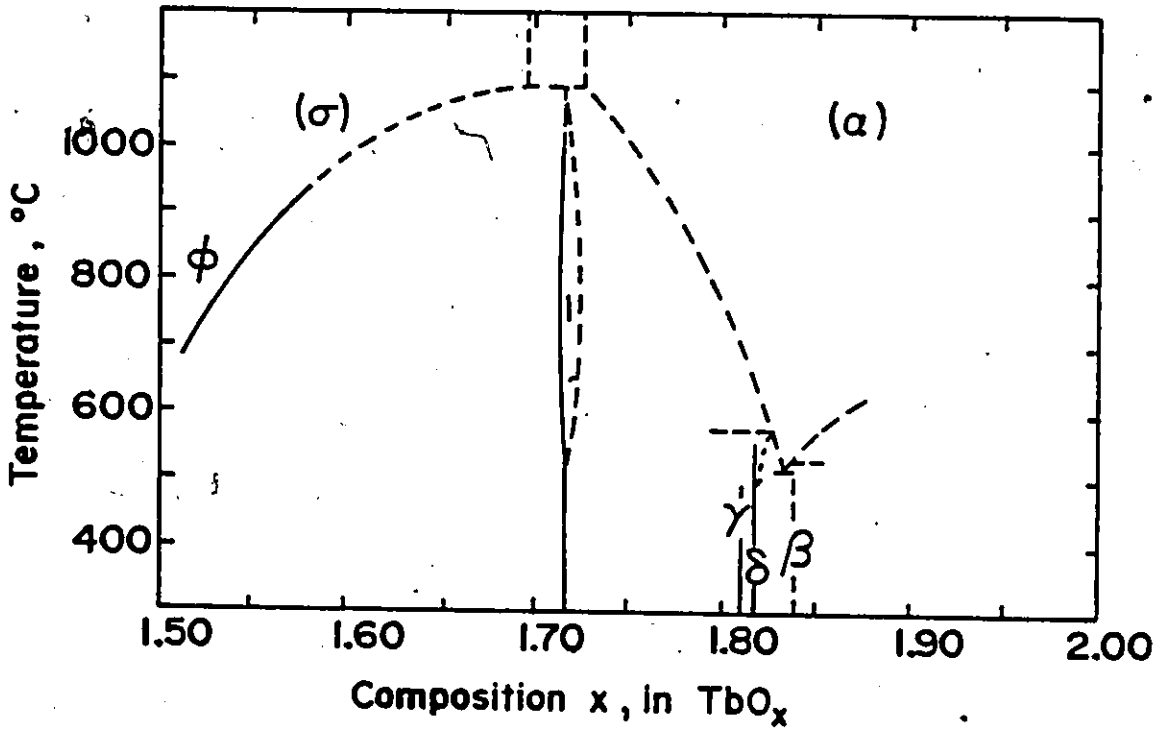

Fig. 2.7 The Tb-O phase diagram. The dashed curves mark the boundaries of the disordered α and σ regions suggested by electron microscopic studies. Notation: ϕ-$TbO_{1.5}$; ι-$TbO_{1.714}$; γ'-$TbO_{1.809}$; δ-$TbO_{1.818}$; β-$TbO_{1.833}$; α-fluorite phase (Ref. 1).

2.5.

Iwasaki and Katsura (35) used a similar technique to study the Ce–O system at temperatures higher than those investigated by Bevan and Kordis. These authors were thus able to study the Ce–O system up to 1300°C.

Campserveux and Gernadian (36) studied the oxygen-rich side of the Ce–O system at 1080°C and measured the partial molar enthalpy of solution of O_2, denoted by $\Delta\bar{H}_{O_2}$, by microcalorimetry. Their values of $\Delta\bar{H}_{O_2}$ are in fair agreement with those obtained by Bevan and Kordis.

Sorensen (37) investigated the oxygen-rich portion ($1.75 \leq x \leq 2.00$) of the Ce–O phase diagram at 900–1400°C. This study indicated that the fluorite phase in the Ce–O system at high temperatures consists of several subregions, each consisting of an apparent nonstoichiometric single phase. The nonstoichiometry in these subregions, characterized by x (in CeO_{2-x}), was assumed to be proportional to $(P_{O_2})^{1/s}$, where s depended upon the nature of lattice defects. Based on their results, these authors divided the oxygen-rich region of the Ce–O phase diagram into different subregions according to the values of s. Their results are shown in Fig. 2.5 at the upper right-hand portion of the diagram.

Recently, Fruehan (38) studied the Ce–O system between 1000 and 1550°C using CO/CO_2 gas mixtures to control P_{O_2}. His results are in fair agreement with those of Bevan and Kordis in the temperature range common to the two studies.

Eyring (1) has extensively reviewed the studies on the Pr–O system. The studies of Hyde et al. (39) and Turcotte et al. (40) form

the basis of his discussion. The phase diagram of the Pr–O system, shown in Fig. 2.6, has been taken from Ref. 39. This diagram gives a good indication of the complex nature of the Pr–O system. As in the Ce–O system, the range of stability of phases depends on the temperature and the oxygen partial pressure. Fig. 2.8, taken from Ref. 39, shows the stability range of the various phases in the Pr–O system.

Most of the work on the Tb–O system has been done by Eyring and his co-workers over several years. These studies have been reviewed by Eyring (40). The phase diagram and the phase stability diagram for the Tb–O system, presented in Figures 2.7 and 2.9, respectively, are based on this work. The Tb–O system appears to be less complex than either the Pr–O or the Ce–O system. However, it is still far from being a simple system.

2.2 Rare Earth Sulfides

Rare earth elements form numerous sulfides having different crystal structures and physico-chemical properties. The rare earths seem to prefer valences lower than +3 in their sulfides. Thus, valences higher than +3 for rare earth ions are rarely encountered in the sulfides. The two most common valence states are +2 and +3.

Another characteristic of rare earth sulfides is related to the coordination of the rare earth ions. Flahaut (41) has pointed out that the rare earth elements have two kinds of coordination polyhedra in their sulfides. One is related to the triangular prism while the other is derived from an octahedron.

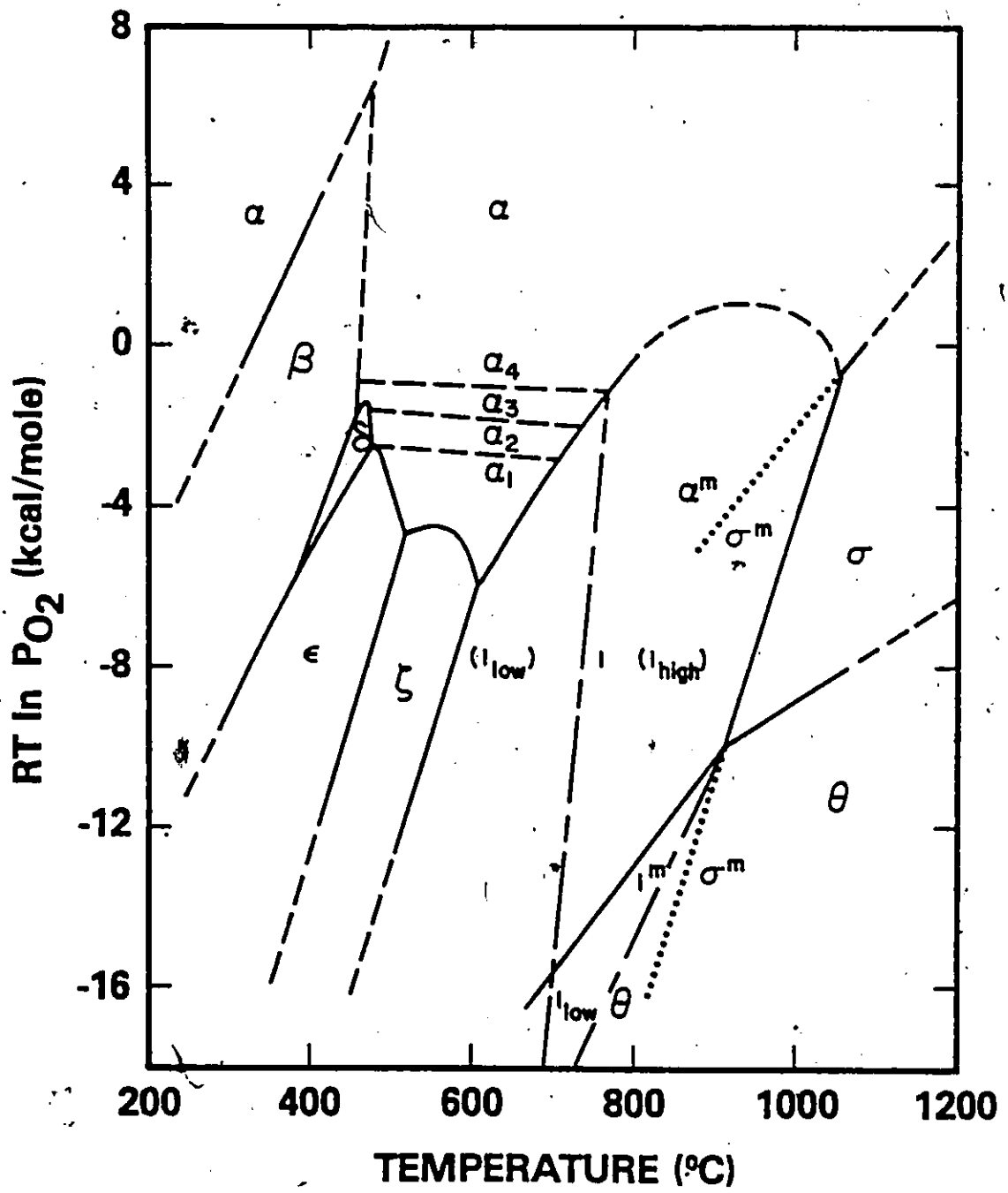

Fig. 2.8 Fields of stability in the Pr-O system. The fluorite phase, α is shown to be complex. Notation: same as Fig. 2.6.

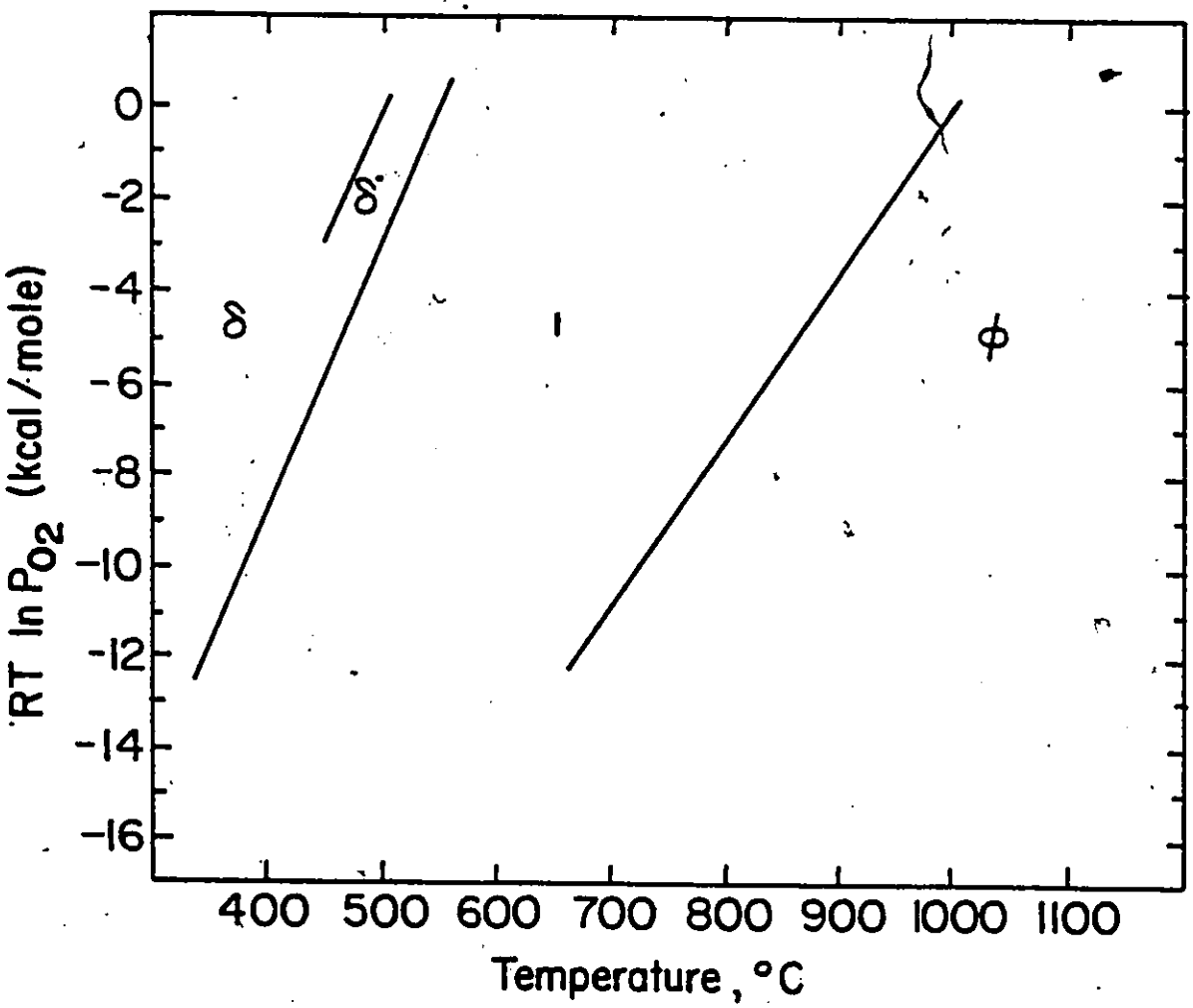

Fig. 2.9 Fields of stability in the Tb-O system. Notation: same as Fig. 2.7.

Numerous structures have been observed in sulfides of rare earths. However, a detailed discussion is beyond the scope of this work. For the present discussion, we will consider only the structures of the most common high temperature modifications, namely the γ-sesquisulfides and the monosulfides. γ-type sesquisulfides have the Th_3P_4 structure while the monosulfides have the NaCl structure.

The thermodynamic properties of only some rare earth sulfides, such as those of europium and cerium, have been extensively studied (43-47). For sulfides of most of the other rare earths, especially those of heavier ones, the thermodynamic information is quite scarce. In order to determine the standard free energy of formation of a RE sulfide from thermochemical data, the following parameters need to be determined:

A. The heat capacities of the rare earth element, sulfur and the sulfide in the temperature range of interest.

B. The standard enthalpy of formation of the sulfide at the reference temperature, chosen as 298K.

C. The standard entropy functions of the rare earth metal, sulfur and the sulfide at a reference temperature, normally chosen as 298K. (These quantities are derived from low temperature heat capacity data).

D. The heats of the transformation undergone by the RE metal, sulfur and sulfide.

Tables 2.3 and 2.4, list the standard enthalpies of formation and the standard entropy functions, respectively, at 298K. As can be seen

TABLE 2.3

STANDARD ENTHALPY OF FORMATION AT 298K, ΔH^{o}_{298}, OF RARE EARTH SULFIDES

Compound	ΔH^{o}_{298} (cal /mole)	Error in ΔH^{o}_{298} (cal /mole)	Reference
LaS(s)	-109000	±5000	42
La_3S_4(s)	-401000	±4000	44*
La_2S_3(s)	-292000	±16000	43
LaS_2(s)	-149000	±8000	43
LaS_2(s)	-144000	±2000	44
CeS(s)	-109100	±2000	43
Ce_3S_4(s)	-395000	±5000	43
Ce_3S_4(s)	-392000	±5000	43
Ce_2S_3(s)	-284000	±3000	43
CeS_2(s)	-146300	±2000	43
CeS_2(s)	-143000	±2000	44
PrS(s)	-108000	±6000	42
PrS(s)	-109200	—	45
Pr_3S_4(s)	-391000	±4000	44*
Pr_2S_3(s)	-275000	±15000	42*
PrS_2(s)	-141000	±2000	44*

TABLE 2.3 (continued)

Compound	ΔH°_{298} (cal /mole)	Error in ΔH°_{298} (cal /mole)	Reference
NdS(s)	-108000	±15000	42*
Nd_3S_4(s)	-388000	±4000	44
Nd_2S_3(s)	-276000	±10000	43
NdS_2(s)	-139000	±2000	44*
SmS(s)	-108000	±20000	42*
SmS(s)	-103200	--	45
Sm_2S_3(s)	-285000	±30000	42*
EuS(s)	-106000	±1200	46
EuS(s)	-97500		45
EuS(s)	-100000	±15000	42*
EuS(s)	-106700	--	47
Eu_3S_4(s)	-355000	±20000	42*
GdS(s)	-110000	±11000	42*
Gd_2S_3(s)	-288000	±30000	42*
TbS(s)	-110000	±10000	42*
Tb_2S_3(s)	-290000	±30000	42*

TABLE 2.3 (continued)

Compound	ΔH°_{298} (cal /mole)	Error in ΔH°_{298} (cal /mole)	Reference
DyS(s)	-110000	±15000	42*
Dy_2S_3(s)	-292000	±30000	42*
Dy_2S_3(s)	-292600	± 8800	91
HoS(s)	-110000	±15000	42*
Ho_2S_3(s)	-293000	±30000	42*
ErS(s)	-110000	±15000	42*
Er_2S_3(s)	-295000	±30000	42*
TmS(s)	-110000	±15000	42*
Tm_2S_3(s)	-297000	±30000	42*
YbS(s)	-108000	±15000	42*
YbS(s)	- 97900	—	45
Yb_2S_3(s)	-280000	±15000	42*
Yb_2S_3(s)	-280600	±8500	91

TABLE 2.3 (continued)

Compound	ΔH^{o}_{298} (cal /mole)	Error in ΔH^{o}_{298} (cal /mole)	Reference
LuS(s)	-110000	±15000	42*
Lu_2S_3(s)	-297000	±30000	42*
YS(s)	-110000	±3000	48
Y_2S_3(s)	-300000	±30000	42*

* Estimated.

TABLE 2.4

STANDARD ENTROPY FUNCTIONS OF RARE EARTH SULFIDES AT 298K

Compound	S°_{298} (cal /mole°K)	Error in S°_{298} (cal /mole°K)	Reference
LaS(s)	17.0	±2.0	42
LaS(s)	16.0	--	49*
La_2S_3(s)	39.43	±0.1	50
LaS_2(s)	21.5	±3.0	51
CeS(s)	18.7	±0.3	52
CeS(s)	17.61	--	49*
Ce_3S_4(s)	61.0	±0.3	42*
Ce_2S_3	43.1	±0.4	52
CeS_2(s)	20.0	±3.0	42*
PrS(s)	18.6	±1.0	42*
PrS(s)	18.62	--	49*
Pr_3S_4(s)	61.2	±3.0	42*
Pr_2S_3(s)	47.5	±2.0	42*
NdS(s)	18.6	±1.0	53
NdS(s)	17.61	--	49*
Nd_2S_3(s)	44.28	±0.13	50

TABLE 2.4 (continued)

Compound	S°_{298} (cal /mole·K)	Error in S°_{298} (cal /mole·K)	Reference
SmS(s)	18.5	±2.0	42*
SmS(s)	24.15	--	49*
Sm_2S_3(s)	48.0	±3.0	42*
EuS(s)	18.5	±2.0	42*
EuS(s)	21.89	--	49*
EuS(s)	22.89	±0.7	46
Eu_3S_4(s)	66.8	±5.0	42*
GdS(s)	18.5	±2.0	42*
GdS(s)	20.69		49*
Gd_2S_3(s)	47.5	±3.0	42*
TbS(s)	18.5	±2.0	42*
Tb_2S_3(s)	49.0	±3.0	42*
DyS(s)	18.5	±2.0	42*
Dy_2S_3(s)	48.0	±3.0	42*

TABLE 2.4 (continued)

Compound	S^{o}_{298} (cal /mole·K)	Error in S^{o}_{298} (cal /mole·K)	Reference
HoS(s)	18.5	±2.0	42*
Ho_2S_3(s)	49.5	±4.0	42*
ErS(s)	18.5	±2.5	42*
Er_2S_3(s)	48.5	±4.0	42*
TmS(s)	18.5	±2.5	42*
Tm_2S_3(s)	46.5	±4.0	42*
YbS(s)	16.5	±2.5	42*
Yb_2S_3(s)	38.5	±5.0	42*
LuS(s)	15.0	±3.0	42*
Lu_2S_3(s)	38.5	±4.0	42*
YS(s)	16.0	±2.0	42*
Y_2S_3(s)	34.0	±4.0	42*

*Estimated.

from these tables, experimental thermodynamic data on the sulfides is very scarce. The heat capacities of very few rare earth sulfides have been measured at high temperatures. The values of heat capacities, used in calculations in subsequent chapters, have been taken from Ref. 42. The thermodynamic data for sulfur is also taken from Ref. 42, whereas, those for the metals have been taken from Ref. 22.

2.3 Oxygen-Sulfur Compounds of the Rare Earths*

Numerous compounds of rare earths with oxygen and sulfur have been reported. However, only the phases stable at high temperatures (above 800°C), and at the oxygen and sulfur partial pressures of interest in this study, are considered here. Therefore, in the present chapter, we will concentrate only on the oxysulfides, oxysulfates and sulfates, of the rare earths.

2.3.1 Rare Earth Oxysulfides (RE_2O_2S)

Rare earth oxysulfides are very stable compounds and have very high melting points (> 2000°C). They are fairly important materials from an industrial viewpoint because of their use as phosphors and their occurrence as inclusions in the rare earth treated steels.

---

* Thiosulfates, sulfites, sulfates with valences other than +3 and oxysulfides like $La_2O_2S_2$ and La_2OS_2 are not considered since they are unimportant at high temperatures and the ranges of oxygen and sulfur potentials under consideration.

Oxysulfides of all the rare earth elements have a Ce_2O_2S type structure. The structure of Ce_2O_2S was determined by Zachariasen (54) and was found to have a hexagonal unit cell with one formula per unit cell and a space group of $C\bar{3}m$. Figure 2.10 shows the unit cell of Ce_2O_2S.

Gschneidner et al. (3) estimated the values of the standard free energy of formation, ΔG_f^o, and the standard enthalpy of formation at 298K, ΔH_{298}^o, of rare earth oxysulfides using information on their preparation and the relationship between ΔG_f^o and the relative unit cell volume for these compounds. Necessary corrections were applied when estimating ΔG_f^o values for Eu_2O_2S and Yb_2O_2S by taking into account the divalence of Eu and Yb in their standard states. Table 2.5 shows the values of ΔG_f^o(1100K) and ΔH_{298}^o of the rare earth oxysulfides estimated by Gschneidner et al. (3).

The estimates of Gschneidner et al. (3) of ΔG_f^o for Y_2O_2S, Ce_2O_2S and Gd_2O_2S at different temperatures can be used to derive analytical expressions for ΔG_f^o in the relevant temperature ranges. These expressions are listed in Table 2.6.

Soschin (55) estimated ΔH_{298}^o for Ce_2O_2S, La_2O_2S and Y_2O_2S from the crystal lattice energies and the sum of the heats of formation of the gaseous ions of the constituent elements. Thus, for RE_2O_2S, ΔH_{298}^o could be expressed as

$$\Delta H_{298}^o = 2\Delta H_{298}^o(RE^{3+}) + 2\Delta H_{298}^o(O^{2-}) + \Delta H_{298}^o(S^{2-}) - U$$

Fig. 2.10 Hexagonal unit cell of cerium oxysylfide.
2 Ce at ±(1/3, 2/3, U_1) where U_1 =0.29;
2 O at ±(1/3, 2/3, U_2) where U_2 =0.64;
1 S at ±(0 , 0 , 0).

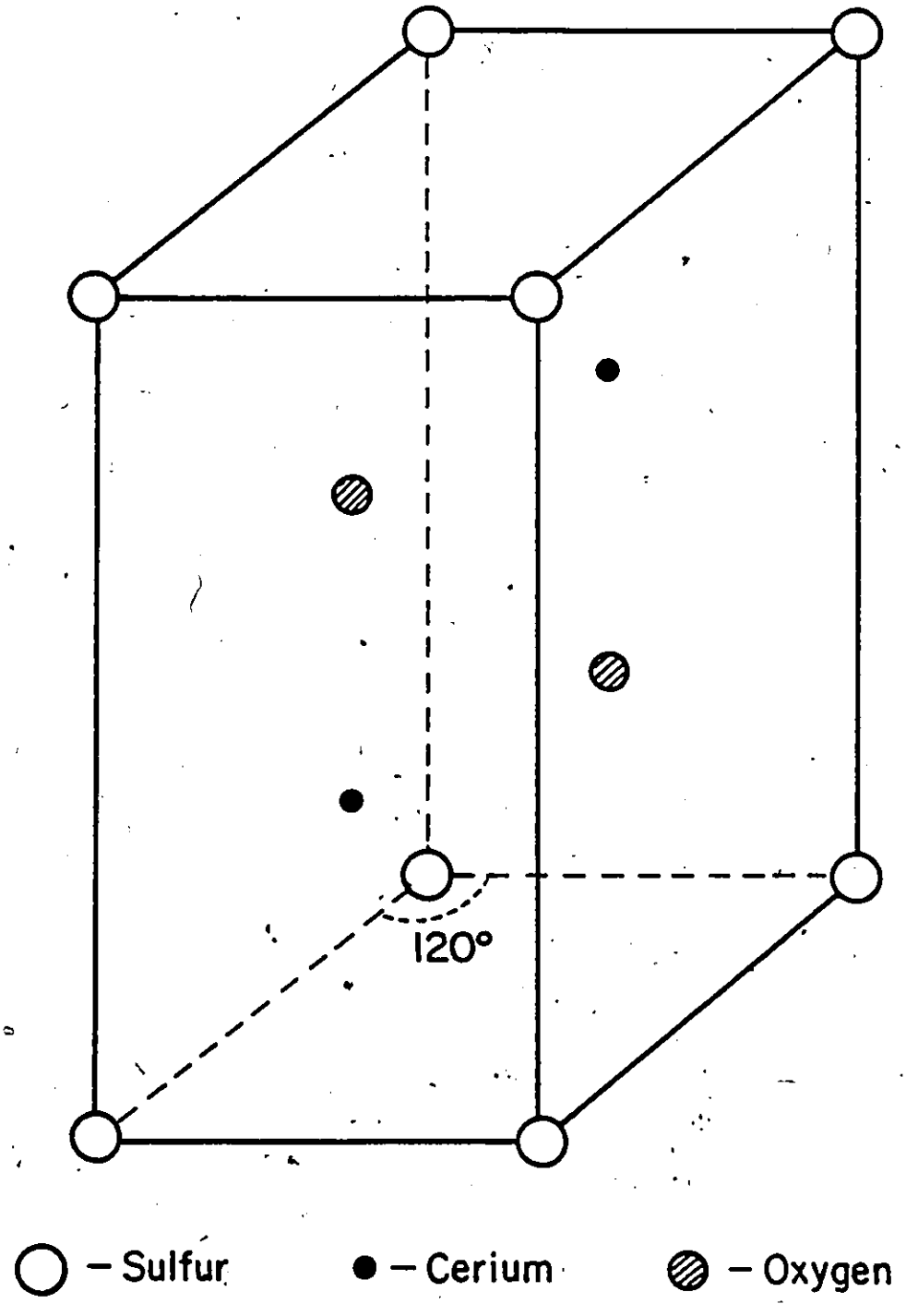
120°
– Sulfur
– Cerium
– Oxygen

TABLE 2.5

THE STANDARD ENTHALPY OF FORMATION AT 298K, ΔH°_{298}, AND THE STANDARD FREE ENERGY OF FORMATION AT 1100K OF RARE EARTH OXYSULFIDES*

Compound	ΔH°_{298}(cal /mole)		ΔG°_{f}(1100)(cal /mole)+
	Gschneidner et al. (3)	Soshchin (55)	Gschreidner et al. (3)
La_2O_2S	-412000	-420000	-337000
Ce_2O_2S	-415000	-433000	-339000
Pr_2O_2S	-416000		-340000
Nd_2O_2S	-416000		-341000
Pm_2O_2S	-417000		-342000
Sm_2O_2S	-419000		-343000
Eu_2O_2S	-379000		-299000
Gd_2O_2S	-420000		-346000
Tb_2O_2S	-422000		-347000
Dy_2O_2S	-423000		-347000
Ho_2O_2S	-424000		-348000
Er_2O_2S	-424000		-348000
Tm_2O_2S	-425000		-348000

TABLE 2.5 (contd.)

Compound	ΔH°_{298}(cal /mole)		ΔG°_{f}(1100)(cal /mole)+
	Gschneidner et al. (3)	Soshchin (55)	Gschreidner et al. (3)
Yb_2O_2S	-403000		-331000
Lu_2O_2S	-426000		-349000
Y_2O_2S	-430000	-439000	-354000

* All the values are estimated

\+ The error limits are estimated at $\pm$ 15000 cals/mole

TABLE 2.6

STANDARD FREE ENERGIES OF FORMATION OF SOME RARE EARTH OXYSULFIDES

Reaction	Temp. Range (K)	ΔG_f^o = A + BT (cal /mole.K) A (cal /mole.K)	B (cal /mole)	Error in ΔG_f^o (cal /mole.K)	Reference
$2Ce(\delta) + O_2(g) + \frac{1}{2}S_2(g) = Ce_2O_2S(s)$	999 - 1071	-415000	69.4	±15000	(3)*
$2Ce(\ell) + O_2(g) + \frac{1}{2}S2(g) = Ce_2O_2S(s)$	1071 - 2000	-410730	65.0	±15000	(3)*
$2Ce(\ell) + O_2(g) + \frac{1}{2}S_2(g) = Ce_2O_2S(s)$	1071 - 1750	-423210	79.5	±4000	(38)
$2La(\ell) + O_2(g) + \frac{1}{2}S_2(g) = La_2O_2S(s)$	1193 - 2000	-407700	65.0	±15000	(3)*
$2Gd(\alpha) + O_2(g) + \frac{1}{2}S_2(g) = Gd_2O_2S(s)$	298 - 1533	-420000	67.0	±18000	(3)*
$2Y(\alpha) + O_2(g) + \frac{1}{2}S_2(g) = Y_2O_2S(s)$	298 - 1752	-429000	67.4	±20000	(3)*

* Estimated

where U is crystal lattice energy. Their estimated values are included in Table 2.5.

Only one work dealing with the determination of the standard free energy of formation of rare earth oxysulfides has been reported. This work has been done by Fruehan (38) for Ce_2O_2S. In this study, the reaction:

$$2CeO_2 + 4CO + SO_2 = Ce_2O_2S + 4CO_2 \qquad (2.1)$$

was studied by heating a sample of CeO_2 in an atmosphere containing a mixture of CO, CO_2 and SO_2. The formation of Ce_2O_2S was detected by analysing the sample after the experiment. The SO_2 content of the gas mixture was bracketed within 8% in order to obtain the composition of gas mixture in equilibrium with CeO_x and Ce_2O_2S. It was pointed out by the author that even though under the experimental conditions equilibrium exists between CeO_x and Ce_2O_2S, and not between CeO_2 and Ce_2O_2S, results can be treated to yield the equilibrium constant for the Reaction 2.1:

$$K_{2.1} = (P_{CO_2}/P_{CO})^4 \cdot (1/P_{SO_2}) \qquad (2.2)$$

From the values of $K_{2.1}$, the standard free energy of formation of Ce_2O_2S can be obtained using the known values of ΔG_f^o (CeO_2).

It is not clear from this work whether equilibrium in the gas phase was attained. Also, an 8% error in bracketing the SO_2 content in the ingoing gases could cause a significant error in the equilibrium gas composition. The authers have estimated the error in the standard free

energy change for Reaction 2.1 to be ± 1.0 kcal . The value of ΔG_f° of Ce_2O_2S determined by these authors is about 12000 cals less negative than that estimated by Gschneidner et al. (3).

Some thermodynamic data on oxysulfides have been reported recently at low temperatures (61, 62). However, the temperature range is too small to yield ΔS_{298}°.

2.3.2 Rare Earth Oxysulfates ($RE_2O_2SO_4$)

All rare earth elements, except cerium, form oxysulfates with a general formula $RE_2O_2SO_4$. The oxysulfates of all rare earth elements are isostructural (56), each having a body centered orthorhombic structure with two formula units per unit cell and a I_{222} space group (57). Figure 2.11 shows the unit cell of the oxysulfate of lanthanum and is taken from Ref. 57. This structure can also be described as being made up of alternate layers of $(La_2O_2)^{2+}$ and SO_4^{2-} groups arranged perpendicular to the C axis. The relative openness of this structure could be the main reason for the unit cell volume of oxysulfates not being affected by the lanthanide contraction.

Thermodynamic properties of the oxysulfates have not been studied at all. Only one work (58), which at best is semiquantitative, has been reported in the literature. In this work, Grezik et al. (58) studied the reaction:

$$2La_2O_3(s) + 3SO_2(g) = 2La_2O_2SO_4(s) + \frac{1}{2}S_2(g). \qquad (2.3)$$

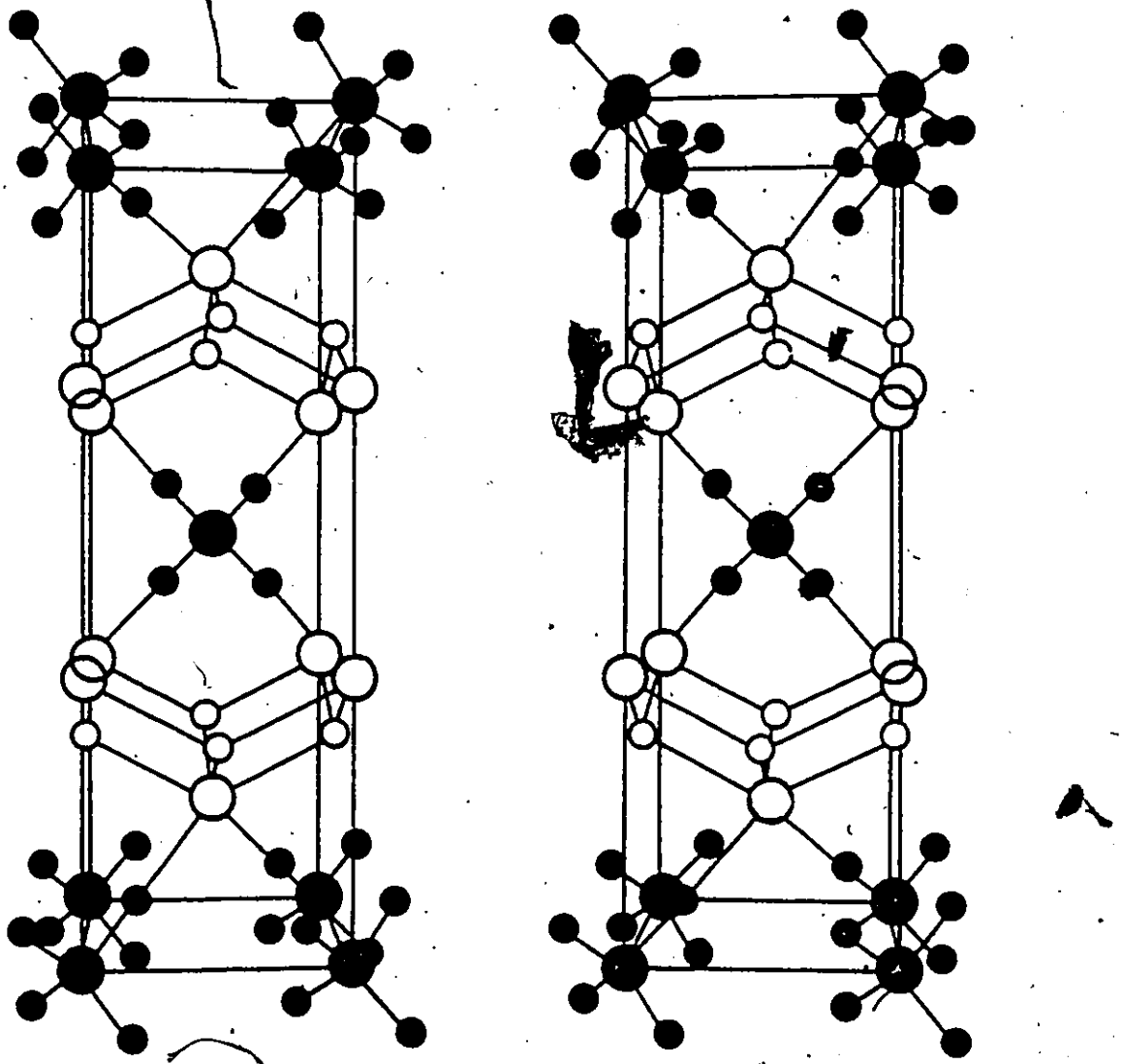

Fig. 2.11 Body centered orthorhombic unit cell of $La_2O_2SO_4$ (Ref.57).

Sulfur deposited in the cold parts of the reaction tube was determined by combustion to SO_2. The rate of sulfur deposition was taken as a measure of the reaction rate. An apparent equilibrium constant was then evaluated for each rate of SO_2 absorbtion. A plot of apparent equilibrium constant against the rate of SO_2 absorbtion, extrapolated to zero absorbtion rate, yielded the equilibrium constant. The P_{S_2} in all these determinations was calculated from the amount of sulfur deposition. It was found that this method worked only below 1173K.

Significant errors could be introduced due to:

1. Difficulties in measuring all the sulfur deposited on the cold parts of the reaction tube.
2. Some of the S_2 vapour may go uncondensed and thus could go unaccounted.
3. Gaseous species other than SO_2 and S_2 may form. This is the reason why this method fails above 1173K.
4. The temperature of the sample could significantly change with the flow-rate of SO_2 even though the controller is maintained at the same setting.
5. Kinetic factors could also play a major role in the temperature range investigated.

Because of the approximate nature of this determination the values of ΔG^o_f ($La_2O_2SO_4$) are not expected to be very reliable. From these determinations, the ΔH^o_{298} and S^o_{298} for $La_2O_2SO_4$ were found to be

-539000 cal /mole and -104 cal /mole.K, respectively. The values of the standard free energies at different temperatures can be used to obtain

$$\Delta G_f^o(La_2O_2SO_4) = -550000 + 88.7T \text{ (cal/mole)} \quad (2.4)$$

in the temperature range 973-1173K.

Recently, low temperature calorimetric data have become available for the oxysulfates of some rare earths (63). However, the temperature range investigated is too small to yield S_{298}^o values.

2.3.3 Rare Earth Sulfates ($RE_2(SO_4)_3$)

Rare earth elements form sulfates which are stable up to fairly high temperatures. Available thermodynamic data at 298K was reviewed by Montgomery (43) in 1959. Krestov (59) has also listed ΔH_{298}^o and S_{298}^o of the rare earth sulfates. However, the source of the data of the latter author is not known. Recently, values of the thermodynamic parameters of $Ce_2(SO_4)_3$ and $Nd_2(SO_4)_3$ have become available (60) at high temperatures.

2.3.4 Oxidation of Rare Earth Oxysulfides to Oxysulfates

Rare earth oxysulfides are known to oxidize to their respective oxysulfates, when heated in air, in a single step. Eick (64) observed that Sm_2O_2S oxidizes to $Sm_2O_2SO_4$ in a single step when heated in air. Haynes and Brown (65) studied the oxidation of La_2O_2S, Gd_2O_2S, Y_2O_2S and Lu_2O_2S in air using thermogravimetric techniques. They also observed

that an oxysulfide oxidized, in a single step, to oxysulfate which subsequently decomposed to oxide. Hale (66) reported results similar to those of the above authors for neodymium oxysulfide. Ozawa (67) studied the oxidation of Y_2O_2S in air at elevated temperatures using thermogravimetric techniques and came to the conclusion that even though the oxidation of the oxysulfide to oxysulfate occurred in a single step there was simultaneous decomposition of the oxysulfate to the oxide. The two steps were found to overlap, thus preventing the preparation and isolation of pure $Y_2O_2SO_4$.

A more complete study on oxidation of the rare earth oxysulfides has been recently reported by Leskela and Niinisto (68). These authors confirmed the observations that the rare earth oxysulfides oxidize to the oxysulfates in a single step, as reported by the previous workers. In addition, these authors reported that the stability range of rare earth oxysulfates in air decreases as the atomic number of the constituent rare earth increases. Their results are summarized in Fig. 2.12.

2.3.5 Decomposition of the Rare Earth Sulfates ($RE_2(SO_4)_3$)

All rare earth sulfates, except that of cerium, decompose to their respective oxysulfates when heated in air. The oxysulfates decompose to the respective oxides on further heating at higher temperatures (65,67,69). The decomposition reactions of the rare earth sulfates and oxysulfates can be written as:

$$RE_2(SO_4)_3(s) = RE_2O_2SO_4(s) + 2\ SO_3(g) \qquad (2.5)$$

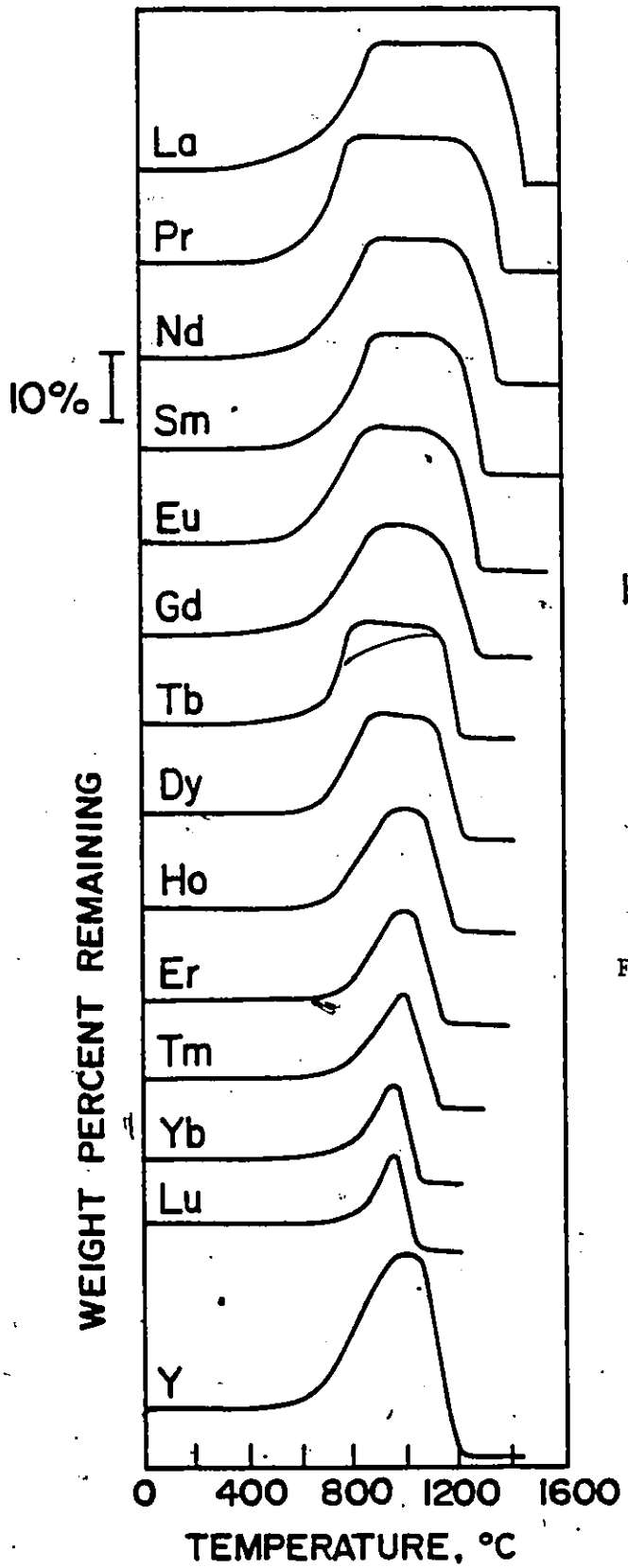

Heating rate = 10°C/min

Fig. 2.12 Weight changes on heating the oxysulfides of rare earths in air (Ref. 68).

and $RE_2O_2SO_4(s) = RE_2O_3(s) + SO_3(g)$ (2.6)

respectively.

The thermodynamics of Reaction (2.5) were studied by Grunzweig (70) in 1913 using static methods, whereby the pressure of gases above the decomposing sulfate was measured. The results are summarized in Table 2.7.

2.3.6 Phase Stability Diagrams

For a three component system, such as the rare earth-oxygen-sulfur system, the stability of a phase depends upon the temperature and the partial pressures of oxygen and sulfur. A plot of the partial pressure of sulfur against the partial pressure of oxygen at a constant temperature helps a great deal in visualizing the equilibria between different phases. This kind of plots are referred to as "Phase Stability Diagrams" (PSD) in the present work. PSD are known as the Kellogg Diagrams in sulfation equilibria and the Inclusion Precipitation Diagrams in steelmaking.

The phase stability diagrams for the cerium-sulfur-oxygen system were constructed by Vahed and Kay (71) at steelmaking temperatures. Ghosh et al. (72) constructed the PSD for the same system at 1273K. The latter diagram is more relevant to the present discussion and is reproduced in Fig. 2.13. This diagram, however, is incomplete since the nonstoichiometry of CeO_2 and the formation of $Ce_2(SO_4)_3$ are not considered in its construction.

TABLE 2.7

STANDARD FREE ENERGY CHANGE FOR DECOMPOSITION OF RARE EARTH SULFATES (70)

Reaction	Temp. Range (K)	ΔG_f^o = A + BT (cal /mole.K) A (cal /mole)	B (cal /mole. K)	Error in ΔG_f^o (cal /mole.K)
$\frac{1}{2}La_2(SO_4)_3(s) = \frac{1}{2}La_2O_2SO_4(s) + SO_3(g)$	1000 - 1300	60480	-38.82	±500
$\frac{1}{3}Ce_2(SO_4)_3(s) = \frac{2}{3}CeO_2(s) + SO_2(g) + \frac{1}{3}O_2(g)$	900 - 1200	63000	-50.97	±500
$\frac{1}{2}Pr_2(SO_4)_3(s) = \frac{1}{2}Pr_2O_2SO_4(s) + SO_3(g)$	1000 - 1300	56600	-37.99	±500
$\frac{1}{2}Nd_2(SO_4)_3(s) = \frac{1}{2}Nd_2O_2SO_4(s) + SO_3(g)$	1000 - 1300	56160	-38.03	±500
$\frac{1}{2}Sm_2(SO_4)(s) = \frac{1}{2}Sm_2O_2SO_4(s) + SO_3(g)$	1000 - 1300	56190	-38.82	±500
$\frac{1}{2}Er_2(SO_4)_3(s) = \frac{1}{2}Er_2O_2SO_4(s) + SO_3(g)$	1000 - 1300	57810	-38.56	±500
$\frac{1}{2}Yb_2(SO_4)_3(s) = \frac{1}{2}Yb_2O_2SO_4(s) + SO_3(g)$	1000 - 1300	57150	-37.48	±500
$\frac{1}{2}Lu_2(SO_4)_3(s) = \frac{1}{2}Lu_2O_2SO_4(s) + SO_3(g)$	1000 - 1300	57840	-37.71	±500
$\frac{1}{2}Y_2(SO_4)_3(s) = \frac{1}{2}Y_2O_2SO_4(s) + SO_3(g)$	1000 - 1300	60070	-39.25	±500

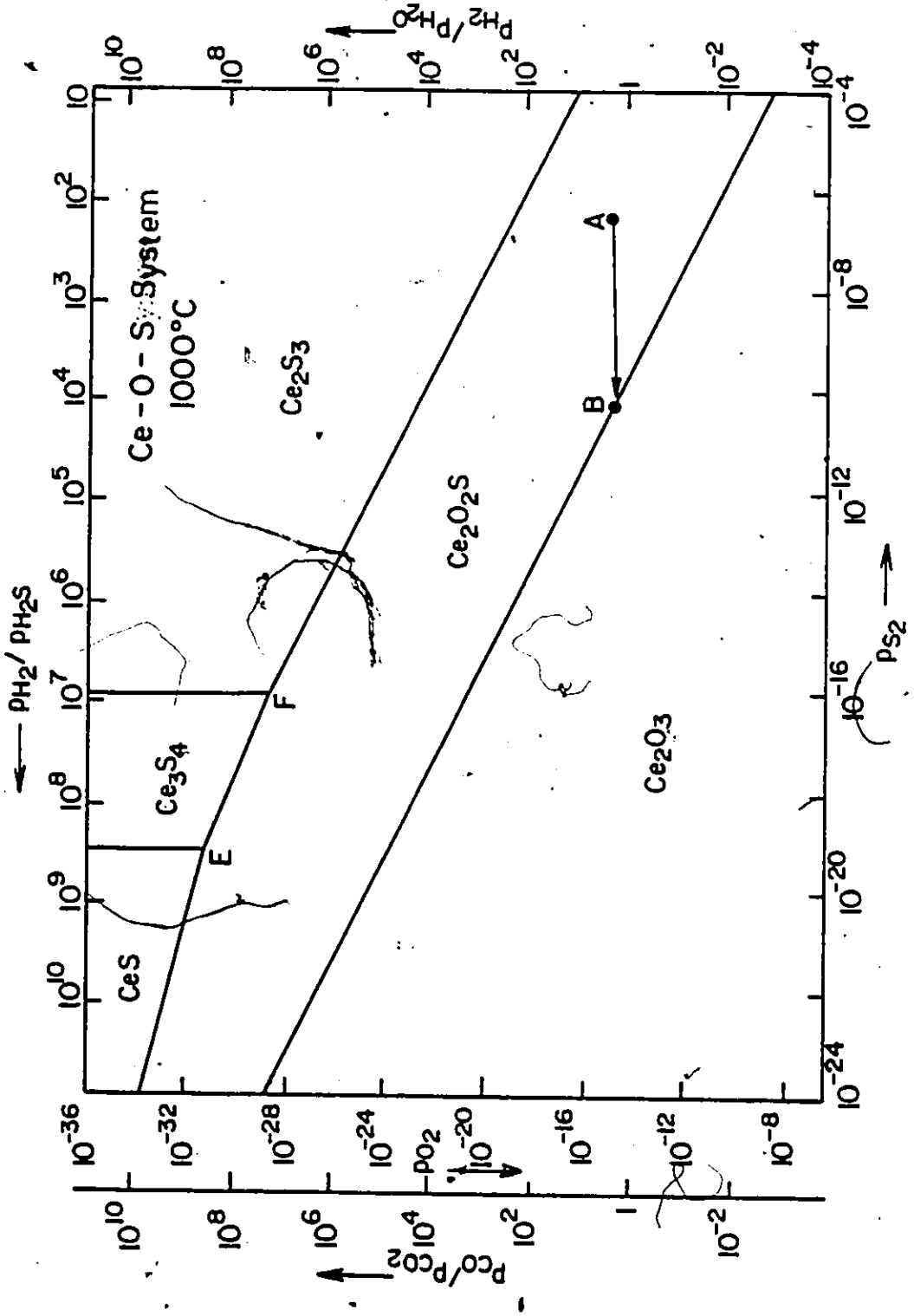

Fig. 2.13 Phase stability diagram of the Ce-O-S system at 1000 C in air.

CHAPTER III

DEVELOPMENT OF ELECTROCHEMICAL TECHNIQUES USING SOLID ELECTROLYTES TO STUDY THE THERMODYNAMICS OF RE-O-S SYSTEMS AT HIGH TEMPERATURES

The research on the development of solid electrolytes and their use in thermodynamic studies at high temperatures received a great impetus due to the poineering work of Kiukkola and Wagner (5, 6). In the last two decades, a tremendous amount of research effort has been devoted to the development of new solid electrolytes and improving properties of the existing ones. The work on development, characterization and use of solid electrolytes have been extensively discussed in the excellent reviews that have appeared in past two decades (73-78). In the present chapter, highlights of solid electrolytes, oxygen concentration cells and their application to the study of metal-oxygen-sulfur systems are presented.

3.1 Solid Electrolytes: Electrical Conductivity, Transference Number and Electrolytic Domain

A solid electrolyte is a material which conducts, predominantly in the ionic mode, over a wide range of temperature. α-Ag_2S, CaF_2, calcia stabilized zirconia (CSZ), and the β-aluminas are some common examples of solid electrolytes. An ionic solid has both electronic and

ionic defects, each of which migrates under the influence of an electrical potential. The conductivity due to a defect species i, denoted by σ_i, can be expressed as:

$$\sigma_i = C_i \, q_i^2 \, B_i \tag{3.1}$$

where C_i is the concentration of the species i in particles/cm^3;

q_i is the electrical charge of the species i in coulombs/particle; and

B_i is the absolute mobility of the species i in particle-cm^2/sec.J.

The transference number, t_i, of a species i is defined as

$$t_i = \frac{\sigma_i}{\sum_i \sigma_i} \tag{3.2}$$

The ionic transference number can thus be written as:

$$t_{ion} = \sum_{ion} \sigma_i / \sum_i \sigma_i \tag{3.3}$$

where $\sum_i \sigma_i$ is total conductivity

and $\sum_{ion} \sigma_i$ is total ionic conductivity.

For an ionic solid to act as a solid electrolyte, t_{ion} should be as close to 1 as possible, a practical criteria being $t_{ion} \geq 0.99$.

Since the mobility of electronic defects is 10^2 - 10^4 times larger than the mobility of ionic defects, from Eqn. 3.1, the concentration of ionic defects should be large compared to the concentration of electronic defects in order that $t_{ion} \geq 0.99$.

Some solid electrolytes, such as α-AgI, have a high concentration of ionic defects whereas others, such as CSZ, need to be doped with aliovalent ions to increase the concentration of ionic defects.

In an ionic solid MX, the concentration of defects depends on both temperature and the partial pressure, P_X , of the anionic species. A similar behaviour is observed for solid electrolytes. However, in this case, there is a large range of P_X in which the concentration of ionic defects is substantially constant. This is schematically illustrated in Fig. 3.1, which was drawn for yttria doped thoria by Rapp and Shores (74). Fig. 3.2 shows the variation of conductivity with the partial pressure of the anionic species, in this case oxygen. This Figure is also taken from the work of the above authors. From the definition of ionic transference number, it follows that for a solid electrolyte, t_{ion} remains constant at a value close to 1.0 in a certain range of partial pressures of the anionic species. This zone, where $t_{ion} \simeq 1.0$, is called the electrolytic domain of the solid electrolyte. Fig. 3.3 schematically illustrates the electrolytic domain of a solid electrolyte.

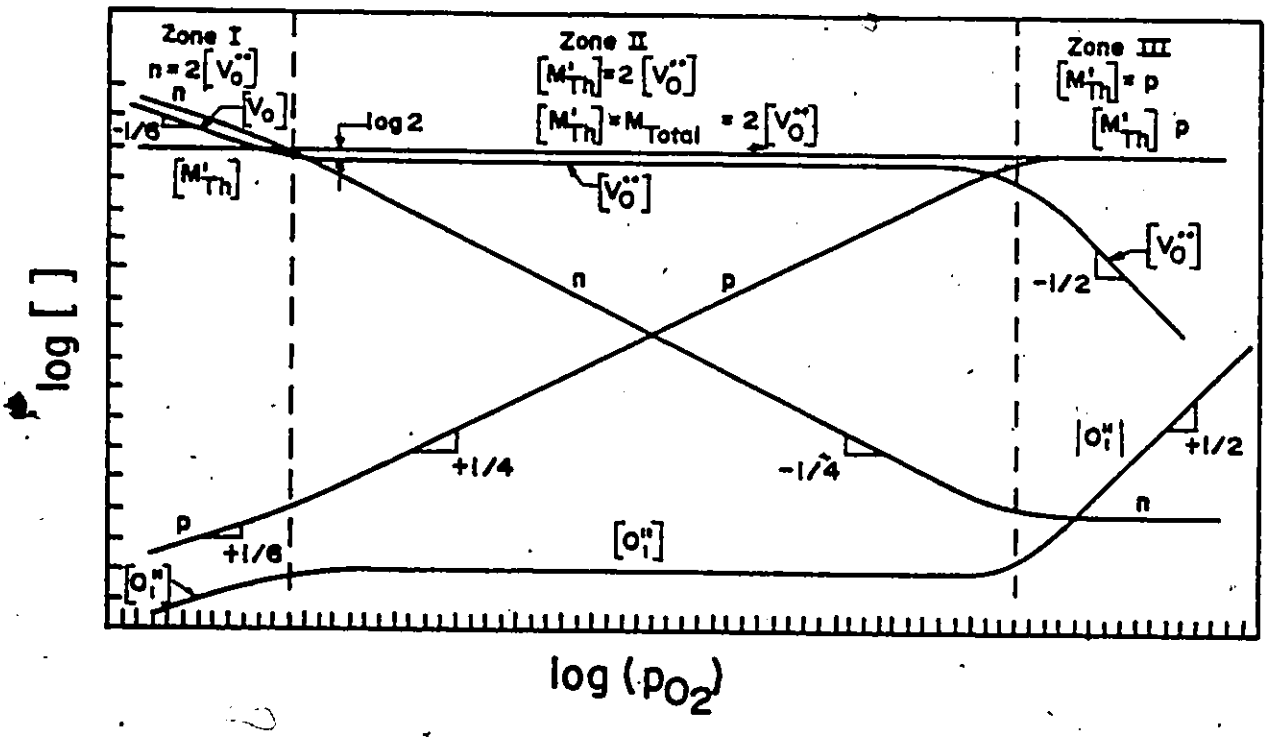

Fig. 3.1 Schematic representation of the change in defect concentration with the partial pressure of oxygen for yttria doped thoria(YDT). Kroger-Vink notations are used to represent the defects(Ref. 74).

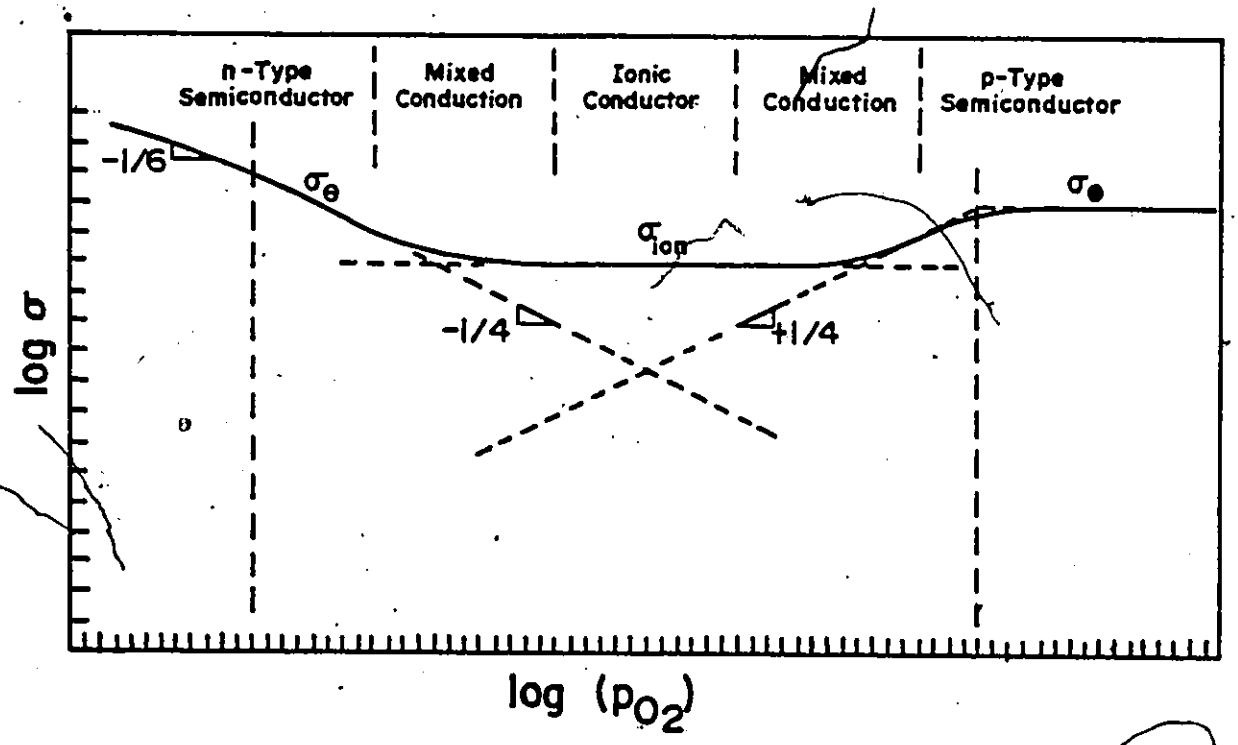

Fig. 3.2 Schematic representation of the change in electrical conductivity with partial pressure of oxygen for an oxygen-conducting solid electrolyte (Ref. 74).

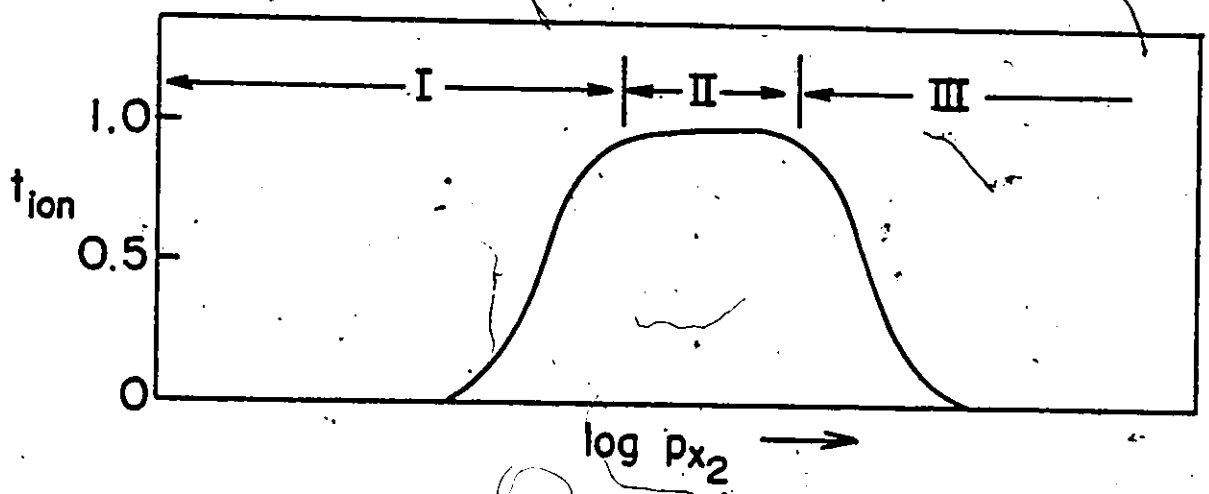

Fig. 3.3 Schematic representation of ionic transference number for an MX_2 compound (Ref. 74).
Zone I : n-type conduction zone
Zone II : ionic conduction zone
Zone III : p-type conduction zone

3.2 Calcia Stabilized Zirconia Solid Electrolytes

Pure ZrO_2 has a monoclinic structure below 1000°C and a tetragonal structure above this temperature. However, when some oxides, such as CaO, Y_2O_3 and MgO are added to ZrO_2, a cubic solid solution is formed. This has the fluorite structure and oxygen ion vacancies as predominant ionic defects. The composition range of the fluorite solid solution is 12-20 mole % CaO in a ZrO_2(CaO) solid solution at elevated temperatures ($\sim$1000°c)(79). The ionic conductivity of csz is a function of CaO concentration with a maximum around 15 mole % CaO, as shown in the Fig. 3.4 (80). The electrolytic domain of calcia stabilized zirconia decreases as the temperature increases. This is shown in Fig. 3.5 which has been taken from Ref. 81.

3.3 Oxygen Concentration Cells

The fact that CSZ can conduct ionically through oxygen ion vacancies at elevated temperatures can be used to form electrochemical cells using electrodes reversible to oxygen ions. Thus, an electrolyte conducting through oxygen ion vacancies and two electrodes reversible to oxygen ions form an oxygen concentration cell. An oxygen concentration cell can be represented as

$$\mu_{O_2}^{I} \mid CSZ \mid \mu_{O_2}^{II} \qquad \mu_{O_2}^{I} < \mu_{O_2}^{II}$$

where $\mu_{O_2}^{I}$ and $\mu_{O_2}^{II}$ are the oxygen potentials at the two electrodes. Based

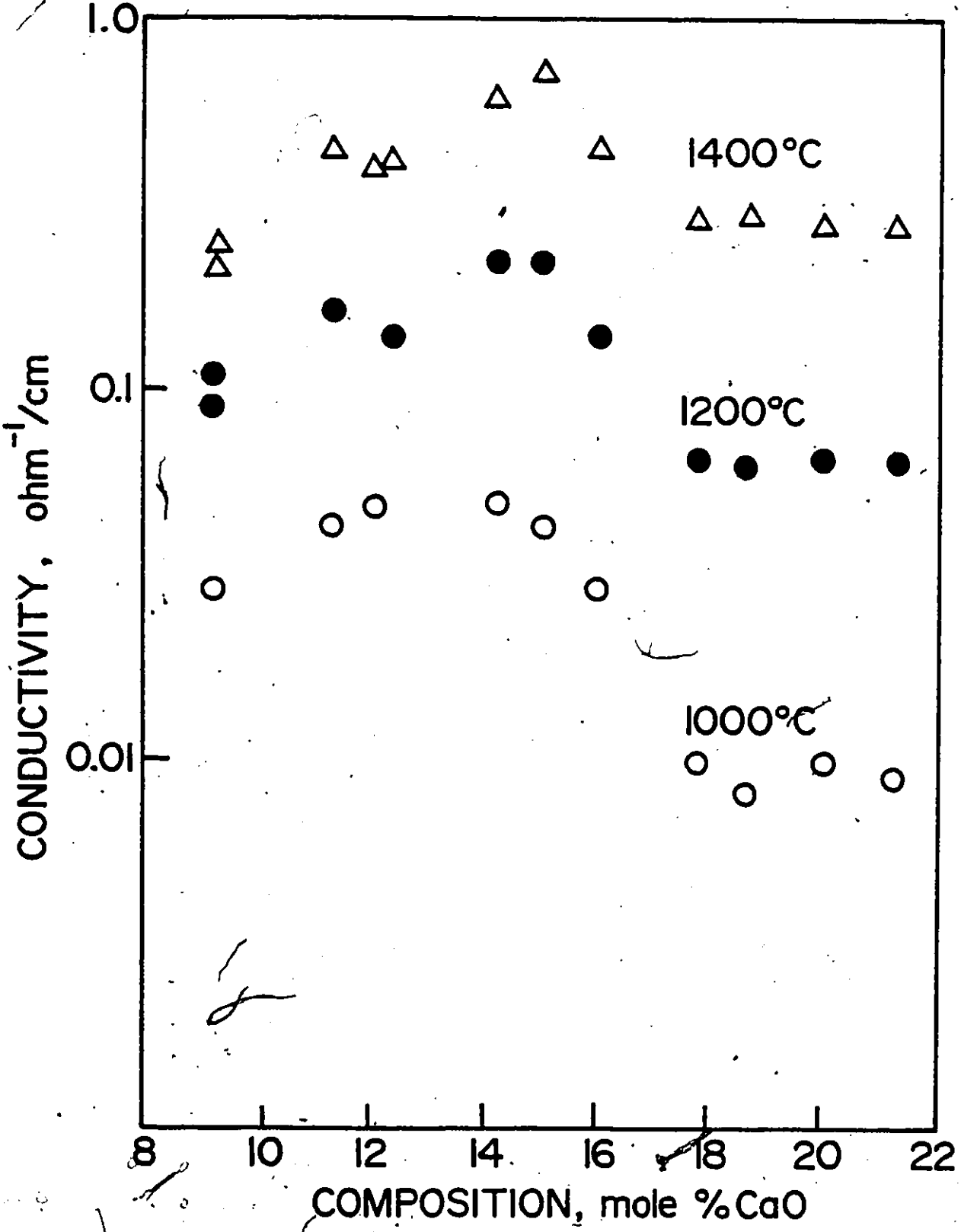

Fig. 3.4 Change in the ionic conductivity of calcia stabilized zirconia with CaO content (Ref. 80).

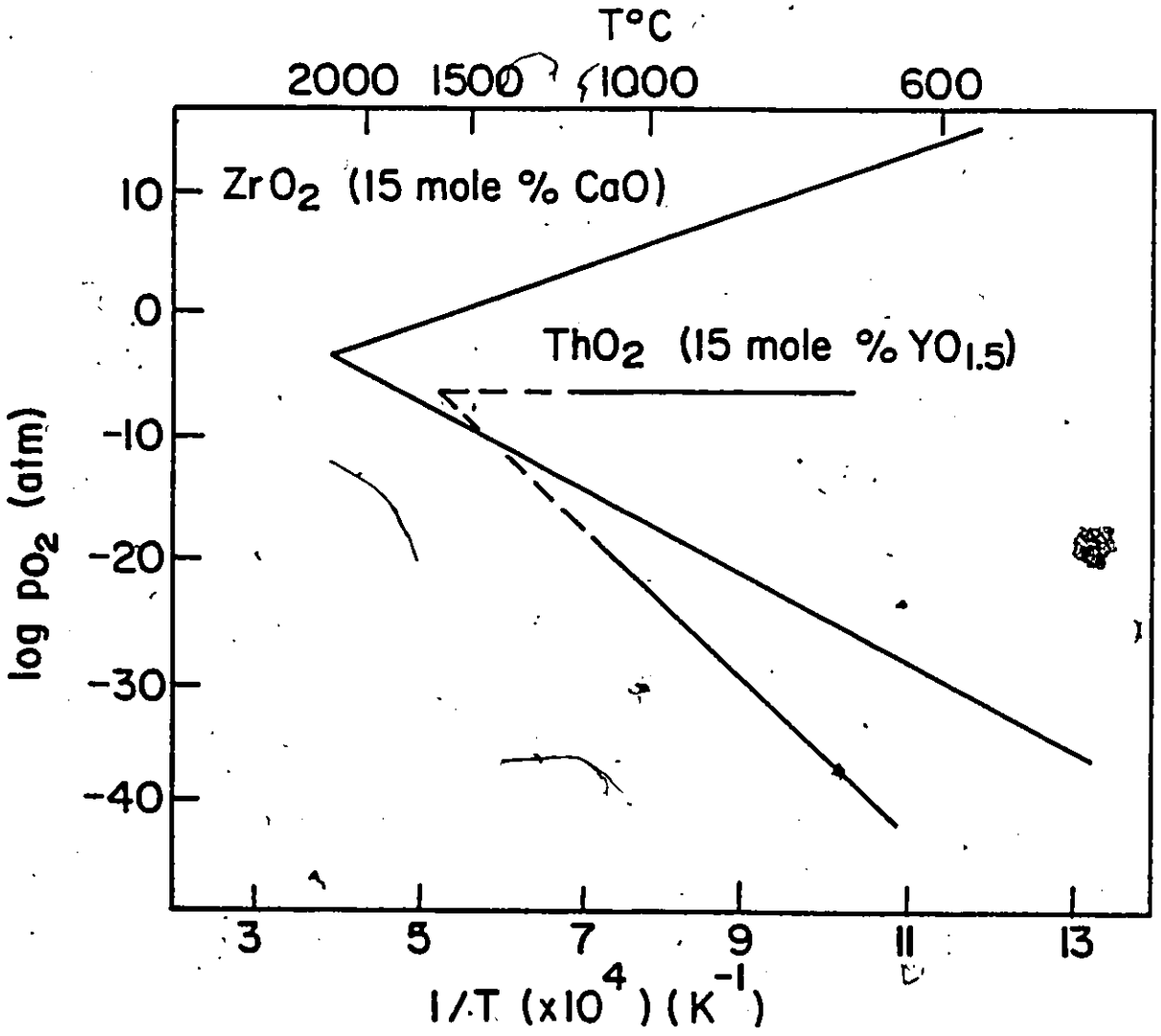

Fig. 3.5 Variation of the electrolytic domain of ZrO_2(15 mole % CaO) and ThO_2(15 mole % $YO_{1.5}$) with oxygen partial pressure and temperature (Ref. 81).

on Wagner's analysis (82), the emf, E, of the above cell can be expressed in terms of the oxygen potentials $\mu_{O_2}^{I}$ and $\mu_{O_2}^{II}$ at the two electrodes and is given by:

$$E = \frac{1}{4F} \int_{\mu_{O_2}^{I}}^{\mu_{O_2}^{II}} t_{O^{2-}} \, d\mu_{O_2} \qquad (F = \text{Faraday's constant}) \qquad (3.4)$$

This expression reduces to:

$$E = \frac{RT}{4F} \ln (P_{O_2}^{II}/P_{O_2}^{I}) \qquad (3.5)$$

when $t_{O^{2-}} \simeq 1.0$ and the activities of oxygen are replaced by its partial pressures.

3.4 Necessary Conditions for Successful Operation of an Oxygen Concentration Cell

The conditions necessary for successful operation of an electrochemical cell using solid electrolytes in general, and an oxygen concentration cell in particular, have been extensively discussed (74, 83-85). These conditions can be summarized as follows:

1. Components at the electrodes should co-exist.
2. The electrolyte should not react with the electrodes.
3. Oxygen partial pressures at the two electrodes should be within the electrolytic domain of the electrolyte at all operating temperatures.
4. It is most desirable to have the two electrode compartments isolated from each other.

5. The temperature gradient along the cell should be minimal.
6. The electrodes should not react with the lead wires.
7. The two electrodes should be completely reversible to oxygen ions.
8. Diffusional transport of oxygen through the electrolyte should be minimized by having oxygen partial pressures at the two electrodes as close to each other as possible.
9. The effect of induction should be minimized by shielding the cell with a grounded metal sheath.
10. Local equilibrium should prevail at the two electrodes.
11. The oxygen potential of the atmosphere around an electrode should be close to the oxygen potential established by the electrode.
12. The electrolyte should be homogeneous, nonporous and mechanically strong.

3.5 Application of Oxygen Concentration Cells to Study Equilibria in Metal - Oxygen - Sulfur Systems

A typical oxygen concentration cell using metal/metal oxide electrodes can be represented by:

Pt | A,AO | CSZ | B,BO | Pt

I II

where A and B are two metals and AO and BO their respective oxides. Consider one of the electrodes, say electrode I, containing metal A and its oxide AO. Since A-O, is a two component system in presence two condensed phases at constant temperature, the system is invariant.

However, if sulfur is also present as a component then an additional degree of freedom is introduced. Thus, for a metal-oxygen-sulfur system, with two condensed phases and a gas phase, there are two degrees of freedom. Therefore, this system will be invariant at a constant temperature only if an additional constraint is introduced.

Larson and Elliott (7) used the principle outlined above to determine the standard free energy of formation of MnS, MoS_2, NbS_2, PtS, TaS_2 and ZnS. Their cell could be written as:

$$Pt \left| \begin{matrix} MO(s),\ MS(s) \\ P_{SO_2} = 1atm. \end{matrix} \right| CSZ \left| P_{O_2} = 1\ atm. \right| Pt \qquad (3.7)$$

where MO and MS are the oxide and sulfide, respectively, of a metal M. The additional constraint was introduced by fixing $P_{SO_2} = 1$ atm.

The anode and cathode reactions can be written as:

$$\frac{2}{3}MS(s) + 2\ O^{2-} = \frac{2}{3}\ MO(s) + \frac{2}{3}SO_2(g) + 4e$$

and $\quad 4e + O_2(1atm.) = 2\ O^{2-}$, respectively.

Flengas (86) has used the same principle to study the equilibrium betwen CoO and $CoSO_4$ at high temerpatures.

Skeaff and Espelund (92) used cells similar to those mentioned above to study oxide/sulfate equilibria in systems involving Mg, Mn, Fe, Ni, Cu and Zn and sulfate/sulfate equilibria in the system involving Fe.

3.6 Application of Oxygen Concentration Cells to Study Equilibria in RE-O-S Systems

The construction of oxygen concentration cells, that can be used to study equilibria in RE-O-S systems, can best be discussed in terms of phase stability diagrams similar to that shown for the La-O-S system in Fig. 3.6. The data used in drawing this diagram are taken from Mills (42) for sulfides; Gschneidner (3) for oxide and oxysulfide; Grunzweig (70) for the phase boundary between $La_2O_2SO_4$ and $La_2(SO_4)_3$; and Grizik (58) for $La_2O_2SO_4$. The values of the standard free energy of formation of SO_2 and SO_3 used in the above calculations are taken from Ref. 87. It should be noted that large errors associated with the thermodynamic data on all of the above compounds, except La_2O_3, may significantly alter the position of each line. The present positions of the phase boundaries is obtained by making their intersections consistent with the phase rule. Therefore, this diagram, at best, is only schematic. However, it clearly shows the important features and the complexity of RE-O-S systems.

As discussed in the previous section, an additional constraint needs to be imposed on a three component system having two condensed phases and a gas phase in order that the system be invariant at constant temperature. In the present work, the additional constraint is imposed by either fixing the sulfur partial pressure using Ag/Ag_2S and Cu/Cu_2S couples (cells of Type II, III and IV) or by introducing an additional condensed phase (Cell of Type I).

For the successful operation of cells using a sulfur potential

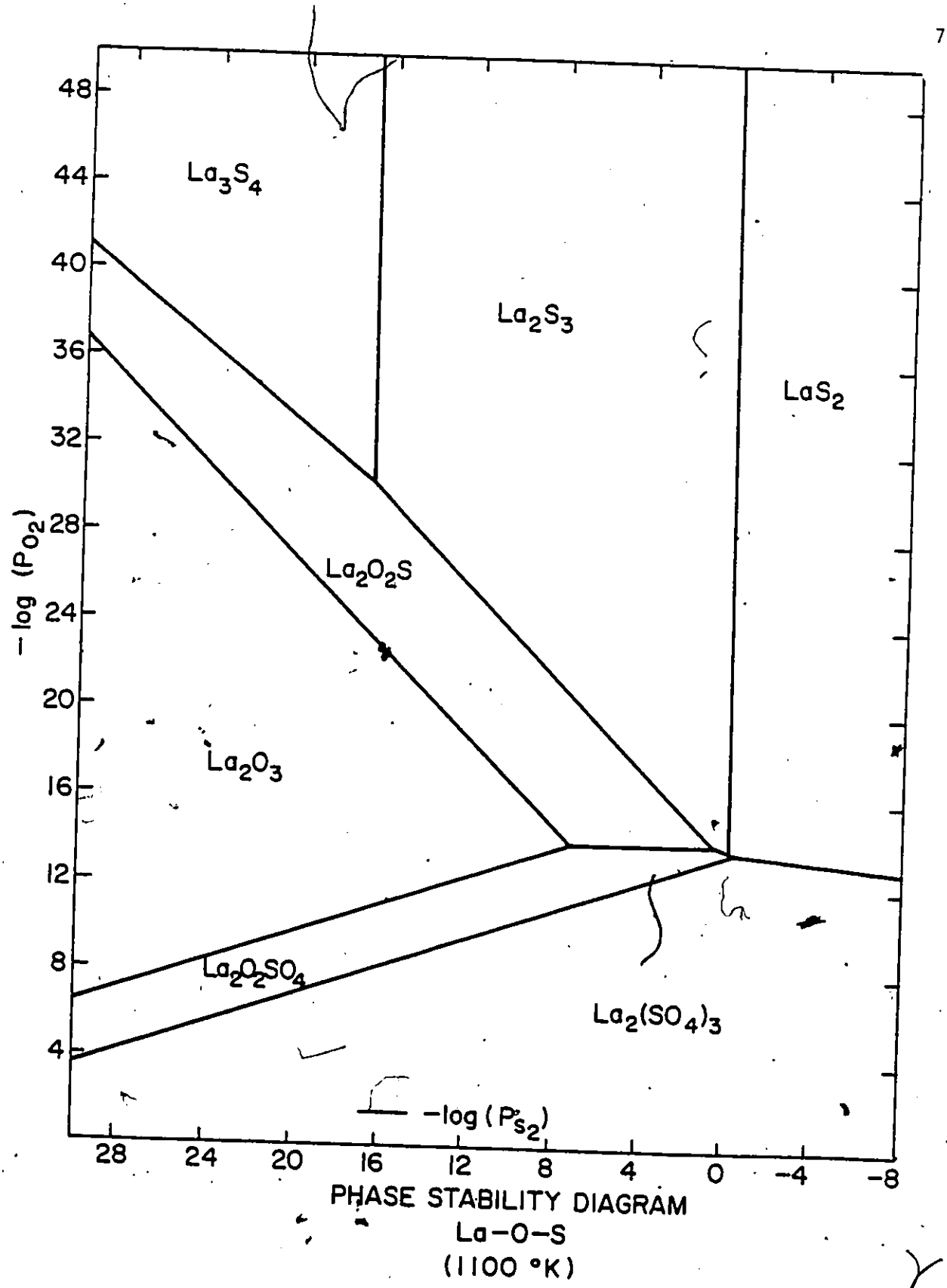

Fig. 3.6 Phase stability diagram of the La-O-S system constructed using available data from the literature. Positions of the phase boundaries are adjusted so as not to violate the phase rule.

fixing couple, one more condition is introduced in addition to those listed in Section 3.4. This condition is that the oxygen partial pressure established at the electrode using a metal/metal sulfide couple, should be several orders of magnitude lower than the oxygen partial pressures corresponding to a) the Ag/Ag_2O, and Ag_2S/Ag_2SO_4 equilibria for electrodes using the Ag/Ag_2S couple, and b) the Cu/Cu_2O equilibria for electrodes using the Cu/Cu_2S couple. This condition is very important and is further discussed later in this work.

CHAPTER IV

EXPERIMENTAL APPARATUS AND PROCEDURE

Following the notation of Section 1.5.2, the oxygen concentration cells studied during the course of this work can be represented as:

Type I Cells

$Pt|La_2O_2S(s), La_2O_2SO_4(s)|CSZ|$ Air | Pt (I.(a))
(in presence of La_2O_3)

$Pt|Pr_2O_2S(s), Pr_2O_2SO_4(s)|CSZ|$ Air | Pt (I.(b))
(in presence of Pr_2O_3)

$Pt|Nd_2O_2S(s), Nd_2O_2SO_4(s)|CSZ|$ Air | Pt (I.(c))
(in presence of Nd_2O_3)

$Pt|Sm_2O_2S(s), Sm_2O_2SO_4(s)|CSZ|$ Air | Pt (I.(d))
(in presence of Sm_2O_3(B))

$Pt|Eu_2O_2S(s), Eu_2O_2SO_4(s)|CSZ|$ Air | Pt (I.(e))
(in presence of Eu_2O_3(B))

$Pt|Gd_2O_2S(s), Gd_2O_2SO_4(s)|CSZ|$ Air | Pt (I.(f))

(in presence of Gd_2O_3(B))

$Pt|Tb_2O_2S(s), Tb_2O_2SO_4(s)|CSZ|$ Air | Pt (I.(g))

(in presence of Tb_2O_3)

$Pt|Dy_2O_2S(s), Dy_2O_2SO_4(s)|CSZ|$ Air | Pt (I.(h))

(in presence of Dy_2O_3)

Type II Cells

$Pt|La_2O_2S(s), La_2O_2SO_4(s)|CSZ|$ Air | Pt (II.(a))

($Ag(s)/Ag_2S(s)$)

$Pt|Nd_2O_2S(s), Nd_2O_2SO_4(s)|CSZ|$ Air | Pt (II.(b))

($Ag(s)/Ag_2S(s)$)

Type III Cells

$Pt|La_2O_3(s), La_2O_2SO_4(s), Cu(s), Cu_2S(s)|CSZ|$ Air | Pt (III.(a))

$Pt|Pr_2O_3(s), Pr_2O_2SO_4(s), Cu(s), Cu_2S(s)|CSZ|$ Air | Pt (III.(b))

$Pt|Nd_2O_3(s), Nd_2O_2SO_4(s), Cu(s), Cu_2S(s)|CSZ|$ Air | Pt (III.(c))

$Pt|Sm_2O_3(B), Sm_2O_2SO_4(s), Cu(s), Cu_2S(s)|CSZ|$ Air | Pt (III.(d))

$Pt|Eu_2O_3(B), Eu_2O_2SO_4(s), Cu(s), Cu_2S(s)|CSZ|$ Air | Pt (III.(e))

$Pt|Gd_2O_3(B), Gd_2O_2SO_4(s), Cu(s), Cu_2S(s)|CSZ|$ Air | Pt (III.(f))

Type IV Cells

$Pt|CeO_x(s), Ce_2O_2S(s), Ag(s), Ag_2S(s)|CSZ|$ Air | Pt (IV.(a))

$Pt|Y_2O_3(s), Y_2O_2S(s), Ag(s), Ag_2S(s)|CSZ|$ Air | Pt (IV.(b))

4.1 Materials

Starting materials along with their source and purity are listed in Table 4.1.

4.1.1 Preparation of Oxysulfates and Oxysulfides

Oxysulfates and oxysulfides of all rare earths, except those of lanthanum and cerium, were prepared from their respective oxides. The oxide was first dissolved in a solution containing 50 vol.% sulfuric acid. The solution was heated and more oxide was added until no more could go into solution. The solution was cooled whereupon the sulfate crystallized out and was removed. The remaining solution was then heated in an oven at around 573K to remove water, leaving behind

TABLE 4.1

MATERIALS AND THEIR PURITY

Material	Source	Purity (wt. %)
La_2O_3 (- 325 mesh)	Cerac Inc.	99.9
Pr_2O_3 (- 325 mesh)	Cerac Inc.	99.9
Nd_2O_3 (- 325 mesh)	Cerac Inc.	99.9
Sm_2O_3 (- 325 mesh)	Cerac Inc.	99.9
Eu_2O_3 (- 325 mesh)	Cerac Inc.	99.9
Gd_2O_3 (- 325 mesh)	Cerac Inc.	99.9
Tb_4O_7 (- 325 mesh)	Cerac Inc.	99.9
Dy_2O_3 (- 325 mesh)	Cerac Inc.	99.9
La_2O_2S (- 200 mesh)	Cerac Inc.	99.9
Ce_2O_2S (- 200 mesh)	Cerac Inc.	99.9
Y_2O_3 (- 325 mesh)	Cerac Inc.	99.9
$Cu_{1.8}S$ (- 200 mesh)	Cerac Inc.	99.9
Ag_2S (- 100 mesh)	Cerac Inc.	99.99
Cu (- 325 mesh)	Cerac Inc.	99.9
CeO_2 (- 325 mesh)	Cerac Inc.	99.9
Ce_2O_3 (- 325 mesh)	Cerac Inc.	99.9
Ho_2O_3 (- 325 mesh)	Cerac Inc.	99.9
Yb_2O_3 (- 325 mesh)	Cerac Inc.	99.9
Er_2O_3 (- 325 mesh)	Cerac Inc.	99.9

sulfate crystals. The sulfate thus obtained, normally, had some water of crystallization which was removed by heating at 870K in a muffle furnace to obtain anhydrous rare earth sulfate.

Rare earth oxysulfates were prepared by heating the respective rare earth sulfates in air at temperatures shown in Table 4.3. By this method, oxysulfates of rare earths up to holmium only could be prepared (cerium does not form an oxysulfate).

Rare earth oxysulfides were prepared by reducing anhydrous rare earth sulfates with unpurified hydrogen at 920-1020K. The rare earth oxysulfides thus obtained had very small crystallites which resulted in diffused intensity peaks in the X-ray diffraction patterns. Therefore, the crystallites were grown by heating the prepared oxysulfides at 900-950°C in argon for about 5 hours. After this treatment, all the oxysulfides gave sharp peaks when examined by X-ray diffraction.

4.2 Characterization of Materials

Oxysulfides and oxysulfates were characterized using X-ray diffraction and thermogravimetric analysis.

4.2.1 X-ray Diffraction Analysis

A Norelco X-ray diffractometer was employed to examine the powdered samples. Cu K_α radiation with a Ni filter was employed to analyse the samples. The X-ray tube was operated at 30kV and 16mA. The X-ray diffraction patterns of oxysulfides and oxysulfates were compared with those available in the literature (88). Diffraction patterns of

some compounds, such as $Pr_2O_2SO_4$ and $Dy_2O_2SO_4$, for which diffraction data are not available were analysed by comparing them with those of similar compounds of other rare earths.

4.2.2 Thermogravimetric Analysis

Thermogravimetric analysis was performed by heating oxysulfides and anhydrous sulfates in air and noting their respective weight changes. About 5 gms of each compound was placed in a Pt crucible and heated at 570-670 K to remove moisture and water of crystallization until a constant weight was attained. In the case of oxysulfides, the sample was heated at 1070-1220K in air for about 12 hrs. For the oxysulfides of the lighter lanthanides, there was a net weight change corresponding to a gain of 2 moles of oxygen per mole of oxysulfide. In contrast to this, oxysulfides of the heavier rare earths directly converted to the respective oxides with a net loss in weight, corresponding to the replacement of a sulfur atom with an oxygen atom in the oxysulfide. Thus, the oxidation of oxysulfides of lighter and heavier lanthanides can respectively be represented by:

$$RE_2O_2S(s) + 2O_2(g) = RE_2O_2SO_4(s) \qquad (4.1)$$

and

$$RE_2O_2S(s) + 3/2O_2(g) = RE_2O_3(s) + SO_2(g). \qquad (4.2)$$

Table 4.2 compares the weight changes accompanying the oxidation of the oxysulfides of light and heavy rare earths. It is clear from this Table that the conversion of an oxysulfide to oxysulfate is complete for rare earth elements up to dysprosium. For elements heavier than dysprosium, and yttrium, oxysulfides directly convert to oxides.

TABLE 4.2

THERMOGRAVIMETRIC ANALYSIS

REACTION: $RE_2O_2S(s) + 2O_2(g) \xrightarrow[\text{air}]{1070-1220K} RE_2O_2SO_4(s)$

Element	Weight Gain Theoretical (%)	Weight Gain Experimental (%)	Final Products (x-ray diffraction analysis)
La	18.72	18.65	oxysulfate
Pr	18.51	18.48	oxysulfate
Nd	18.16	18.08	oxysulfate
Sm	17.55	17.48	oxysulfate
Eu	17.40	17.31	oxysulfate
Gd	16.91	16.78	oxysulfate
Tb	16.76	16.66	oxysulfate
Dy	16.45	16.20	oxysulfate + oxide
Ho	16.25	-4.03	oxide (c)*
Er	16.06	-4.01	oxide (c)
Yb	15.61	-3.92	oxide (c)
Y	26.47	-6.64	oxide (c)

* c indicates the c-type rare earth sesquioxides.

In order to charactarize the oxysulfates and sulfates of the rare earths, the reaction given with Table 4.3 was used. In this case, a sample of anhydrous rare earth sulfate was heated at 900-950°C in air and the weight change in the sample was measured after cooling it to room temperature. For the sulfates of light rare earths, the weight changes closely corresponded to a loss of 2 moles of SO_2 and 1 mole of O_2 per mole of $RE_2(SO_4)_3$. The X-ray diffraction analysis confirmed the formation of oxysulfates. In contrast to this, when sulfates of the heavier rare earth elements were heated, the final product was either a mixture of oxysulfate and oxide, or only oxide. The results of this analysis are presented in Table 4.3. It is clear from these results that the conversion of a sulfate to oxysulfate is complete in the case of the lighter rare earths. The sulfates of heavier rare earths convert to oxysulfates which simultaneously decompose to oxides.

4.3 Characterization of the Solid Electrolyte

The solid electrolytes used in the present investigation consisted of 350mm long calcia stabilized zirconia (15 mole % CaO) tubes having a 7.4mm outer diameter and a flat closed end. The tubes were supplied by ZIRCOA. All tubes used in this investigation were He leak tested under a vacuum of 10^{-6} torr. The electrolytes were further characterized for ionic conduction using the electrochemical cell:

$$Pt|Ni,NiO|CSZ|Cu, Cu_2O|Pt.$$

The reversible emf of this cell compared very well with the estabilshed values given in the literature, as shown in Fig. 4.1.

TABLE 4.3

THERMOGRAVIMETRIC ANALYSIS

REACTION: $RE_2(SO_4)_3(s) \xrightarrow[air]{\Delta} RE_2O_2SO_4(s) + 2\ SO_2\uparrow + O_2\uparrow$

Element	Temperature Range (K)	Weight Loss Theoretical (%)	Weight Loss Experimental (%)	Final Products (by x-ray diffraction analysis)
La	1170-1220	28.28	28.25	oxysulfate
Pr	1170-1220	28.08	28.00	oxysulfate
Nd	1170-1220	27.76	27.70	oxysulfate
Sm	1070-1120	27.18	27.10	oxysulfate
Eu	1070-1120	27.03	26.97	oxysulfate
Gd	1070-1120	26.56	26.50	oxysulfate
Tb	1070-1120	26.41	27.60	oxysulfate + oxide (c)
Dy	1070-1120	26.10	27.21	oxysulfate + oxide (c)
Ho	1070-1120	25.90	(38.70)	oxide (c)
Er	1070-1120	25.70	(38.41)	oxide (c)
Yb	1070-1120	25.23	(37.74)	oxide (c)
Y	1070-1120	34.35	(51.42)	oxide (c)

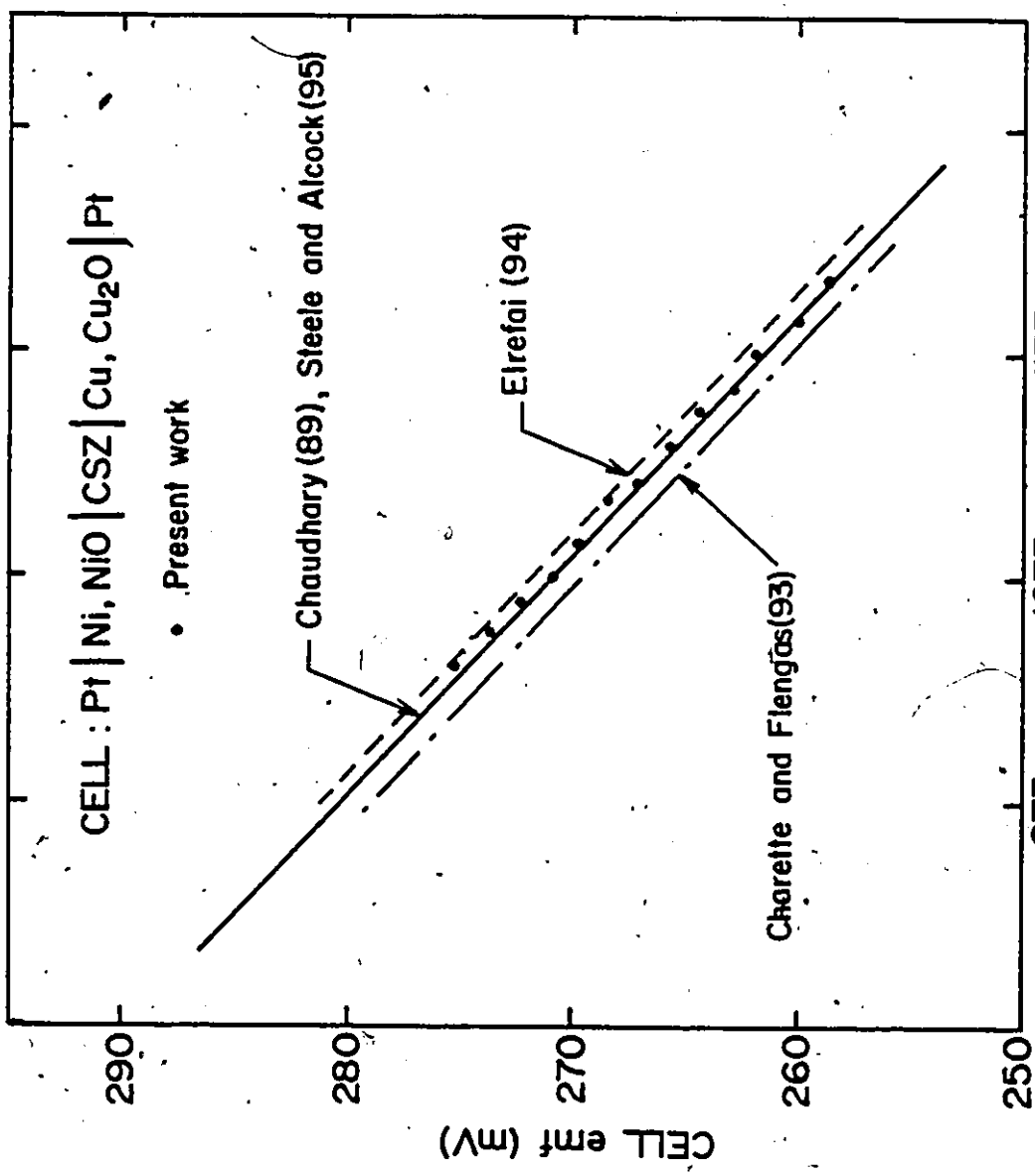

Fig. 4.1 Variation of emf with temperature for the cell:
Pt/NiO, Ni / CSZ / Cu_2O; Cu /Pt.

4.4 The Apparatus

The apparatus used in the present study had the following major components.

4.4.1 Furnace

Two tubular furnaces, one platinum-wound and the other Kanthal-wound, were used to heat the cell assembly in the present investigation. The lengths of both furnaces were 300mm and the internal diameters of the furnace tubes were about 75mm. The furnace assembly is schematically shown in Fig. 4.2. A furnace tube was protected from the inconel tube by an alumina tube placed between them. Inside the inconel tube, a working tube of recrystallized alumina was placed. The hot zone of each furnace was 27mm long. In order to find the radial temperature distribution in the working tube, a differential chromel-alumel thermocouple was used. One junction of the thermocouple was located at a point along the diameter of the working tube while the other was moved in a radial direction from the center of the working tube. The temperature emf was measured by the potentiometer described in the Section 4.7. It was found that the temperature of two diametrically opposite points, and also, the temperature at the center and the circumfrence of the working tube, did not differ by more than 0.5K. The temperature in the furnace was controlled by a Barber-Coleman (621A-24060-067) proportional controller within 2K, measured at the center of the working tube.

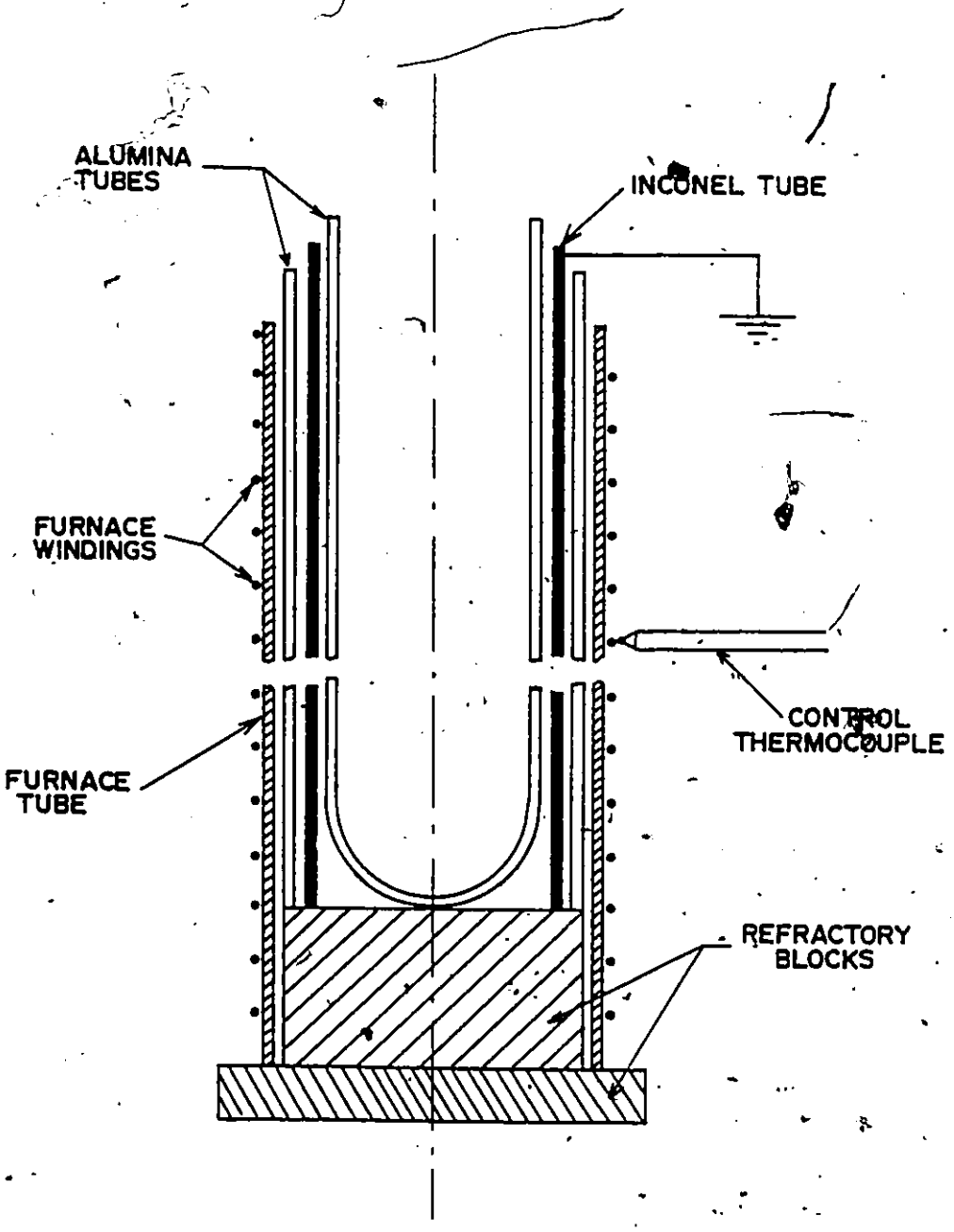

Fig. 4.2 The furnace assembly.

4.4.2 The Cell Assembly

The cell assembly used in the present investigation is shown in Fig. 4.3. A calcia stabilized zirconia solid electrolyte tube, described in Section 4.3, was joined to a stainless steel tube of the same outer diameter through a stainless steel O-ring coupling. A thick-walled spring-loaded alumina tube was placed inside the CSZ tube to compact the electrode mixture. Another alumina tube, open at both ends, was placed inside this alumina tube to insulate the Pt lead wire. A Pt wire was also used to make the connection with the outer electrode. The thermocouple used for measuring the temperature was placed very close to the cell. The stainless steel tube was connected to a vacuum pump through a vacuum valve. Thus, the CSZ tube could be evacuated and isolated by alternatively opening and closing the vacuum valve.

4.5 Configurations of the Anode

Whereas the cathode was constructed by wrapping Pt gauze on the outer side of the CSZ tube and was fairly simple in construction, three different configurations were used to construct the anode. These are shown in Fig. 4.4.

Configuration I was used for the cells of Type I and this was the most obvious choice when the electrode mixture did not contain a metallic component.

Configuration II and III were used for cells of Type II, III and IV. In configuration II, the rare earth compounds, mixed in a molar ratio of 1:1, formed the bottom layer of the electrode while the

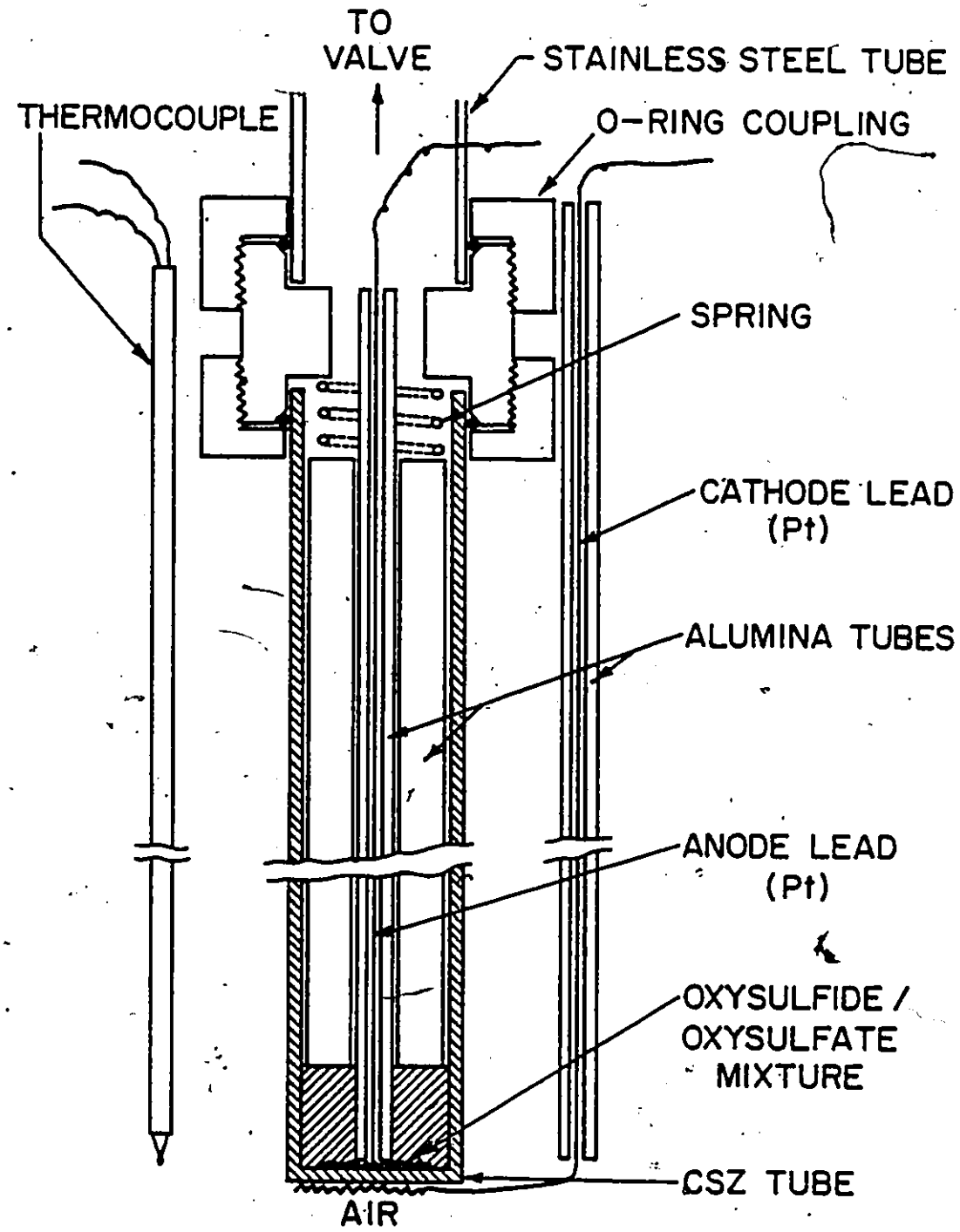

Fig. 4.3 The cell assembly.

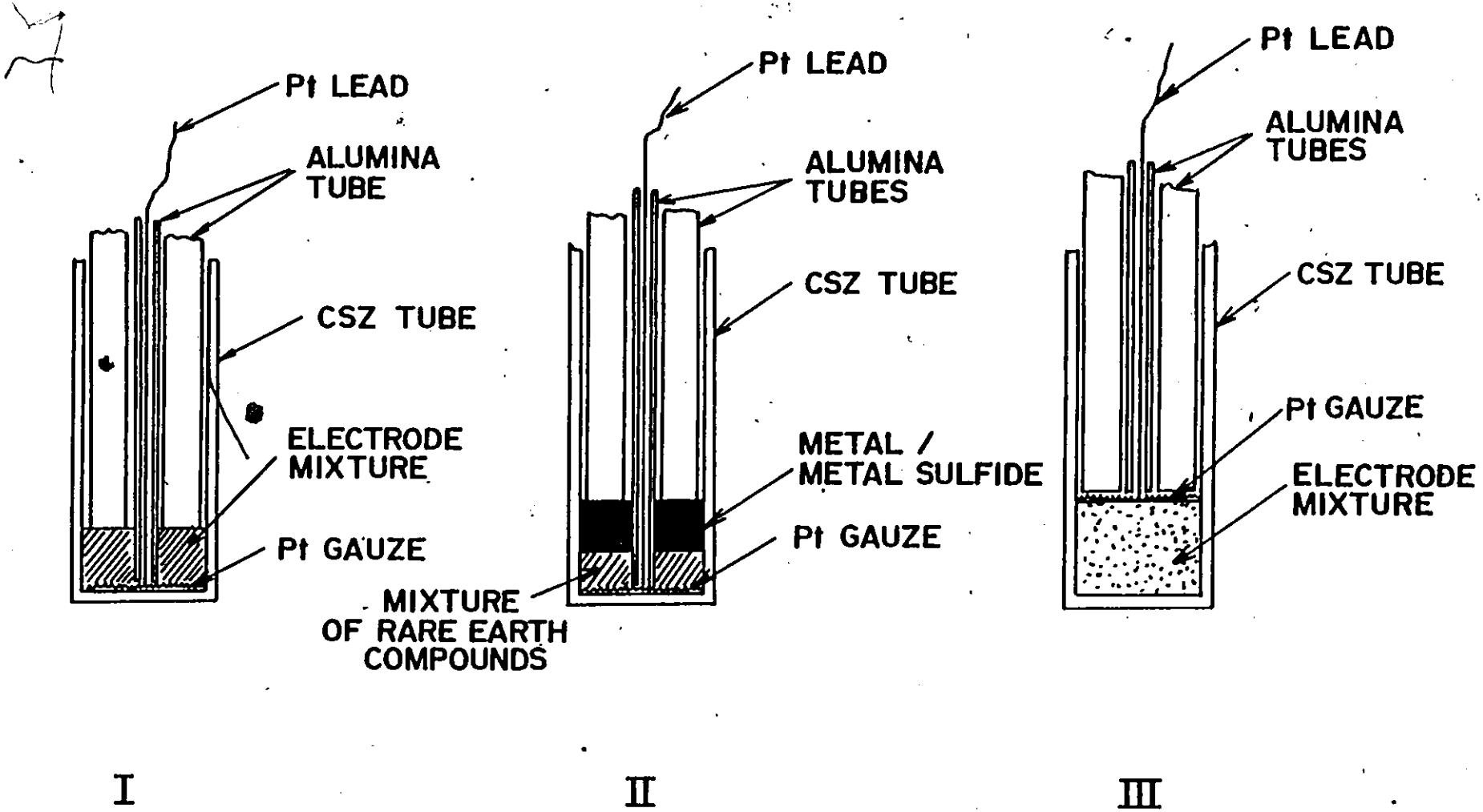

Fig. 4.4 Anode configurations.

metal/metal sulfide (Ag/Ag_2S or Cu/Cu_2S) couple formed the upper layer. The advantage of this arrangement was that there was minimal contact between the rare earth compounds and the metal/metal sulfide, so that chemical reactions, if any, between the components in the two layers were kinetically hindered. Also at high temperatures, the metal/metal sulfide mixture sintered together and effectively sealed the electrode, whereby the oxygen potential at the electrode/electrolyte interface was not affected by the level of vacuum.

In configuration III, the two rare earth compounds (RE_2O_3/RE_2O_2S, $RE_2O_3/RE_2O_2SO_4$ or $RE_2O_2S/RE_2O_2SO_4$), the metal sulfide and the metal were present in a ratio 1:1:1:3 or 1:1:2:4, the cell emf being independent of this ratio. In this case, the Pt lead wire made the contact with the electrode mixture at the top, so as to minimize the effect of a reaction, between the Pt wire and the metal, on the interfacial oxygen potential. This mixture also sintered together to form a compact mass which effectively sealed off the electrolyte/electrode interface.

4.6 Construction of the Anode

Rare earth compounds used in making an anode were dried at 670K, while Ag_2S and $Cu_{1.8}S$ were dried at 200°C. The copper and silver powders used in the anode were heated in hydrogen at 770-820K in order to reduce the oxide coating formed on the metal particles. The ratio of components used in the anode are indicated in Table 4.4.

Components were mixed in the ratios listed in Table 4.4 in an

TABLE 4.4

CONSTITUTION OF THE ANODE

Configuration	Cells	Components	Molar Ratio
I	I	RE_2O_2S, $RE_2O_2SO_4$	1:1
II upper layer	II & IV	Ag, Ag_2S	1:1
II lower layer	II	RE_2O_2S, $RE_2O_2SO_4$	1:1
II lower layer	III	RE_2O_3, $RE_2O_2SO_4$	1:1
II lower layer	IV	RE_2O_3, RE_2O_2S	1:1
II upper layer	III	Cu, Cu_2S	1:1
II lower layer	III	RE_2O_3, $RE_2O_2SO_4$	1:1
III	II	RE_2O_2S, $RE_2O_2SO_4$, Ag_2S, Ag	1:1:1:3 or 1:1:2:4
III	III	RE_2O_3, $RE_2O_2SO_4$, Cu_2S, Cu	1:1:1:3

agate mortar. When constructing an anode of Configuration I, the Pt gauze and the Pt lead wire along with the insulating alumina tube were placed in position first and then the electrode mixture was poured in. The mixture was tamped using the outer thick-walled alumina tube. A similar procedure was followed in construction of an anode in the Configuration II.

When constructing an anode of Configuration III, the electrode mixture was first poured in and then the Pt contact and the alumina tubes were placed in position. Figure 4.5 shows an electrode constructed in Configuration III.

4.7 Temperature Measurement

Thermocouples used for temperature measurement were constructed from Pt and Pt-13%Rh wires, each 0.5mm in diameter. The wires were first annealed at about 1500K for 15 hours to relieve stresses and were then used to make a thermocouple with two junctions. The reference junction was placed in a water/ice bath. After every experiment about 3mm of the thermocouple wires, measured from the hot junction, were clipped off and a new bead was made, in order to reduce errors due to interdiffusion of the metals at the hot junction.

All thermocouples used in the present investigation were calibrated against a thermocouple which in turn was calibrated within 1K of the International Practical Temperature Scale of 1968. Thermocouples were also checked against the melting point of silver covered with graphite powder.

Fig. 4.5 Anode in Configuration III

The thermocouple emf was measured by a fully guarded Leeds and Northrup (K-3) potentiometer having a gauranteed accuracy of ±.01% of the reading plus 0.5μV. This potentiometer was calibrated by the supplier. The standard cell used to calibrate the potentiometer was supplied by Eppley Lab. Inc. (B8718).

The overall accuracy of temperature measurement is estimated to be ±2K.

4.8 Measurement of Cell EMF

The cell emf was measured using a Keithley 616 Electrometer with an impedance of over $10^{14}\Omega$. This electrometer was checked against the potentiometer and a new electrometer of the same make. The readings shown by the new and the old electrometer were found to be identical. Readings of the electrometer and the potentiometer differed by less than 2mV. However in this case, the electrometer is expected to be more accurate than the potentiometer. The overall accuracy in the measurement of the cell emf is estimated to be ±1mV.

4.9 Operation of the Cells

After assembling, a cell was lowered into the hot zone of the furnace and the furnace top was covered with a refractory cap. The assembly was then evacuated to 10^{-4} torr and the furnace was turned on. The system was isolated from the vacuum pump by closing the vacuum valve, after temperature inside the furnace reached 570K. The furnace temperature was then raised to around 1120K (except for the Type IV

cells which were heated to 1020K) and the cell was equilibrated for 15 hours before readings were taken. In most cells, 3 to 4 hours were sufficient for equilibration and to give a steady emf. A reading was taken only if the emf did not vary by more than 1mV in 2 hours.

Reversibility of the cells was tested by passing a small current through the cell by connecting the potentiometer across it, the latter being slightly off-balance, and noting recovery of the cell emf to the original value with time.

Cells of Type II, III and IV were found to be extremely reversible and it took less than a minute for the cell emf to recover to the original value after polarization. However, cells of Type I were more lethargic and took up to 5 minutes to attain the original cell emf.

No reaction between the electrode materials and the electrolyte was observed for any of the cells. The Pt lead wire was found to have a black coat, presumably of platinum sulfide, in the cooler portions of the cell. However, near the electrolyte/electrode interface the Pt wire was not attacked.

Most of the cells were operated for a period of 3 to 4 days without any sign of deterioration. The reproducibility of the cells was excellent. For most of the cells of Type I at least three runs were made. However, for some of the cells of Type I, such as those involving lanthanum compounds, as many as six runs were done. For cells of Types II, III and IV, two runs, one each in anode Configurations II and III, were made. The electrode-products from the cells with anodes constructed in Configurations I and II were examined by X-ray diffraction, in order to verify coexistence of the compounds in the anode.

CHAPTER V

EXPERIMENTAL RESULTS

Cells of all types were standardized before use in actual experimental runs. A variety of standardization procedures were used in order to test the reliability and reproducibility of the cells, and to establish firmly the cell reaction occurring in each case. These standardization procedures are described in the first few sections of this chapter. The experimental results and a brief discussion on the cells of each type follow.

5.1 Verification of the Coexistence of the Components in the Anode

Coexistence of the components in the anode compartment is the primary requirement for a cell to yield useful thermodynamic information. Thus, mutual coexistence of all components in the anode of a cell was verified using X-ray diffraction techniques in most cases.

5.1.1 Coexistence of RE_2O_2S with $RE_2O_2SO_4$

In order to establish the coexistence of RE_2O_2S with $RE_2O_2SO_4$ for cells of Type I, a mixture of the two compounds containing 50 mole % of each, was pelletized and sealed in an evacuated quartz capsule. The capsule was then heated at a predetermined temperature for 120 hours, air-cooled and the products examined by X-ray powder diffraction. The

X-ray intensity patterns thus obtained were compared with those obtained using the original mixture of components. Figure 5.1 presents the X-ray diffraction patterns of La_2O_2S + $La_2O_2SO_4$ mixtures before and after various heattreatments. It should be noted that $La_2O_2SO_4$ did not decompose even at 1373K, the highest temperature used in coexistence studies. In contrast to this, oxysulfates of heavier rare earths decomposed to oxides at a temperature which depended upon the system being investigated. Such behavior is illustrated for gadolinium oxysulfate in Fig. 5.2. In this case, the X-ray diffraction analysis was performed before and after heatbtreating a mixture of Gd_2O_2S and $Gd_2O_2SO_4$. The results clearly show that $Gd_2O_2SO_4$ decomposes to oxide at high temperatures. The results of similar investigations for other systems are summarized in Table 5.1.

5.1.2 Coexistence of RE_2O_2S with $RE_2O_2SO_4$ at Sulfur Partial Pressures Corresponding to Ag/Ag_2S and Cu/Cu_2S Equilibria

The coexistence of RE_2O_2S with $RE_2O_2SO_4$ at sulfur partial pressures corresponding to Ag/Ag_2S and Cu/Cu_2S equilibria was studied by enclosing an $RE_2O_2S/RE_2O_2SO_4$ pellet with metal/metal sulfide pellets in a quartz capsule. The capsule was then evacuated, sealed and heated at temperatures shown in Table 5.1 for 120 hours. The sample was air-cooled and examined using X-ray diffraction techniques.

The results of the investigation performed on various mixtures are given in Table 5.1. It should be noted that the oxysulfides of the rare earths, considered here, coexist with their respective oxysulfates

Fig. 5.1 Results of X-ray diffraction analysis performed on a mixture of La_2O_2S and $La_2O_2SO_4$ after various heat-treatments. Notation: D - oxysulfide; T - oxysulfate; θ - angle of diffraction; I/I_{max} - relative intensity.

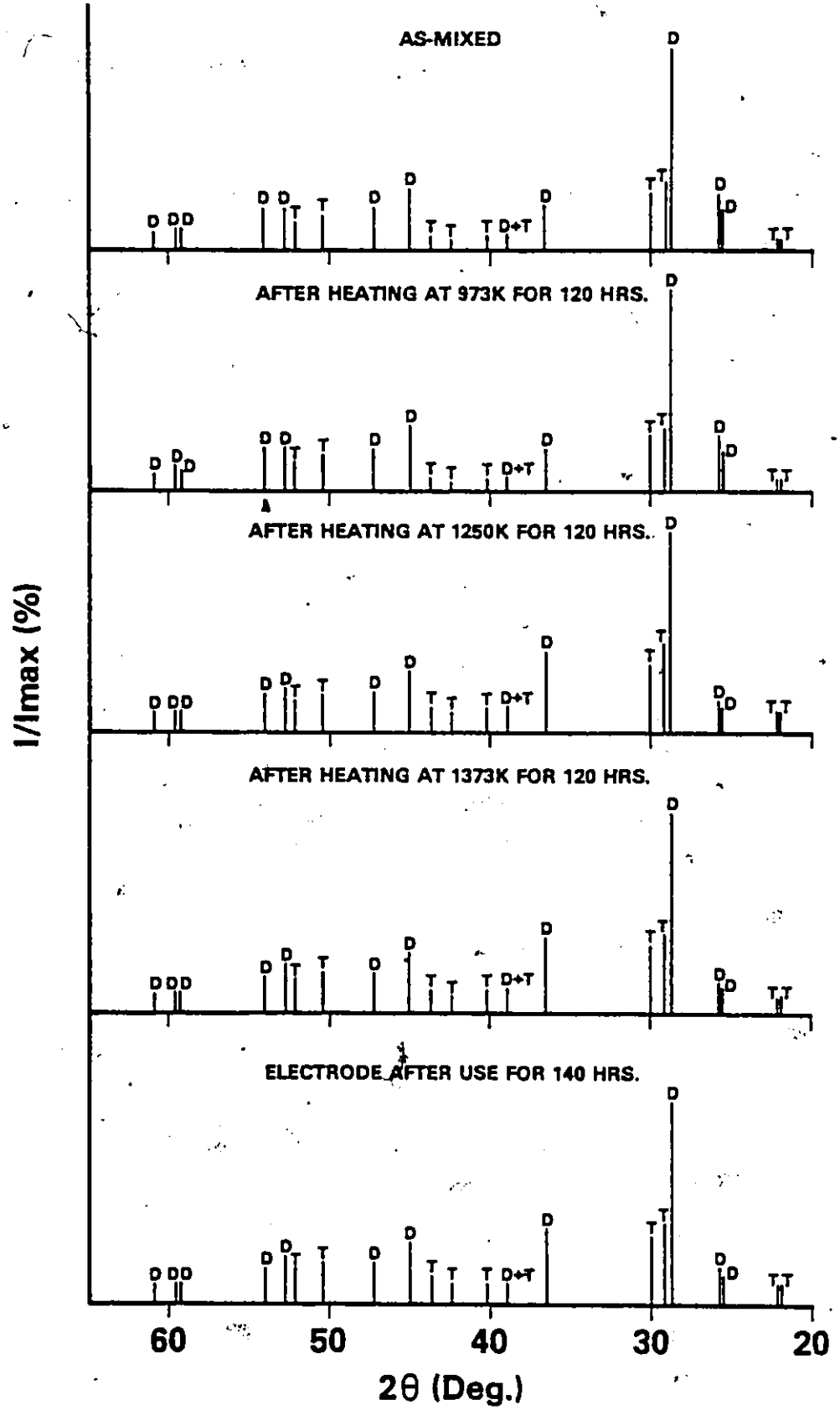
AS-MIXED
AFTER HEATING AT 973K FOR 120 HRS.
AFTER HEATING AT 1250K FOR 120 HRS.
AFTER HEATING AT 1373K FOR 120 HRS.
ELECTRODE AFTER USE FOR 140 HRS.
I/Imax (%)
60
50
40
30
20
2θ (Deg.)

Fig. 5.2 Results of X-ray diffraction analysis performed on a mixture of Gd_2O_2S and $Gd_2O_2SO_4$ after various heat-treatments. Notation: D - oxysulfide; T - oxysulfate; O - oxide; θ - angle of diffraction ; and I/I_{max} -relative intensity. The oxysulfate in the sample heated at 1373K decomposed to the oxide.

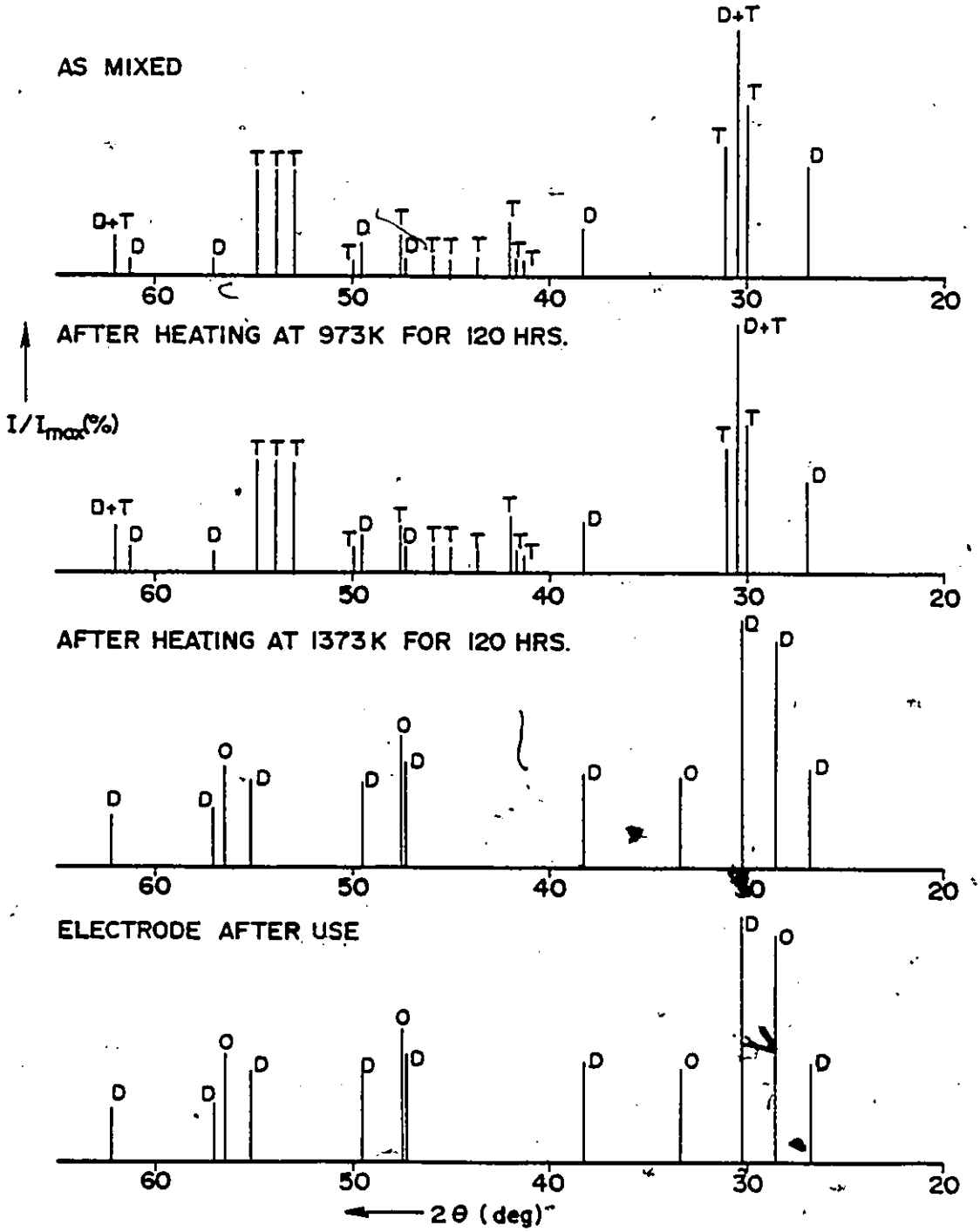
AS MIXED
AFTER HEATING AT 973K FOR 120 HRS.
AFTER HEATING AT 1373K FOR 120 HRS.
ELECTRODE AFTER USE
I/I_max(%)
2θ (deg)
60
50
40
30
20
D+T
T
D
O

TABLE 5.1

RESULTS FROM COEXISTENCE STUDIES

Composition of the Mixture (molar ratio)	Purpose	Heattreatment*	Composition of the Products	Comments
$La_2O_2S + La_2O_2SO_4$ (1:1)	To verify coexistence of oxysulfide with oxysulfate	Heated at 973, 1250 and 1373 K for 120 hrs.	$La_2O_2S + La_2O_2SO_4$	Proportion of $La_2O_2SO_4$ slighly increased in the sample heated at 1373 K.
$Pr_2O_2S + Pr_2O_2SO_4$ (1:1)	Same as above.	Same as above.	$Pr_2O_2S + Pr_2O_2SO_4$	Some Pr_2O_3 (A type) was also present in the sample heated at 1375 K.
$Nd_2O_2S + Nd_2O_2SO_4$ (1:1)	Same as above.	Same as above.	$Nd_2O_2S + Nd_2O_2SO_4$	Proportion of $Nd_2O_2SO_4$ increased in samples heated at 1373 K.
$Sm_2O_2S + Sm_2O_2SO_4$ (1:1)	Same as above.	Heated at 973 and 1250 K for 120 hrs.	$Sm_2O_2S + Sm_2O_2SO_4$	
$Sm_2O_2S + Sm_2O_2SO_4$ (1:1)	Same as above.	Heated at 1373 K	Sm_2O_3 (B type) + Sm_2O_2S	$Sm_2O_2SO_4$ decomposed to oxide.
$Eu_2O_2S + Eu_2O_2SO_4$ (1:1)	Same as above.	Heated at 973 to 1250 K for 120 hrs.	$Eu_2O_2S + Eu_2O_2SO_4$	
$Eu_2O_2S + Eu_2O_2SO_4$ (1:1)	Same as above.	Heated at 1373 K for 120 hrs.	Eu_2O_3 (B type) + Eu_2O_2S	$Eu_2O_2SO_4$ decomposed to oxide.
$Gd_2O_2S + Gd_2O_2So_4$ (1:1)	Same as above.	Heated at 973, 1250 and 1373 K for 120 hrs.	Gd_2O_3 (C type) + Gd_2O_2S	$Gd_2O_2SO_4$ decomposed to oxide for samples heated at 1250 and 1375 K.
$Tb_2O_2S + Tb_2O_2SO_4$ (1:1)	Same as above.	Heated at 973 and 1173 K for 120 hrs.	$Tb_2O_2S + Tb_2O_2SO_4$	

TABLE 5.1 (cont'd)

Composition of the Mixture (molar ratio)	Purpose	Heattreatment*	Composition of the Products	Comments
$Tb_2O_2S + Tb_2O_2SO_4$ (1:1)	Same as above.	Heated at 1250 K for 120 hrs.	Tb_2O_3 (C type) + Tb_2O_2S	$Tb_2O_2SO_4$ decomposed to oxide.
$Dy_2O_2S + Dy_2O_2SO_4$ (1:1)	Same as above.	Heated at 1000 and 1100 K for 120 hrs.	$Dy_2O_2S + Dy_2O_2SO_4$	Some Dy_2O_3 was present in the products.
$Ho_2O_2S + Ho_2O_2SO_4$ (1:1)	Same as above.	Heated at 1000 and 1100 K for 120 hrs.	$Ho_2O_3 + Ho_2O_2S + Ho_2O_2SO_4$	Ho_2O_3 was found in the sample heated at 1000 K and complete decomposition had occurred in the sample heated at 1100 K.
$La_2O_2S + La_2O_2SO_4$ (1:1) in presence of Ag/Ag_2S	To verify coexistence of oxysulfide with oxysulfate at a sulphur partial pressure corresponding to Ag/Ag_2S equilibria.	Heated at 1000 and 1200 K for 120 hrs. in presence of Ag/Ag_2S	$La_2O_2S + La_2O_2SO_4$	Relative proportion of $La_2O_2SO_4$ increased significantly.
$Nd_2O_2S + Nd_2O_2SO_4$ (1:1) in presence of Ag/Ag_2S	Same as above.	Same as above.	$Nd_2O_2S + Nd_2O_2SO_4$	Reltive proportion of $Nd_2O_2SO_4$ increased significantly.
$La_2O_2S + La_2O_2SO_4$ (1:1) in presence of Cu/Cu_2S	To study coexistence of oxysulfide with oxysulfate at sulfur partial pressures corresponding to Cu/Cu_2S equilibria.	Heated at 1100 and 1300 K for 120 hrs. in presence of Cu/Cu_2S.	$La_2O_3 + La_2O_2SO_4$	La_2O_2S does not coexist with $La_2O_2SO_4$ at partial pressures determined by Cu/Cu_2S equilibria.

TABLE 5.1 (cont'd)

Composition of the Mixture (molar ratio)	Purpose	Heattreatment*	Composition of the Products	Comments
Gd_2O_2S + $Gd_2O_2SO_4$ (1:1) in presence of Cu/Cu_2S	Same as above.	Heated at 1000 and 1200 K for 120 hrs. in presence of Cu/Cu_2S.	Gd_2O_3 (C Type) + $Gd_2O_2SO_4$	Gd_2O_2S does not coexist $Gd_2O_2SO_4$ at partial pressures determined by Cu/Cu_2S equilibria.
La_2O_3 + $La_2O_2SO_4$ (1:1) in presence of Cu/Cu_2S	To verify coexistence of oxide with oxysulfate at sulfur partial pressures corresponding to Cu/Cu_2S equilibria.	Heated at 973 and 1300 K for 120 hrs. in presence of Cu/Cu_2S.	La_2O_3 + $La_2O_2SO_4$	Proportion of $La_2O_2SO_4$ increased.
Pr_2O_3 + $Pr_2O_2SO_4$ (1:1) in presence of Cu/Cu_2S	Same as above.	Heated at 1100 and 1300 K for 120 hrs. in presence of Cu/Cu_2S.	Pr_2O_3 + $Pr_2O_2SO_4$	Relative proportion of $Pr_2O_2SO_4$ increased in the samples.
Nd_2O_3 + $Nd_2O_2SO_4$ (1:1) in presence of Cu/Cu_2S	Same as above.	Heated at 1100 and 1300 K for 120 hrs. in presence of Cu/Cu_2S.	Nd_2O_3 + $Nd_2O_2SO_4$	Relative proportion of $Nd_2O_2SO_4$ increased in the samples.
Sm_2O_3 (B type) + $Sm_2O_2SO_4$ (1:1) in presence of Cu/Cu_2S	Same as above.	Heated at 1100 and 1300 K for 120 hrs. in presence of Cu/Cu_2S.	Sm_2O_3 (B type) + $Sm_2O_2SO_4$	Relative proportion of $Sm_2O_2SO_4$ increased after heating.
Eu_2O_3 (B type) + $Eu_2O_2SO_4$ (1:1) in presence of Cu/Cu_2S.	Same as above.	Heated at 1100 and 1300 K for 120 hrs. in presence of Cu/Cu_2S.	Eu_2O_3 (B type) + $Eu_2O_2SO_4$	Relative proportion of $Eu_2O_2SO_4$ increased.

TABLE 5.1 (cont'd)

Composition of the Mixture (molar ratio)	Purpose	Heattreatment*	Composition of the Products	Comments
Gd_2O_3 (C type) + $Gd_2O_2SO_4$ in presence of Cu/Cu_2S.	Same as above.	Heated at 1100 and 1200 K for 120 hrs. in presence of Cu/Cu_2S.	Gd_2O_3 (C type) + $Gd_2O_2SO_4$	Relative proportion of $Gd_2O_2SO_4$ increased.
La_2O_2S + La_2O_3 (1:1) in presence of Cu/Cu_2S	To verify coexistence of oxysulfide with oxide at sulfur partial pressures corresponding to Cu/Cu_2S equilibria.	Heated at 1100 and 1300 K for 120 hrs.	La_2O_2S + La_2O_3	
Sm_2O_3 (B type) + Sm_2O_2S (1:1) in presence of Cu/Cu_2S	Same as above.	Same as above.	Sm_2O_3 (B type) + Sm_2O_2S	
La_2O_3 + La_2O_2S (1:1) in presence of Ag/Ag_2S	To study coexistence of oxide with oxysulfide at sulfur partial pressures corresponding to Ag/Ag_2S equilibria.	Heated at 1000 and 1200 K.	La_2O_2S + $La_2O_2SO_4$	Stronger lines of La_2O_2S.
Y_2O_3 + Y_2O_2S (1:1) in presence of Ag/Ag_2S	To study coexistence of oxide with oxysulfide at sulfur partial pressures corresponding to Ag/Ag_2S equilibria.	Heated at 1000 and 1200 K for 120 hrs.	Y_2O_3 + Y_2O_2S	
La_2O_3 + Ag_2S	To investigate the chemical reactions between the compounds.	Heated at 1000 and 1250 K for 120 hrs.	La_2O_3 + Ag_2S	No reaction between Ag_2S and La_2O_3

TABLE 5.1 (cont'd)

Composition of the Mixture (molar ratio)	Purpose	Heattreatment*	Composition of the Products	Comments
$La_2O_2S + Ag_2S$	Same as above.	Heated at 1000 and 1250 K for 120 hrs.	$La_2O_2S + Ag_2S$	No reaction between Ag_2S and La_2O_2S.
$La_2O_2SO_4 + Ag_2S$	Same as above.	Heated at 1000 and 1250 K for 120 hrs.	$La_2O_2SO_4 + Ag_2S$	No reaction between Ag_2S and $La_2O_2SO_4$.
$La_2O_3 + Cu_2S$	Same as above.	Heated at 1100 and 1300 K for 120 hrs.	$La_2O_3 + Cu_2S$	No reaction between Cu_2S and La_2O_3.
$La_2O_2S + Cu_2S$	Same as above.	Heated at 1100 and 1350 K for 120 hrs.	$La_2O_2S + Cu_2S$	No reaction between Cu_2S and La_2O_2S.
$La_2O_2SO_4 + Cu_2S$	Same as above.	Heated at 1100 to 1300 K for 120 hrs.	$La_2O_2SO_4 + Cu_2S$.	No reaction between Cu_2S and $La_2O_2SO_4$.

* All samples were air-cooled after the heattreatment.

at sulfur potentials corresponding to Ag/Ag_2S equilibria but not at those corresponding to Cu/Cu_2S equilibria. At the sulfur potentials corresponding to Cu/Cu_2S equilibria only oxide and oxysulfate were found among the products.

5.1.3 Coexistence of RE_2O_3 with $RE_2O_2SO_4$ at Sulfur Partial Pressures Corresponding to Cu/Cu_2S Equilibria

The experimental procedure followed in order to verify the coexistence of RE_2O_3 with $RE_2O_2SO_4$ at sulfur partial pressures corresponding to Cu/Cu_2S equilibria was similar to that discussed in the previous section. The results of the study done on a mixture of lanthanum compounds are presented in Fig. 5.3. The results for the compounds of other rare earths are summarized in Table 5.1.

5.1.4 Coexistence of RE_2O_3 with RE_2O_2S at Sulfur Partial Pressures Corresponding to Cu/Cu_2S and Ag/Ag_2S Equilibria

The experimental procedure adopted in this case was similar to the one discussed in Section 5.1.2. The results of this investigation are summarized in Table 5.1.

5.1.5 Reaction of Ag_2S or Cu_2S with RE_2O_3, RE_2O_2S and $RE_2O_2SO_4$

Reactions between Ag_2S or Cu_2S, and a rare earth compound were studied by pressing a pellet of a mixture of the two and sealing it in an evacuated quartz capsule. The capsule was subsequently heated, held at the reaction temperature, air-cooled and the products analysed using

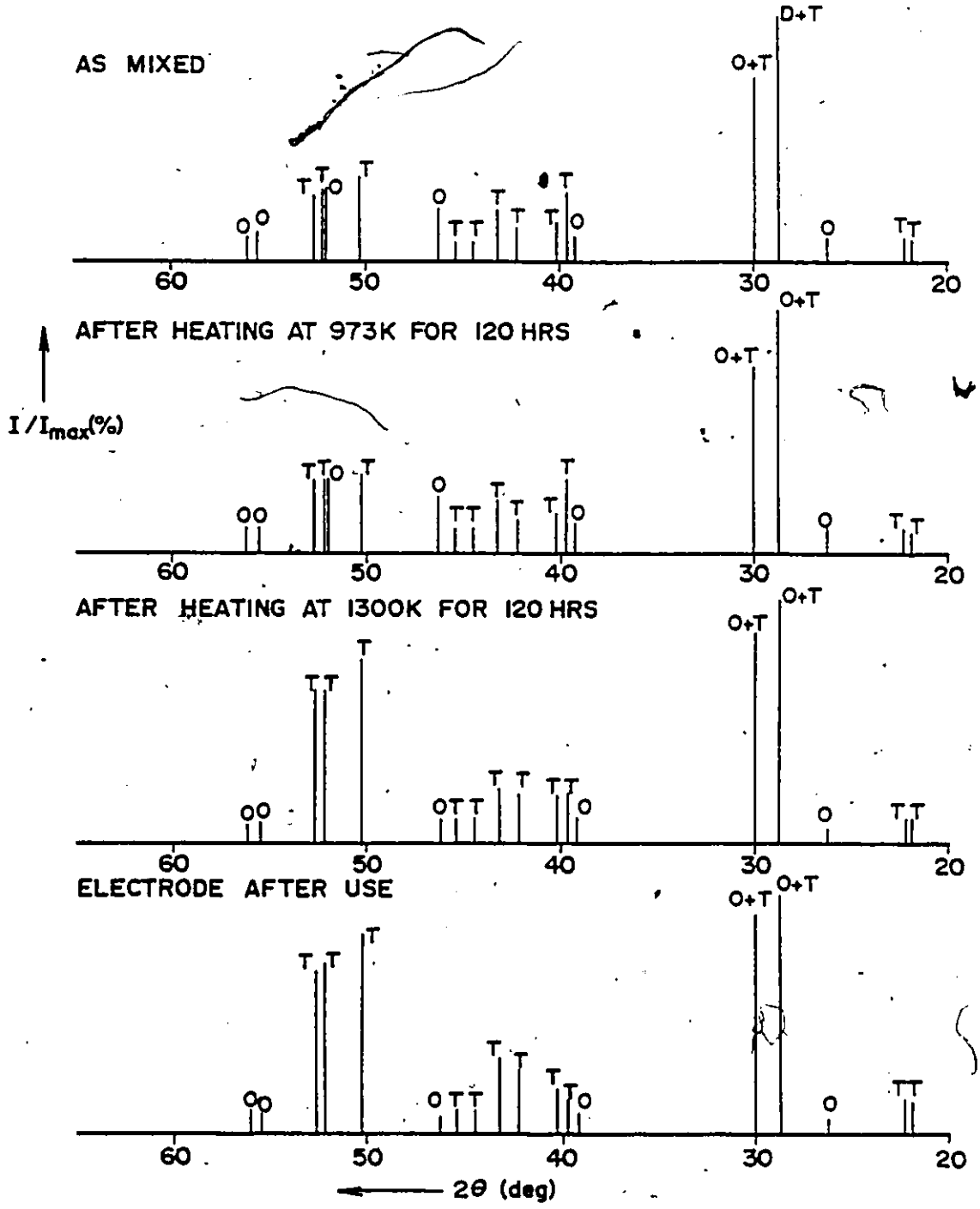

Fig. 5.3 Results of X-ray diffraction analysis performed on a mixture of La_2O_3 and $La_2O_2SO_4$ in presence of Cu/Cu_2S. Notation: same as in Fig. 5.2.

X-ray diffraction analysis. It was found that the rare earth compounds did not react with either Ag_2S or Cu_2S. The results of this investigation are summarized in Table 5.1.

5.1.6 Discussion on the Coexistence of Anode Components

From studies on the coexistence of oxysulfides with oxysulfates, it can be concluded that the oxysulfides of rare earth elements coexist with the respective oxysulfates up to a certain temperature above which decomposition given by the reaction:

$$RE_2(SO_4)_3(s) = RE_2O_3(s) + 3SO_2(g) + 3/2O_2(g), \qquad (5.1)$$

occurs.

It was noticed, while studying the coexistence of RE_2O_2S with $RE_2O_2SO_4$ in the presence of Ag/Ag_2S, that the proportion of $RE_2O_2SO_4$ in $RE_2O_2S|RE_2O_2SO_4$ mixtures increased significantly after heating. This can be attributed to coversion of RE_2O_2S to $RE_2O_2SO_4$, given by the reaction:

$$RE_2O_2S(s) + 2O_2(g) = RE_2O_2SO_4(s). \qquad (5.2)$$

The oxygen needed for the above reaction may come from the remnants of moisture in the anode, the decomposition of Ag_2O, the dissolved oxygen in Ag or from the atmosphere by diffusion through the walls of the quartz capsule. Since no such reaction was observed when oxysulfate/oxysulfide mixtures were heated in the absence of Ag/Ag_2S (Section 5.1.1), it seems that the last of the listed factors does not

contribute significantly to Reaction 5.2. A similar reaction also occurred when $RE_2O_3/RE_2O_2SO_4$ mixtures were heated in the presence of Cu/Cu_2S, in which case RE_2O_3 was presumably converted to $RE_2O_2SO_4$ by the reaction:

$$RE_2O_3(s) + 3/2O_2(g) + 1/2S_2(g) = RE_2O_2SO_4(s) \qquad (5.3)$$

Oxysulfides of all the rare earths investigated were found to coexist with their respective oxides at sulfur partial pressures corresponding to Cu/Cu_2S equilibria.

5.1.7 Summary of Coexistence Studies

Based on the experimental observation discussed above, the following conclusions can be drawn:

1. Oxysulfides of rare earth elements from lanthanum to dysprosium coexist with their respective oxysulfates.
2. Oxysulfides of neodymium and lanthanum coexist with the respective oxysulfates in the presence of Ag/Ag_2S (probably true for other rare earth compounds).
3. Oxides of rare earth elements from lanthanum to gadolinium coexist with their respective oxysulfates in presence of Cu/Cu_2S.
4. Oxides of La, Sm and Y (probably true for all RE elements even though only La, Sm and Y compounds were studied) coexist with their respective oxysulfides in the presence of Cu/Cu_2S.
5. No reactions of Cu_2S or Ag_2S with rare earth compounds are observed.
6. External sources of oxygen tend to influence the study by a slow

conversion of a compound to one that is stable at higher oxygen potentials.

5.2 Results from Type I Cells

5.2.1 EMF Data from Type I Cells

The emf data from cells of Type I are presented in Table 5.2. The same data is presented in Figs. 5.4(a)-(h). For all cells, except those involving La compounds, the cell emf was found to vary linearly with temperature up to a certain temperature, above which a deviation from linear behaviour was observed. For the lanthanum system, no variation from linear behaviour was observed (Fig. 5.4 (a)). The temperature at which a cell showed a deviation from linear behaviour, varied from one run to another for the same system. Table 5.3 shows the temperatures at which a deviation from linear behaviour was observed for various runs of a cell. In Figs. 5.4 (b)-(h) only the highest temperatures, at which a deviation from linear behaviour was observed, are shown. Only readings taken below the temperatures at which deviation from linear behaviour was observed, are processed to yield thermodynamic information.

The linear portions of the cell emf vs. temperature plots were analysed using linear regression analysis. Equations of the 'best-fit' lines are presented in Table 5.4. Fig. 5.5 summarizes the data from all cells of Type I.

TABLE 5.2

EMF DATA FOR THE CELLS OF TYPE I

Temperature (K)	Cell emf (V)
Lanthanum System (Type I(a))	
1107.50	.692
1134.40	.676
1191.00	.649
1202.60	.643
1249.50	.622
1263.60	.617
1273.80	.613
1284.80	.608
1295.70	.602
1305.70	.599
1315.80	.595
1328.10	.589
1347.60	.580
1361.60	.575
1250.80	.624
1198.50	.646
1142.60	.670
1196.90	.645
1195.90	.645
1245.60	.626
1276.90	.614
1277.90	.613
1322.00	.593
1363.00	.572
1392.00	.557
1418.30	.546
1440.90	.536
1438.00	.536
1462.90	.526
1348.30	.578
1196.50	.646
1228.70	.633
1227.30	.634
1260.00	.620
1295.30	.603
1485.40	.517
1463.00	.526
1485.40	.517

TABLE 5.2 (continued)

Temperature (K)	Cell emf (V)
Praseodymium System (Type I (b))	
1157.00	.649
1115.00	.666
1209.50	.627
1215.00	.623
1243.00	.610
1184.00	.636
1234.00	.614
1234.00	.614
1274.00	.596
1149.00	.655
1101.00	.673
1139.60	.654
1172.70	.639
1214.00	.623
1250.00	.607
1284.00	.592
1315.50	.578
1386.00	.544
1359.00	.557
1330.00	.571
1305.00	.585
1262.00	.598
1230.00	.613
1196.00	.628
1160.00	.643
1123.00	.658

TABLE 5.2 (continued)

Temperature (K)	Cell emf (V)
Neodymium System (Type I(c))	
1135.00	.650
1113.00	.661
1153.00	.642
1167.00	.636
1179.00	.630
1192.00	.624
1210.00	.616
1228.00	.607
1250.00	.597
1265.00	.591
1278.00	.585
1344.00	.555
1362.00	.548
1390.00	.535
1410.00	.526
1279.40	.587
1303.00	.574
1327.40	.562
1343.50	.553
1351.70	.549
1400.00	.529
1376.80	.539
1425.00	.517
1287.00	.578
1287.30	.578
1285.00	.579
1285.80	.579
1320.00	.563
1320.00	.563
1363.60	.544

TABLE 5.2 (continued)

Temperature (K)	Cell emf (V)
Samarium System (Type I(d))	
1046.00	.688
1105.00	.663
1140.00	.646
1179.00	.628
1211.00	.614
1242.00	.599
1276.00	.583
1305.00	.570
1338.00	.555
1338.00	.553
1369.00	.542
1172.00	.628
1156.50	.633
1198.00	.614
1179.50	.623
1220.50	.603
1242.00	.593
1264.00	.582
1285.00	.572
1295.00	.567
1305.70	.563
1320.40	.557
1224.60	.599
1309.00	.560

TABLE 5.2 (continued)

Temperature (K)	Cell emf (V)
Europium System (Type I(e))	
1110.00	.654
1136.00	.644
1096.00	.660
1066.00	.676
1046.00	.684
996.00	.700
1028.00	.688
1053.00	.679
1077.00	.668
1109.00	.653
1144.00	.637
1172.00	.624
1171.00	.624
1189.00	.616
1211.00	.606
1232.00	.596
1253.00	.587
1272.00	.578
1294.00	.568
1316.00	.559

TABLE 5.2 (continued)

Temperature (K)	Cell emf (V)
Gadolinium System (Type I(f))	
1026.00	.688
1050.50	.678
1072.00	.669
1094.50	.658
1118.00	.646
1136.50	.640
1172.30	.624
1173.00	.621
1192.00	.612
1222.00	.600
1242.50	.589
1261.50	.581
1282.00	.572
1263.00	.582
1276.00	.576
1016.00	.694
1040.00	.682
1053.50	.677
1080.00	.663
1108.00	.651
1126.00	.642
1131.00	.641
1153.00	.629
1185.00	.617
1208.00	.606
1233.00	.593
1259.00	.582

TABLE 5.2 (continued)

Temperature (K)	Cell emf (V)
Terbium System (Type I(g))	
1028.00	.695
1066.00	.667
1070.00.	.672
1072.00	.668
1032.00	.680
1066.00	.667
1110.00	.650
1130.00	.641
1152.00	.630
1174.00	.620
1195.00	.611
1190.00	.611
1162.00	.625
1140.00	.635
1120.00	.645
1094.00	.657
1080.00	.664
1057.00	.675
1045.00	.683
Dysprosium System (Type I(h))	
1042.00	.676
1063.70	.664
1089.30	.653
1108.80	.645
1128.30	.636
1150.10	.624
1172.30	.616

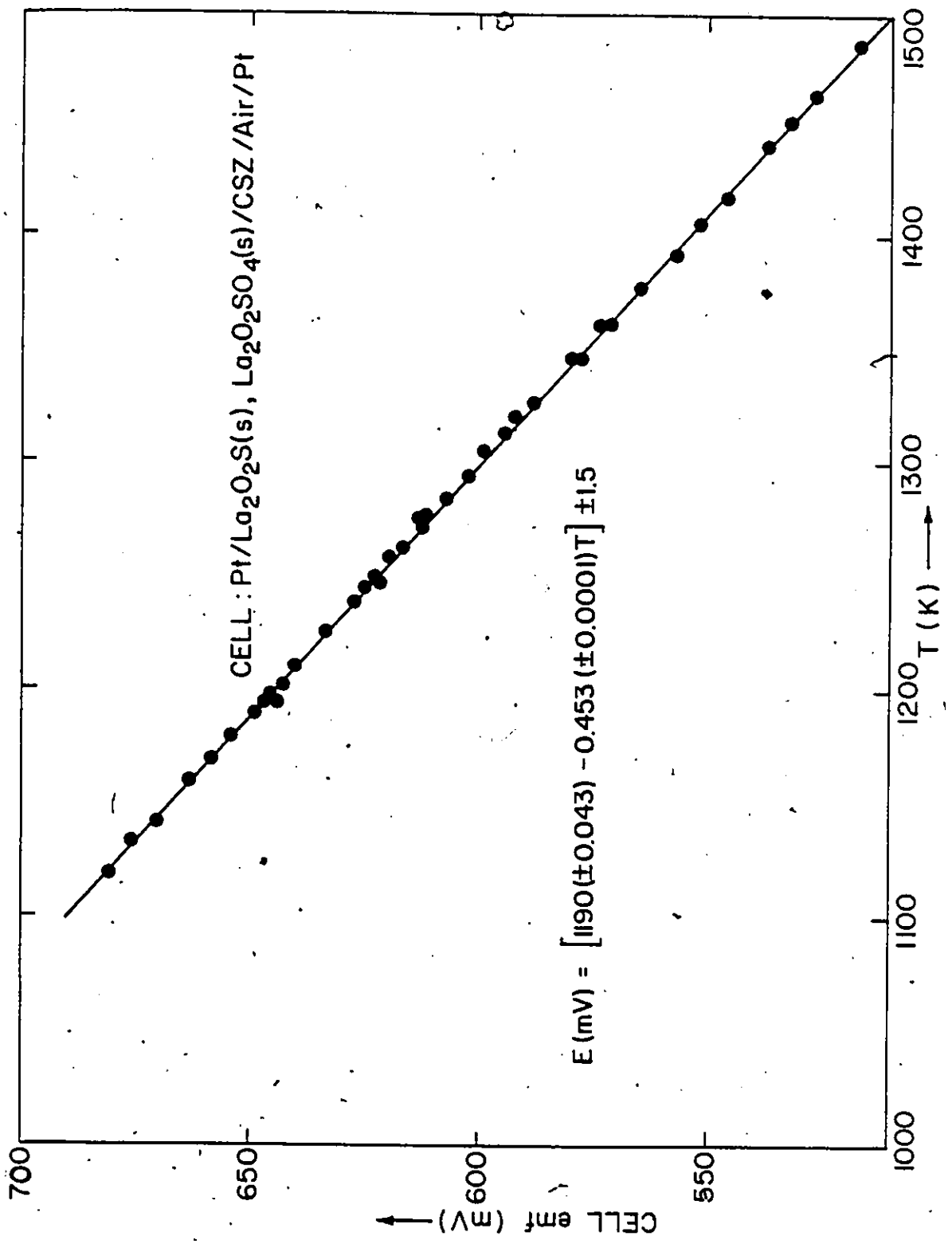

Fig. 5.4(a) The variation of emf with temperature for Cell I(a).

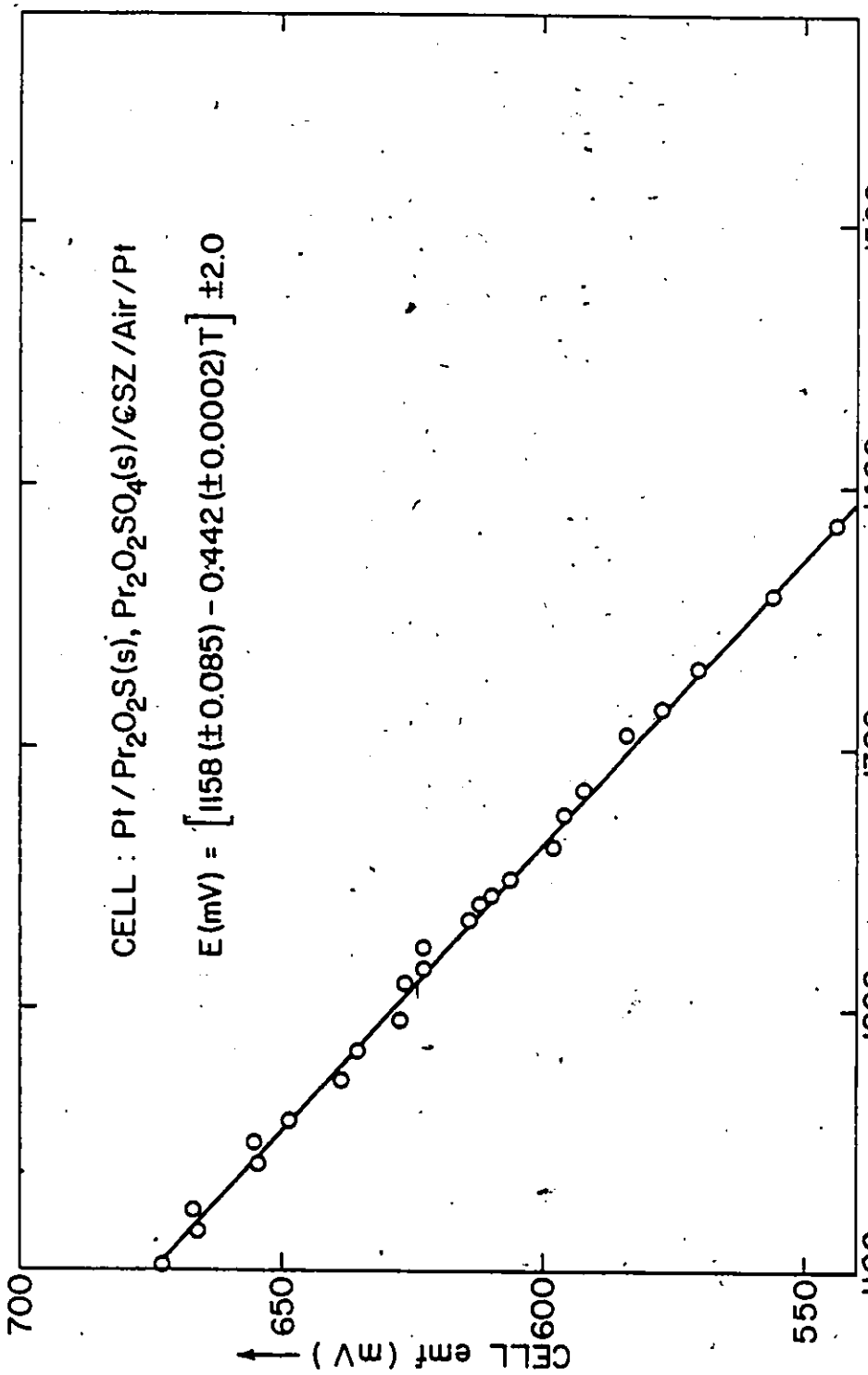

Fig. 5.4(b) The variation of emf with temperature for Cell I(b).

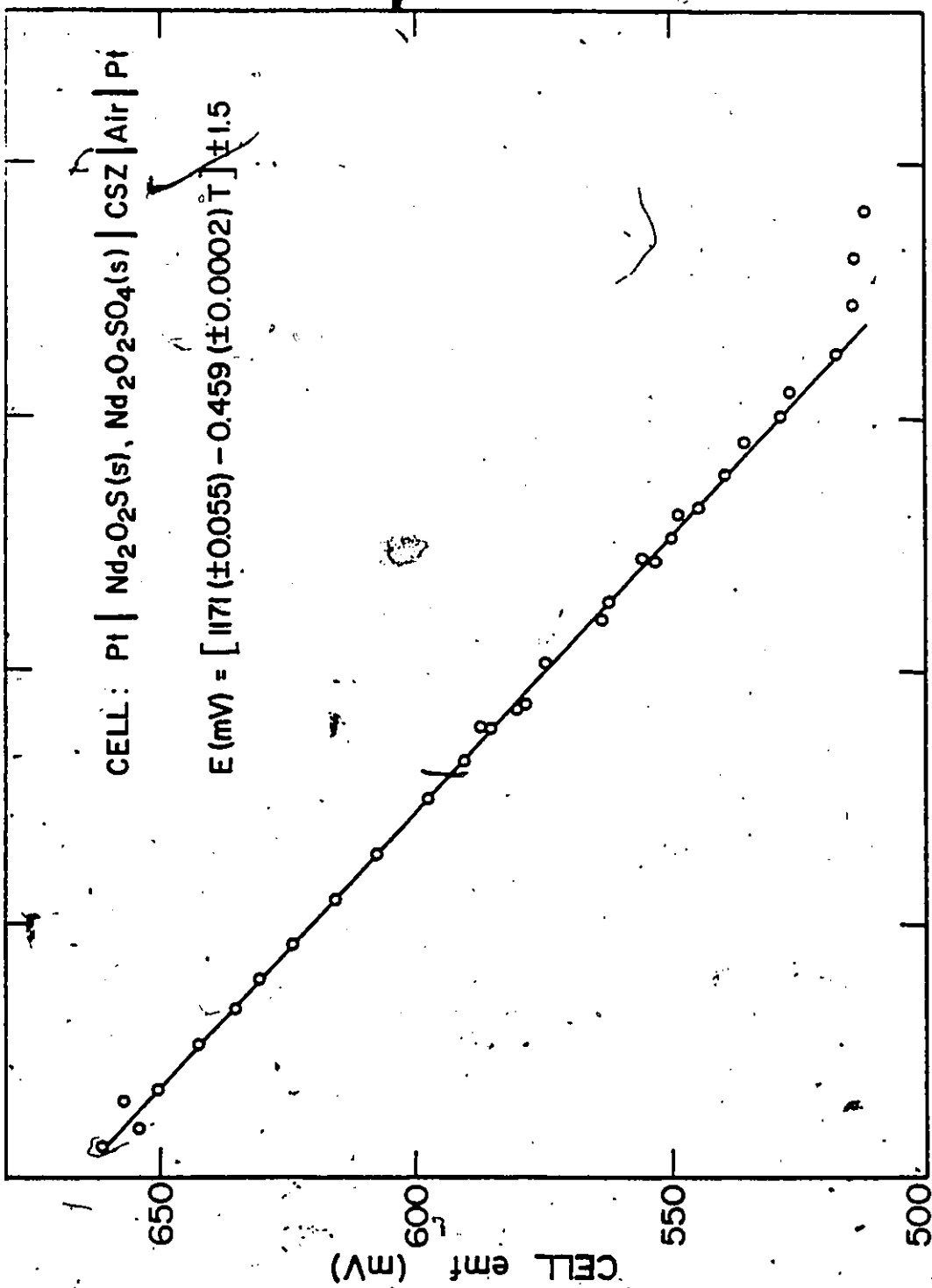

Fig. 5.4(c) The variation of emf with temperature for Cell I(c).

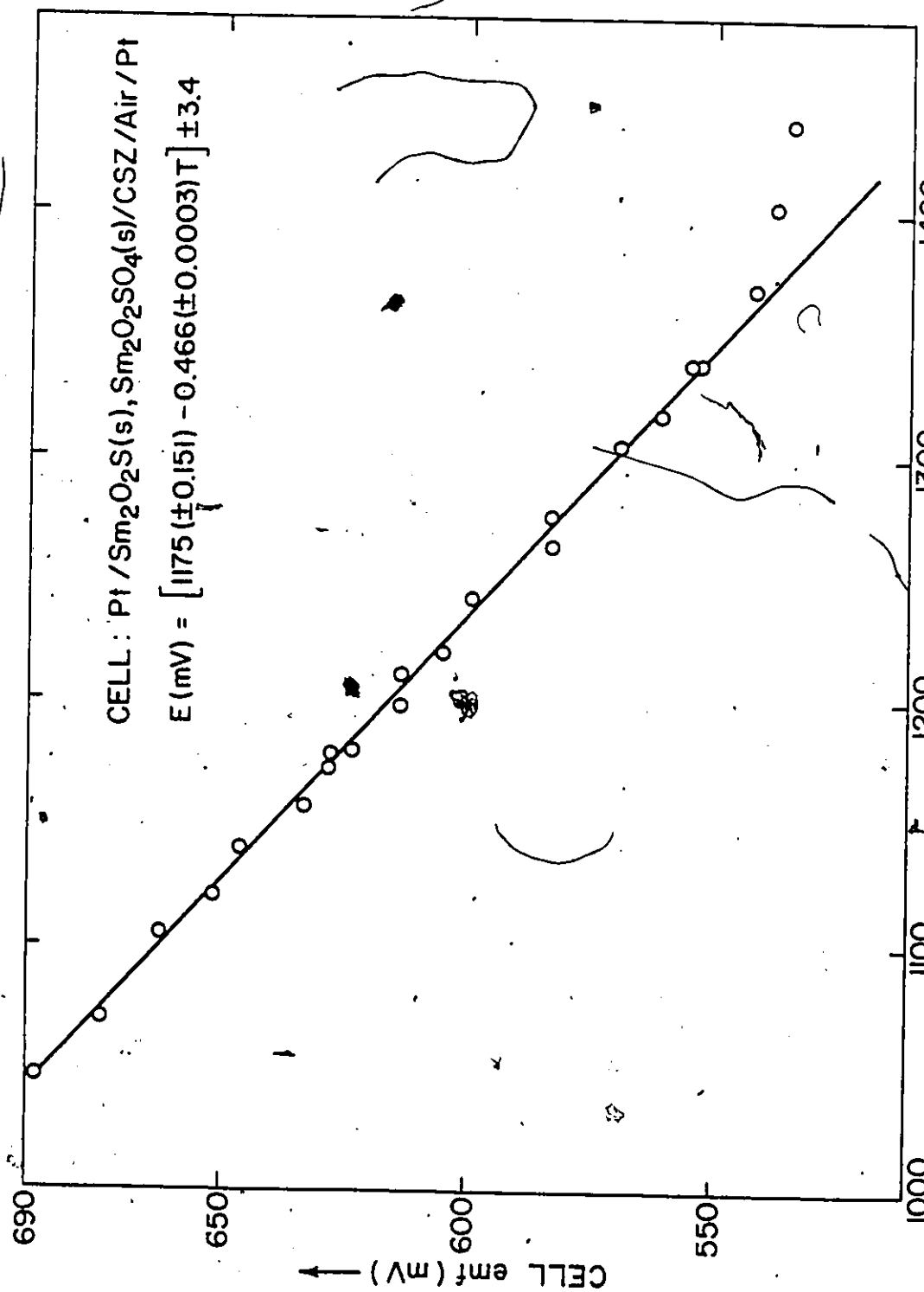

Fig. 5.4(d) The variation of emf with temperature for Cell I(d).

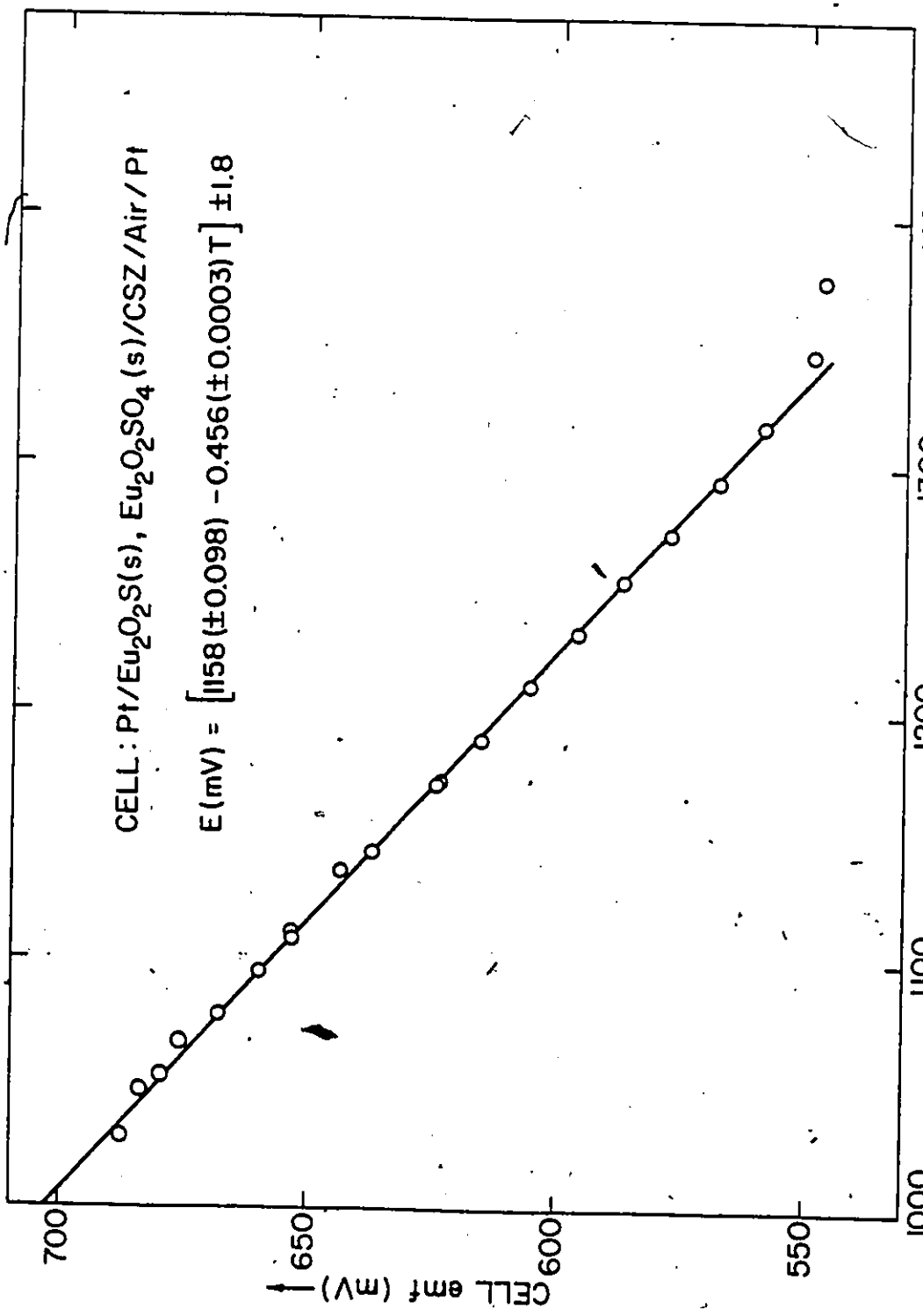

Fig. 5.4(e) The variation of emf with temperature for Cell I(e).

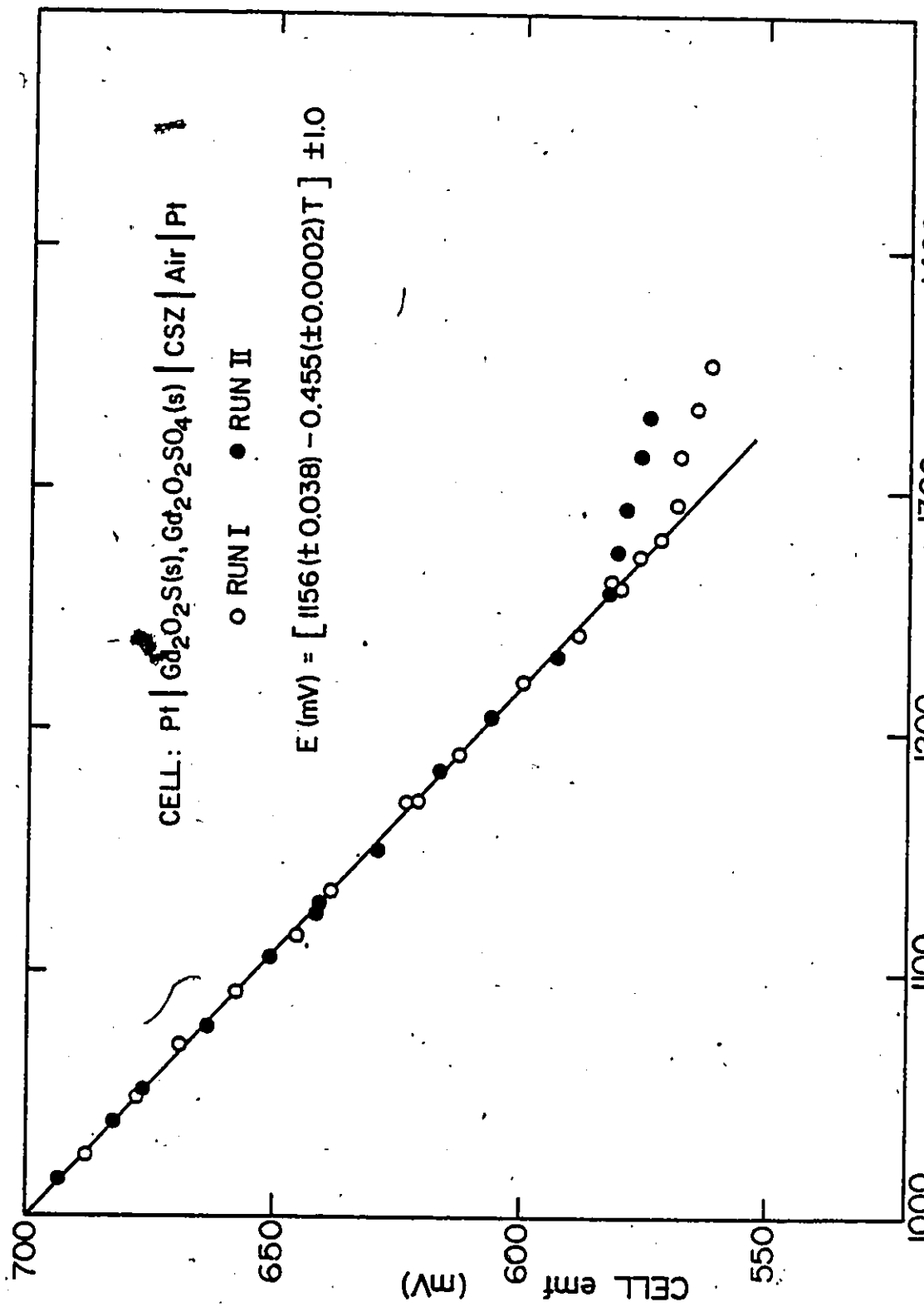

Fig. 5.4(f) The variation of emf with temperature for Cell I(f).

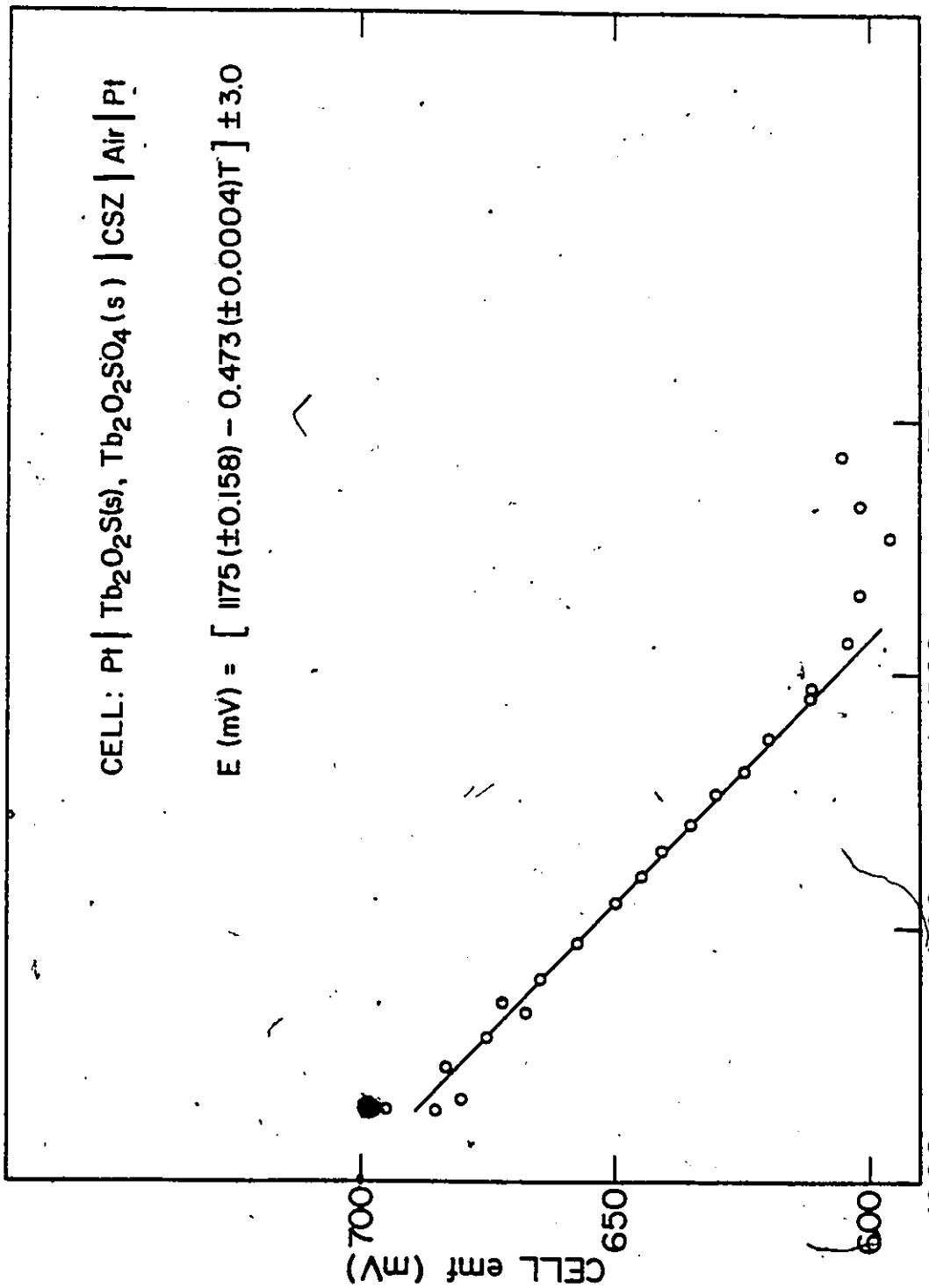

Fig. 5.4(g) The variation of emf with temperature for Cell I(g).

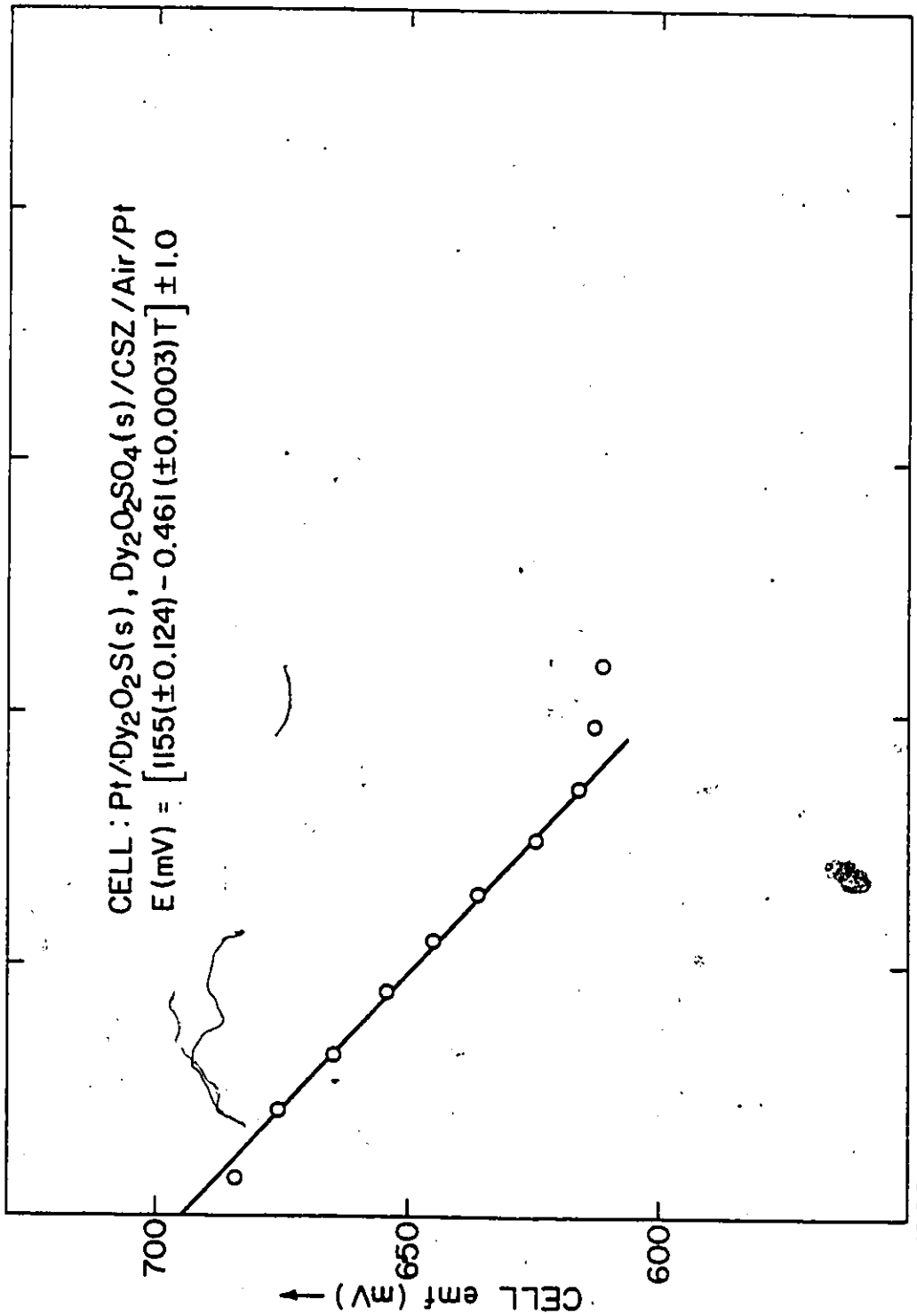

Fig. 5.4(h) The variation of emf with temperature for Cell I(h).

TABLE 5.3

TEMPERATURES AT WHICH A DEVIATION FROM THE LINEAR BEHAVIOUR WAS OBSERVED FOR THE CELLS OF TYPE I

RE (Cell No.)	Temperature (K)	Average Temperature (K)
La (I(a))	> 1500	--
Pr (I(b))	1410, 1370, 1380	1387
Nd (I(c))	1430, 1350, 1410	1397
Sm (I(d))	1320, 1360, 1300	1327
Eu (I(e))	1335, 1300, 1290	1308
Gd (I(f))	1280, 1260, 1200	1247
Tb (I(g))	1190, 1150, 1180	1173
Dy (I(h))	1170, 1160, 1170	1167

TABLE 5.4

LEAST SQUARE ANALYSIS OF EMF DATA FROM THE CELLS OF TYPE I

RE (Cell No.)	Temperature Range (K)	$E(mV) = A(\pm S_A) + B(\pm S_B)T$				Standard Deviation (mV)	Correlation Coefficient
		A (mV)	S_A (mV)	B (mV/K)	S_B (mV/K)		
La (I(a))	1100-1500	1190	0.043	-0.453	0.0001	1.5	-0.9995
Pr (I(b))	1100-1400	1158	0.085	-0.442	0.0002	2.0	-0.9980
Nd (I(c))	1100-1430	1171	0.055	-0.459	0.0002	1.5	-0.9992
Sm (I(d))	1050-1370	1175	0.151	-0.466	0.0003	3.4	-0.9961
Eu (I(e))	1020-1320	1158	0.098	-0.456	0.0003	1.8	-0.9991
Gd (I(f))	1000-1280	1156	0.038	-0.455	0.0002	1.0	-.9997
Tb (I(g))	1020-1200	1175	0.158	-0.473	0.0004	3.0	-.9939
Dy (I(h))	1040-1180	1155	0.124	-0.461	0.0003	1.0	-.9994

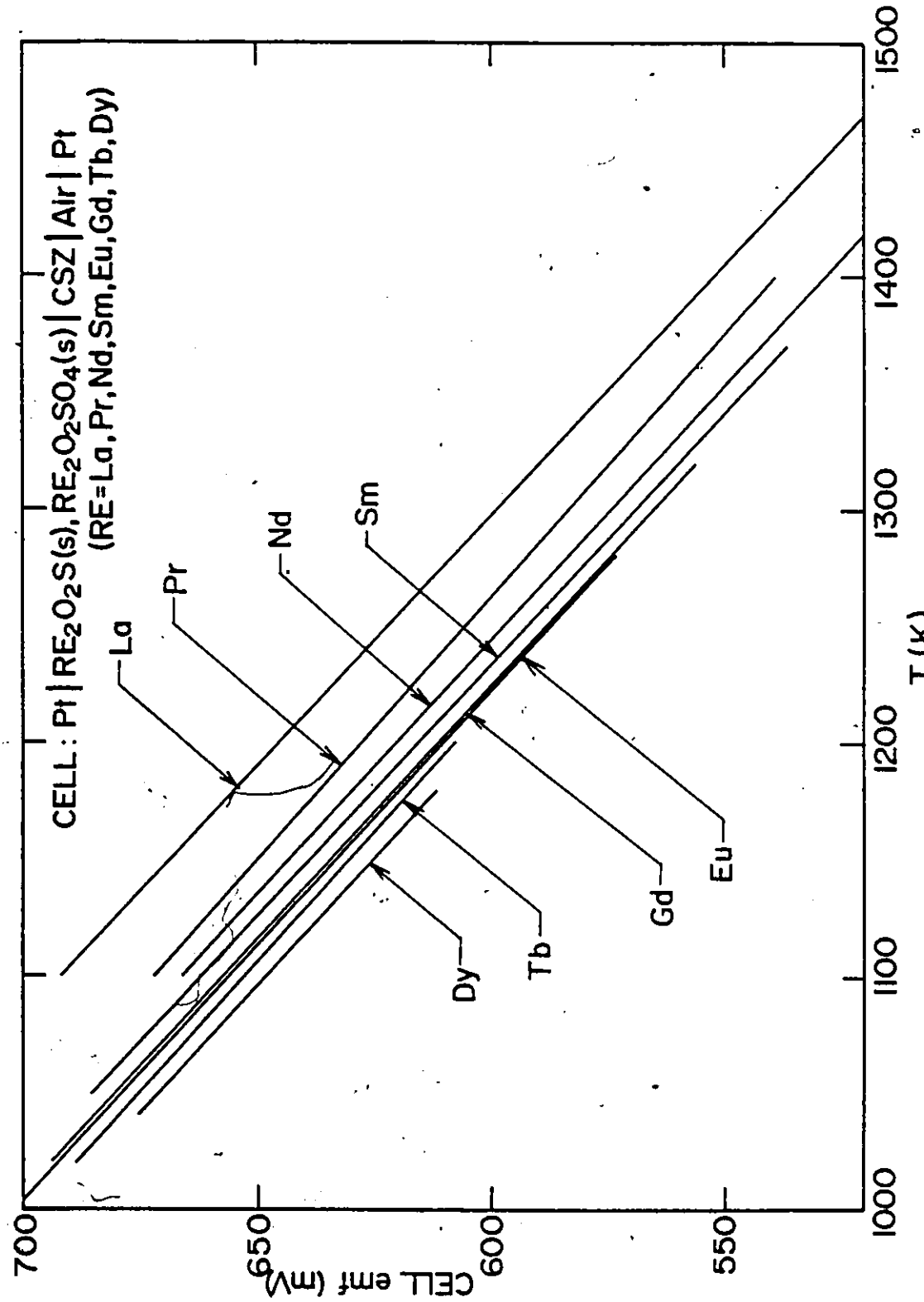

Fig. 5.5 The variation of emf with temperature for cells of Type I.

5.2.2 Analysis of the Electrode-mixtures Using X-ray Diffraction

Anode-mixtures were analysed before and after operation of a cell using X-ray diffraction. The results of such analyses for cells I(a) and I(f) are included in Figs. 5.1 and 5.2, respectively. Similar results were obtained for other Type I cells. These results confirmed the observations made in Section 5.1.1, and are presented in Table 5.5.

5.2.3 Standard Free Energies of Oxidation of Rare Earth Oxysulfides to Oxysulfates

A cell of Type I can be represented as:

$$Pt \mid RE_2O_2S(s),\ RE_2O_2SO_4(s) \mid CSZ \mid Air \mid Pt$$

The two electrode reactions can be represented as follows:

Anode: $\frac{1}{2}\ RE_2O_2S(s) + 2O^{=} = \frac{1}{2}\ RE_2O_2SO_4(s) + 4e$

Cathode: $O_2(.21\ atm) + 4e = 2O^{=}$

Thus, the virtual cell reaction can be represented by:

$$\frac{1}{2}\ RE_2O_2S(s) + O_2(.21\ atm) = \frac{1}{2}\ RE_2O_2SO_4(s)\ . \qquad (5.4)$$

From Eqn. 3.5, for a cell of Type I:

$$E = \frac{RT}{4F} \ln [P_{O_2}(.21\ atm)/P_{O_2}(Anode)]. \qquad (5.5)$$

TABLE 5.5

X-RAY DIFFRACTION ANALYSIS OF THE ELECTRODE MIXTURE

RE (Cell No.)	Composition Before Operation of the Cell	Composition Before the Break in Cell e.f vs. Temperature Plot	Composition After the Break in Cell emf vs. Temperature Plot
La (I(a))	$La_2O_2S + La_2O_2SO_4$	$La_2O_2S + La_2O_2SO_4$	-
Pr (I(b))	$Pr_2O_2S + Pr_2O_2SO_4$	$Pr_2O_2S + Pr_2O_2SO_4$	$Pr_2O_3 + Pr_2O_2S$
Nd (I(c))	$Nd_2O_2S + Nd_2O_2SO_4$	$Nd_2O_2S + Nd_2O_2SO_4$	$Nd_2O_3 + Nd_2O_2S$
Sm (I(d))	$Sm_2O_2S + Sm_2O_2SO_4$	$Sm_2O_2S + Sm_2O_2SO_4$	Sm_2O_3 (B type) + Sm_2O_2S
Eu (I(e))	$Eu_2O_2S + Eu_2O_2SO_4$	$Eu_2O_2S + Eu_2O_2SO_4$	Eu_2O_3 (B-type) + Eu_2O_2S
Gd (I(f))	$Gd_2O_2S + Gd_2O_2SO_4$	$Gd_2O_2S + Gd_2O_2SO_4$	Gd_2O_3 (C-type) + Gd_2O_2S
Tb (I(g))	$Tb_2O_2S + Tb_2O_2SO_4$	$Tb_2O_2S + Tb_2O_2SO_4$	$Tb_2O_3 + Tb_2O_2S$
Dy (I(h))	$Dy_2O_2S + Dy_2O_2SO_4$	$Dy_2O_2S + Dy_2O_2SO_4$	$Dy_2O_3 + Dy_2O_2S$

Therefore, from the measured values of E and T, the partial pressures of oxygen corresponding to oxysulfide/oxysulfate coexistence may be calculated. These values of log (P_{O_2}) are listed in Table 5.6. The standard free energy change for the reaction:

$$\frac{1}{2} RE_2O_2S(s) + O_2(g) = \frac{1}{2} RE_2O_2SO_4(s) \qquad (5.6)$$

is given by:

$$\Delta G^{o}_{5.6} = 2.303 \log(P_{O_2}(.21 \text{ atm})) - 4FE \qquad (5.7)$$

Utilizing Eqn. 5.7, from the experimentally determined values of E, $\Delta G^{o}_{5.6}$ values for various rare earth systems are calculated and are listed in Table 5.7.

5.2.4 Break in the Cell emf vs. Temperature Plot: Decomposition of Oxysulfates

A break in Cell emf vs. temperature plots was observed in all cells of Type I except those involving lanthanum compounds. The temperature at which the break occurred varied from one run to another as indicated in Table 5.3. X-ray diffraction analysis of the anode products indicated that the break occurred due to the decomposition of oxysulfate to oxide (Table 5.5).

This behaviour can be explained in terms of the diagram shown in Fig. 5.6, drawn for the gadolinium system. This diagram has been drawn using thermodynamic data from the present work and those from Ref. 3.

TABLE 5.6

OXYGEN PARTIAL PRESSURES CORRESPONDING TO OXYSULFIDE/OXYSULFATE COEXISTENCE

RE	Temperature Range (K)	$\log (P_{O_2}) = A + B/T$ (P_{O_2} in atms.)	
		A	B
La	1100–1500	8.46	-24000
Pr	1100–1400	8.23	-23360
Nd	1100–1430	8.57	-23600
Sm	1050–1370	8.72	-23670
Eu	1020–1320	8.51	-23350
Gd	1000–1280	8.50	-23300
Tb	1020–1200	8.86	-23690
Dy	1040–1180	8.61	-23290

TABLE 5.7

STANDARD FREE ENERGY CHANGES FOR OXIDATION OF OXYSULFIDE TO OXYSULFATE

REACTION: $\frac{1}{2}\ RE_2O_2S(s) + O_2(g) = \frac{1}{2}\ RE_2O_2SO_4(s)$

RE	Temperature Range (K)	ΔG^o = A + BT (cal /mole O_2) A (cal /mole O_2)	B (cal /K·mole O_2)	Standard Deviation about the Fitted Line (cal /mole O_2)	95% Conf. Interval for A (cal /mole O_2)	95% Conf. Interval for B (cal /mole O_2·K)
La	1100-1500	-109930	38.91	±140	±46	±.035
Pr	1100-1400	-106890	37.67	±180	±79	±.064
Nd	1100-1430	-108000	39.21	±140	±54	±.042
Sm	1050-1370	-108410	39.92	±310	±136	±.110
Eu	1020-1320	-106860	38.95	±180	±80	±.069
Gd	1000-1280	-106520	38.88	±90	±35	±.030
Tb	1020-1200	-108410	40.56	±280	±130	±.119
Dy	1040-1180	-106560	39.39	±90	±76	±.068

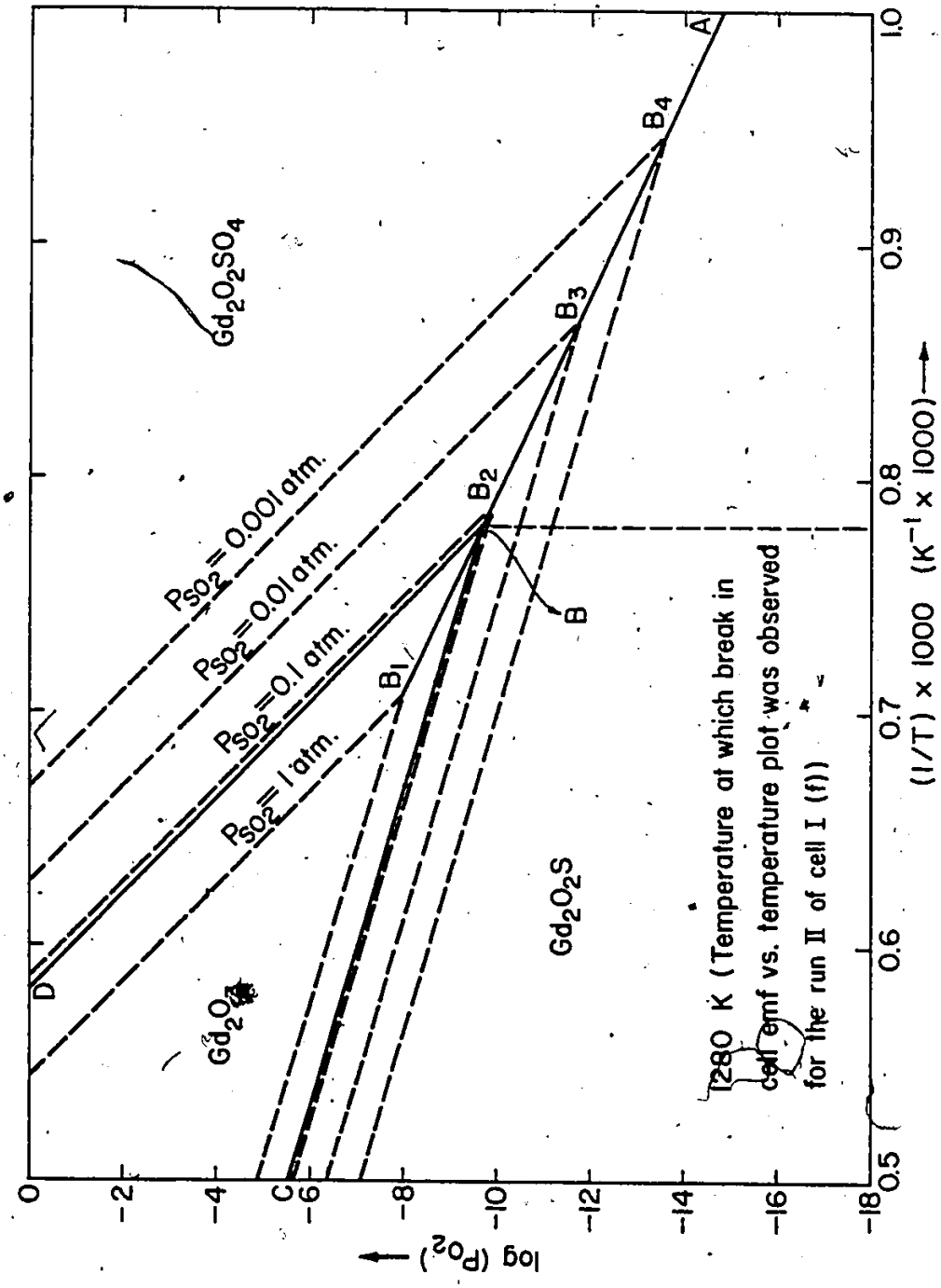

Fig. 5.6 Phase stability diagram showing the range of operation for cells of Type I and the decomposition oxysulfate in the anode. This figure has been drawn for the Gd-O-S system. Cell I(f) operates along AB. The break in the emf vs. T plot occurred at B.

It is basically a plot log (P_{O_2}) against 1/T at various constant partial pressures of SO_2. The phase boundaries between the important phases in this study are clearly indicated. From this figure, under conditions of oxysulfide/oxysulfate coexistence, the cell operates along the line AB, so that the oxygen potential established is independent of P_{SO_2}. The P_{SO_2} inside the anode is established by the partial decomposition of oxysulfate to oxide. Therefore, inside the anode compartment we actually have three condensed phases, namely, oxysulfide, oxysulfate and the oxide. Thus, AB is simply the locus of the point, determined by the above three phases. As the temperature of the cell increases, the P_{SO_2} corresponding to the oxide-oxysulfide-oxysulfate coexistence increases, causing more oxysulfate to decompose in order to establish the P_{SO_2} demanded by the above equilibrium. A condition is reached when the P_{SO_2} demanded by the oxide-oxysulfide-oxysulfate coexistence is more than that can be established by complete decomposition of the oxysulfate. At this temperature the cell no longer operates along the line AB but deviates along line BC, which corresponds to the oxide/oxysulfide equilibrium, giving a break in the cell emf vs. temperature plot. Therefore, the temperature at which a break is observed depends upon the maximum P_{SO_2} that can be established in the anode, which in turn depends upon the absolute amount of the oxysulfate present in the anode compartment. It is for this reason the break-temperature varies from one run to another.

5.2.5 Standard Entropy Change of the Reaction:

$$\frac{1}{2}\,RE_2O_2S(s) + O_2(g) = \frac{1}{2}RE_2O_2SO_4(s)$$

If it is assumed that the standard enthalpy change, $\Delta H^{\circ}_{5.6}$ and the standard entropy change, $\Delta S^{\circ}_{5.6}$, of Reaction 5.6 do not vary with temperature, then $\Delta S^{\circ}_{5.6}$ and $\Delta H^{\circ}_{5.6}$ can be equated to -B and A, in Table 5.7, respectively. It is noticed that $\Delta S^{\circ}_{5.6}$ does not vary much from one rare system to another and has an average value of about -39 cal /K.mole O_2. Since $\Delta S^{\circ}_{5.6}$ can also be written as:

$$\Delta S^{\circ}_{5.6} = \frac{1}{2}\,S^{\circ}_{RE_2O_2SO_4} - \frac{1}{2}\,S^{\circ}_{RE_2O_2S} - S^{\circ}_{O_2}$$

where S° denotes the standard entropy function of a substance and $S^{\circ}_{O_2}$ is about 60 cal /K.mole in the temperature range under consideration, we obtain:

$$S^{\circ}_{RE_2O_2SO_4} - S^{\circ}_{RE_2O_2S} \approx 40 \text{ cal /mole.K}$$

A positive value of $(S^{\circ}_{RE_2O_2SO_4} - S^{\circ}_{RE_2O_2S})$ indicates that the structure of $RE_2O_2SO_4$ is substantially disordered* compared to that of RE_2O_2S. The structure of oxysulfates, determined by Fahey (57), when compared with the hexagonal close-packed structure of oxysulfides, confirms this point.

---

* considering only configurational entropy.

5.2.6 Errors in the Standard Free Energy Changes for the Reaction:

$\frac{1}{2}RE_2O_2S(s) + O_2(g) = \frac{1}{2}RE_2O_2SO_4(s)$.

In addition to the statistical error (Appendix A gives details), there are experimental errors arising mainly from the measurement of cell emf and temperature. A 2K uncertainty in the measurement of temperature and a 1mV uncertainty in the measurement of cell emf will together contribute an error of about $\pm$180 cal in $\Delta G^{\circ}_{5.7}$ in addition to the statistical error.

5.2.7 Limitations of the Cells of Type I

Cells of Type I are applicable only to rare earth systems which have a stable oxysulfate in the temperature and oxygen partial pressure ranges in which calcia stabilized zirconia acts as an electrolyte. Thus, the systems involving rare earths heavier than dysprosium can not be studied using cells of Type I because the oxysulfate is unstable in the temperature range in which CSZ is a fully ionic conductor. Even in cases where Type I cells are applicable, the working temperature range is restricted by the decomposition of the oxysulfate and the resistance polarization of the cells. These are important limitations of Type I cells.

5.3 Results from the Cells of Type II

5.3.1 EMF Data from the Cells of Type II

EMF data from the cells of Type II are presented in Table 5.8 and Figures 5.7 (a) and (b). The cell emf is found to vary linearly with temperature. The data from these cells when compared with the data from the corresponding cells of Type I indicate that the two are identical. Table 5.9, in which the emf values obtained from cells of Type II for La and Nd are compared with those obtained from the corresponding cells of Type I, clearly demonstrates this point. Thus, for a particular system, cells of Type I and II really examine the same phase boundary, i.e., the phase boundary between the oxysulfide and oxysulfate. This also indicates that the phase boundary between the oxysulfide and oxysulfate in a phase stability diagram (similar to Fig. 3.6) is parallel to the $\log(P_{S_2})$ axis.

Tables 5.10 and 5.11 list the results obtained from cells of Type II.

5.3.2 Analysis of Anode Products

Anodes constructed in Configuration II were examined by X-ray diffraction. The components in the lower and upper layers were easily identifiable. However, anodes constructed in Configuration III, when examined by X-ray diffraction, gave lines corresponding to silver only, due to its large amount. Thus, in this case, other components in the anode could not be identified. Therefore, anodes constructed in Configuration III (Fig. 4.4) were examined metallographically. Since

TABLE 5.8

EMF DATA FOR THE CELLS OF TYPE II

Temperature (K)	Cell emf (V)
Lanthanum System (Type II(a)	
1246.50	.623
1233.80	.629
1208.20	.641
1201.50	.644
1186.70	.651
1154.90	.666
1132.40	.676
1113.20	.684
1088.80	.695
1065.70	.705
1037.00	.717
1015.50	.726
1015.50	.727
990.90	.738
959.10	.753
953.00	.756
1075.00	.701
1076.00	.701
1035.00	.722
1040.10	.721
964.10	.750
980.70	.743
1024.70	.723
1193.20	.648
1174.00	.657
1152.50	.667
1139.50	.673
1126.20	.679
1118.00	.683
1109.50	.687
1104.70	.689
1087.80	.697
1051.70	.714
951.90	.760
986.80	.745
1024.00	.726
1094.40	.692
1059.60	.708
1061.30	.707
977.60	.740

TABLE 5.8 (continued)

Temperature (K)	Cell emf (V)
Neodymium System (Type II(b))	
1063.70	.684
1049.30	.690
1035.00	.697
1021.10	.702
1037.00	.696
1029.40	.697
1082.00	.677
1199.60	.619
1187.00	.627
1160.00	.639
1151.00	.645
1133.00	.653
1115.50	.661
1099.60	.668
1081.00	.677
1054.50	.690
1056.20	.689
1033.00	.699
1017.60	.705
1018.00	.704

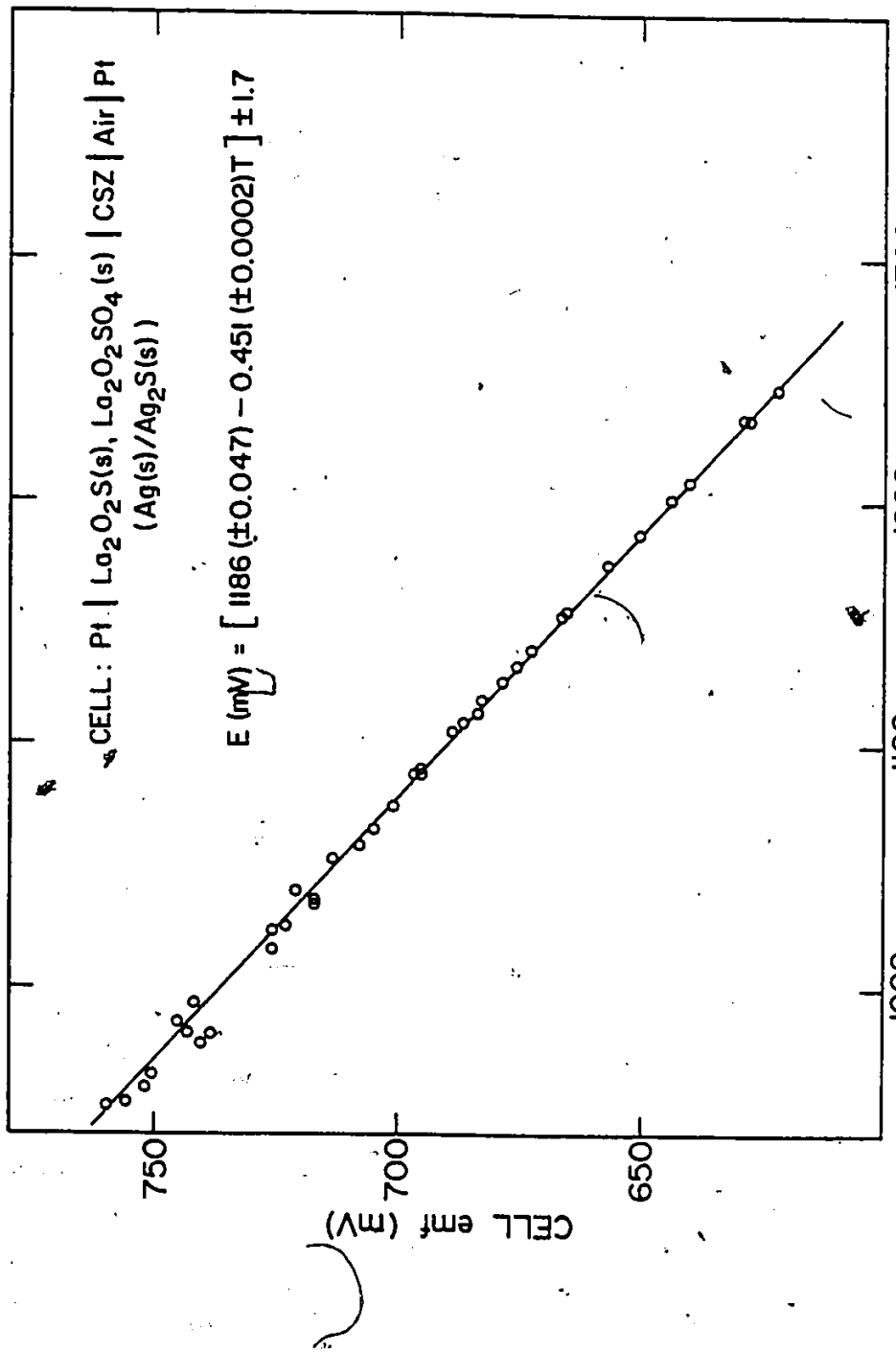

Fig. 5.7(a) The variation of emf with temperature for Cell II(a).

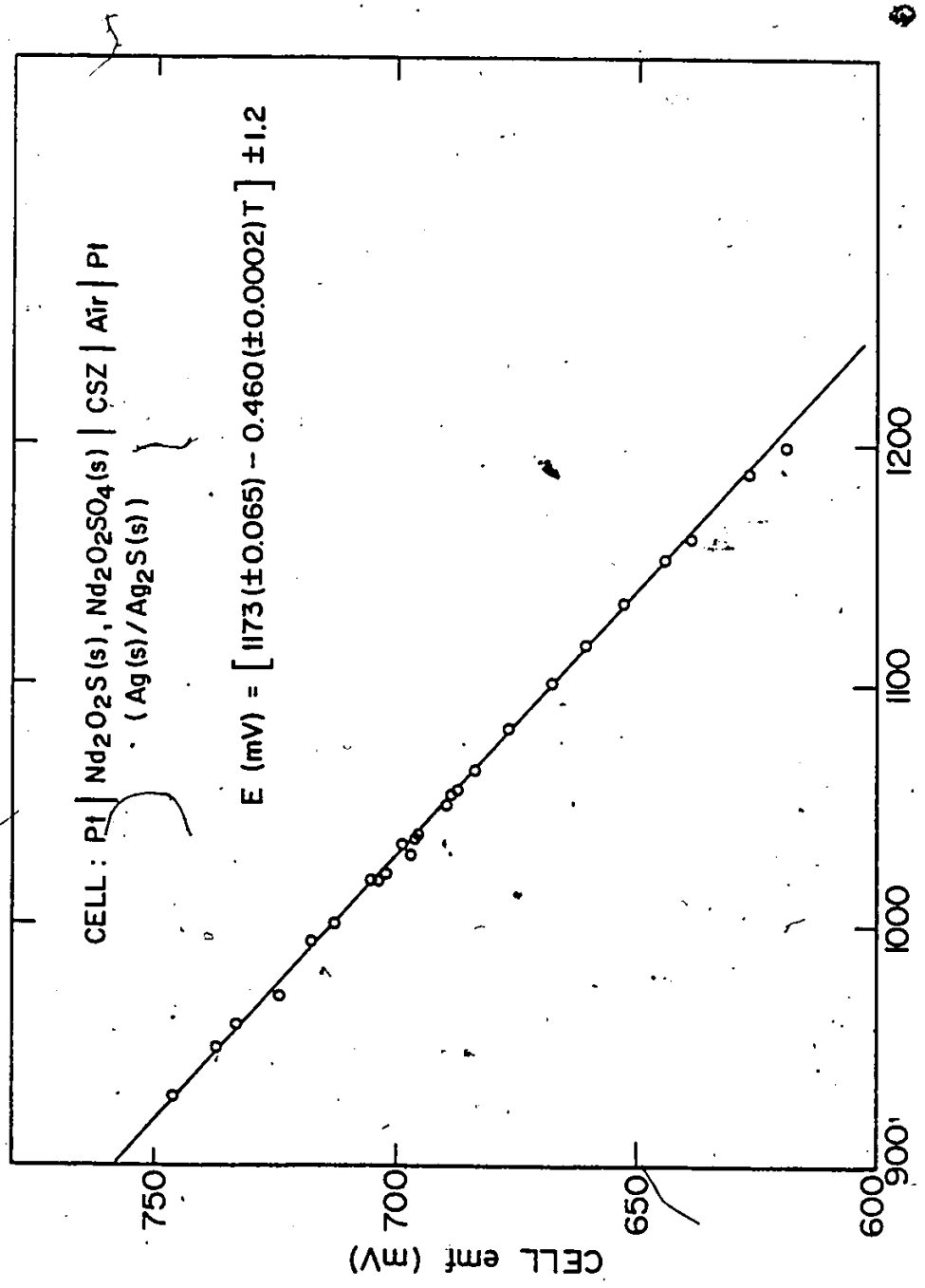

Fig. 5.7(b) The variation of emf with temperature for Cell II(b).

TABLE 5.9

COMPARISON OF THE EMF DATA OBTAINED FROM THE CELLS OF TYPE I AND TYPE II

Temperature (K)	Lanthanum System Cell emf (mV) Type I	Type II	Difference	Neodymium System Cell emf (mV) Type I	Type II	Difference
1000	737*	735	+2	712*	713	-1
1050	714*	712	+2	689*	690	-1
1100	692	690	+2	666	667	-1
1150	669	667	+2	643	644	-1
1200	647	645	+2	620	621	-1
1250	623	621	+2	597	598*	-1
1300	601	599*	+2	574	575*	-1
1350	578	576*	+2	551	552*	-1
1400	556	554*	+2	528	529*	-1
1450	533	531*	+2	505*	506*	-1
1500	511	509*	+2	482*	483*	-1

* Extrapolated

TABLE 5.10

LEAST SQUARE ANALYSIS OF EMF DATA FROM THE CELLS OF TYPE II

RE (Cell No.)	Temperature Range (K)	$E(mV) = A(\pm S_A) + B(\pm S_B)T$				Standard Deviation (mV)	Correlation Coefficient
		A (mV)	S_A (mV)	B (mV/K)	S_B (mV/K)		
La (II(a))	940-1250	1186	.047	-.451	.0002	1.7	-.9989
Nd (II(b))	930-1200	1173	.065	-.460	.0002	1.2	-.9989

TABLE 5.11

STANDARD FREE ENERGY CHANGE FOR OXIDATION OF OXYSULFIDE TO OXYSULFATE IN PRESENCE OF

Ag/Ag_2S, REACTION: $\frac{1}{2} RE_2O_2S(s) + O_2(g) = \frac{1}{2} RE_2O_2SO_4(s)$

RE	Temperature Range (K)	$\Delta G^\circ = A + BT$ (cal /mole O_2)		Standard Deviation about the Fitted Line (cal /mole O_2)	95% Conf. Interval for A (cal /mole O_2)	95% Conf. Interval for B (cal /mole O_2·K)
		A (cal /mole O_2)	B (cal /K·mole O_2)			
La	940-1250	-109460	38.49	160	50	.046
Nd	930-1200	-108240	39.32	110	56	.051

the anode components, RE_2O_2S, $RE_2O_2SO_4$, Ag_2S and Ag, were present in a molar ratio of 1:1:2:4 or 1:1:1:3, it was difficult to identify phases other than Ag and Ag_2S. However, in some cells which were heated beyond the melting point of silver, the rare earth compounds segregated together and it was possible to see them under a microscope. Figs. 5.8 (a) and (b) show micrographs of electrodes used in a Type II cell heated to temperatures below and above the melting point of silver, respectively. Under metallographic examination only three phases (Ag, Ag_2S and an RE containing phase) were identifiable. The segregated portion of the electrode was examined by x-ray diffraction which indicated that the RE containing phase was a mixture of oxysulfide and oxysulfate, the latter being present in larger proportions. This observation confirms the results of coexistence studies reported in Section 5.1.

5.3.3 Possibility of Secondary Reactions within the Anode

Because of the presence of four condensed phases, namely, RE_2O_2S, $RE_2O_2SO_4$, Ag and Ag_2S, in the anode compartment, the possibility of reactions other than the one represented by the virtual cell reaction has to be considered. As noted in Section 5.1.5, no reaction takes place between the rare earth compounds and Ag or Ag_2S.

Palazzi et al. (90) have reported the formation of a compound between Ag_2S and La_2O_2S with a chemical formula (LaO)AgS. The authors have also reported that this compound decomposes into Ag_2S and La_2O_2S at about 1023K. In the present study, no evidence indicating the formation

Fig. 5.8 Micrographs of the electrode mixture consisting of La_2O_2S, $La_2O_2SO_4$, Ag_2S and Ag in a molar ratio 1:1:2:4 after use at a temperature
(a) below the melting point of Ag_2S
(b) above the melting point of Ag
The bright phase is Ag; the darker phase is Ag_2S; and the rare earth phases are dispersed in the Ag_2S phase.

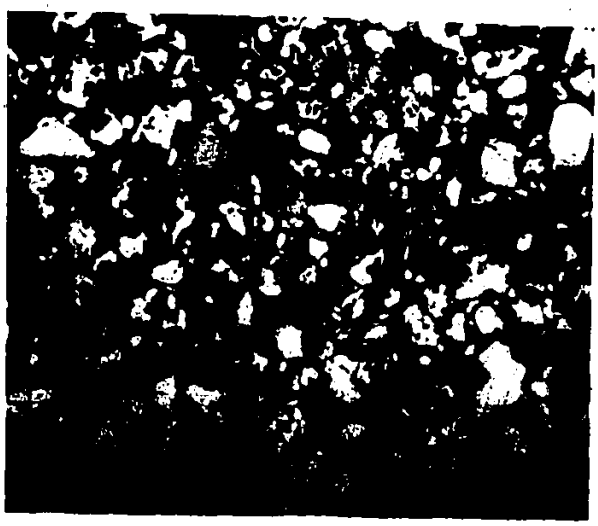

(a) X600

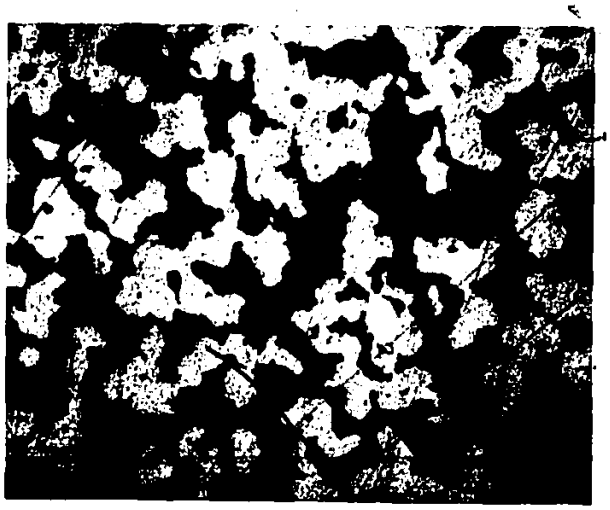

(b) X600

of such a compound was found. Since emf values of the Type II cell are very close to those obtained in the corresponding Type I cell, La_2O_2S and $La_2O_2SO_4$ present in the anode of Type II cell must be in an uncombined form (x-ray diffraction analysis in Section 5.3.2 confirms this assertion).

There is no possibility of Ag_2O formation at the temperatures and oxygen partial pressures prevailing in the anode compartment, since Ag_2O is extremely unstable under these conditions. Also, the possibility of Ag_2SO_4 formation may be discounted because the oxygen partial pressures required for the conversion of Ag_2S to Ag_2SO_4 are much higher than those prevailing inside the anode compartment of a cell of Type II. The above two points are illustrated in Fig. 5.8.

5.4 Results from Type III Cells

5.4.1 EMF Data from Type III Cells

The experimental data from cells of Type III are presented in Tables 5.12 and Figures 5.10 (a) to (f). Figure 5.11 summarizes the results from all cells of Type III. A straight line relationship between the cell emf and temperature is followed in the temperature range in which cells of Type III are operational. All cells of Type III were operated up to the liquidus temperature of sulfur saturated Cu containing some oxygen (the oxygen content depends upon the rare earth system under study). When the Cu phase melts, it combines with the Pt lead wire and renders the cell inoperable. A discussion on this phenomenon and the limitations of cells of Type III will follow in

Fig. 5.9 Variation of anode oxygen partial pressure with temperature for Cell II(a) and II(b). The higher values of $\log(P_{O_2})$ for Ag_2O/Ag and Ag_2S/Ag_2SO_4 equilibria indicate that the formation of Ag_2O and Ag_2SO_4 is highly unlikely.

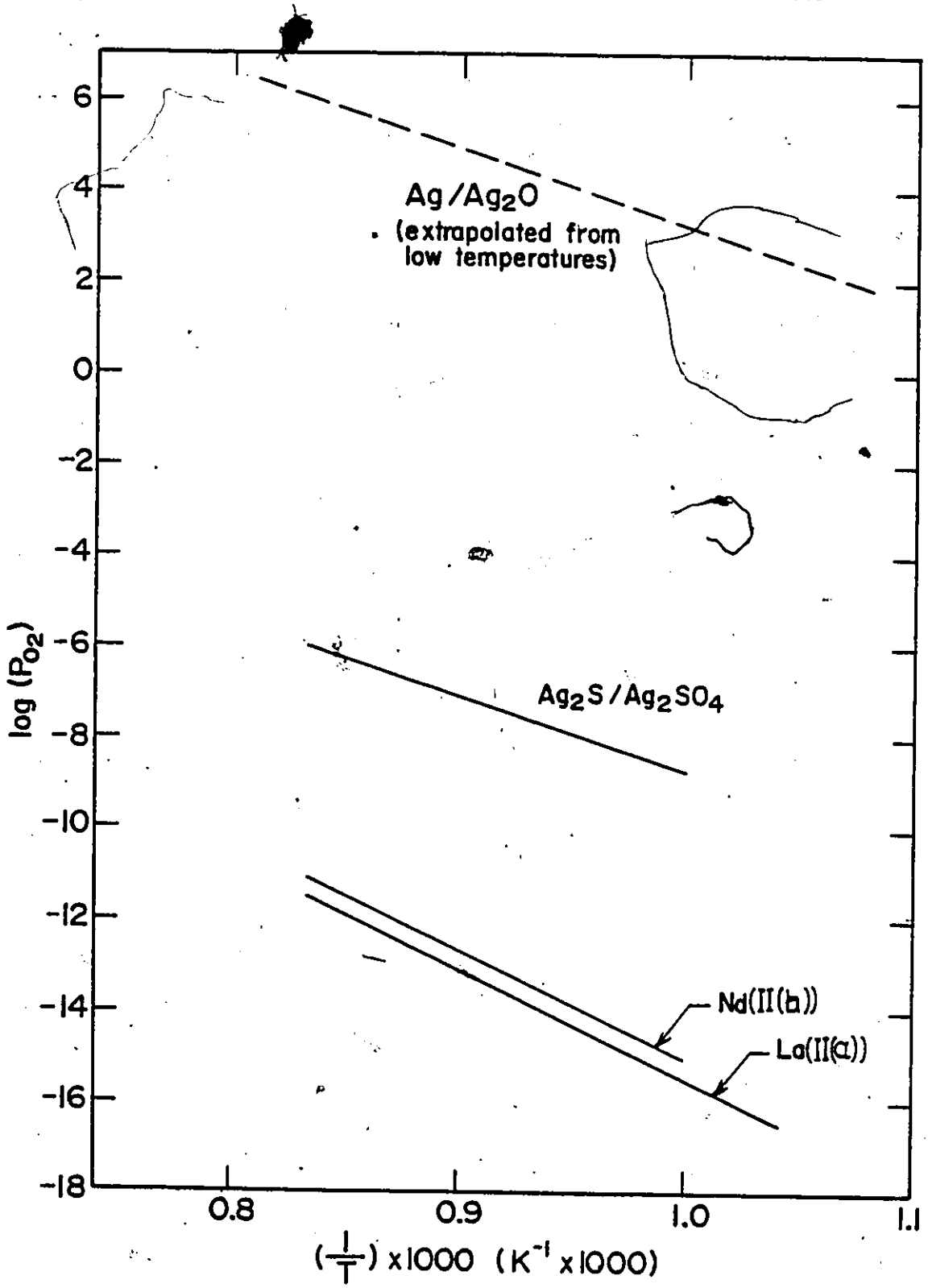
Ag/Ag2O
(extrapolated from low temperatures)
Ag2S/Ag2SO4
Nd(II(b))
La(II(a))
log (Po2)
6
4
2
0
-2
-4
-6
-8
-10
-12
-14
-16
-18
0.8
0.9
1.0
1.1
(1/T) x1000 (K-1 x1000)

TABLE 5.12

EMF DATA FOR THE CELLS OF TYPE III

Temperature (K)	Cell emf (V)
Lanthanum System (Type III(a))	
1140.60	.630
1140.60	.630
1140.50	.630
1162.00	.619
1179.00	.611
1196.00	.602
1212.30	.593
1231.30	.583
1249.20	.573
1251.20	.573
1266.60	.564
1282.30	.555
1302.50	.544
1302.00	.545
1318.00	.536
1331.00	.528
1347.60	.520
1364.00	.513
1376.80	.507
Praseodymium System (Type III(b))	
1181.60	.573
1212.30	.556
1240.00	.541
1150.80	.588
1116.00	.608
1083.00	.623
1098.00	.616
1128.20	.600
1165.70	.582
1195.90	.564
1225.60	.548
1255.00	.533
1274.80	.522
1288.00	.514
1309.70	.503
1329.00	.493
1347.60	.484

TABLE 5.12 (continued)

Temperature (K)	Cell emf (V)
Neodymium System (Type III(c))	
1230.20	.535
1261.00	.518
1210.20	.545
1186.20	.557
1185.70	.558
1137.00	.582
1106.70	.600
1045.20	.624
1285.00	.504
1284.00	.506
1304.50	.494
1339.40	.475
1300.00	.495
1087.20	.609
1161.00	.570
1247.10	.525
Samarium System (Type III(d))	
1103.00	.576
1143.60	.555
1160.50	.547
1189.00	.532
1179.50	.537
1125.50	.561
1108.00	.569
1209.00	.522
1230.00	.511
1252.70	.500
1273.80	.488
1297.80	.473

TABLE 5.12 (continued)

Temperature (K)	Cell emf (V)
Europium System (Type III(e))	
1103.00	.556
1117.00	.550
1134.00	.542
1150.00	.535
1164.00	.528
1180.00	.520
1198.00	.510
1217.00	.501
1235.00	.492
1254.00	.483
1276.00	.472
1292.00	.461
1310.00	.454
1324.00	.443
1336.00	.435
Gadolinium System (Type III(f))	
1159.00	.518
1190.00	.504
1219.40	.490
1238.00	.481
1261.00	.469
1285.50	.455
1292.00	.453
1288.00	.454
1311.00	.448
1176.00	.512
1206.00	.497
1248.00	.475
1276.00	.461

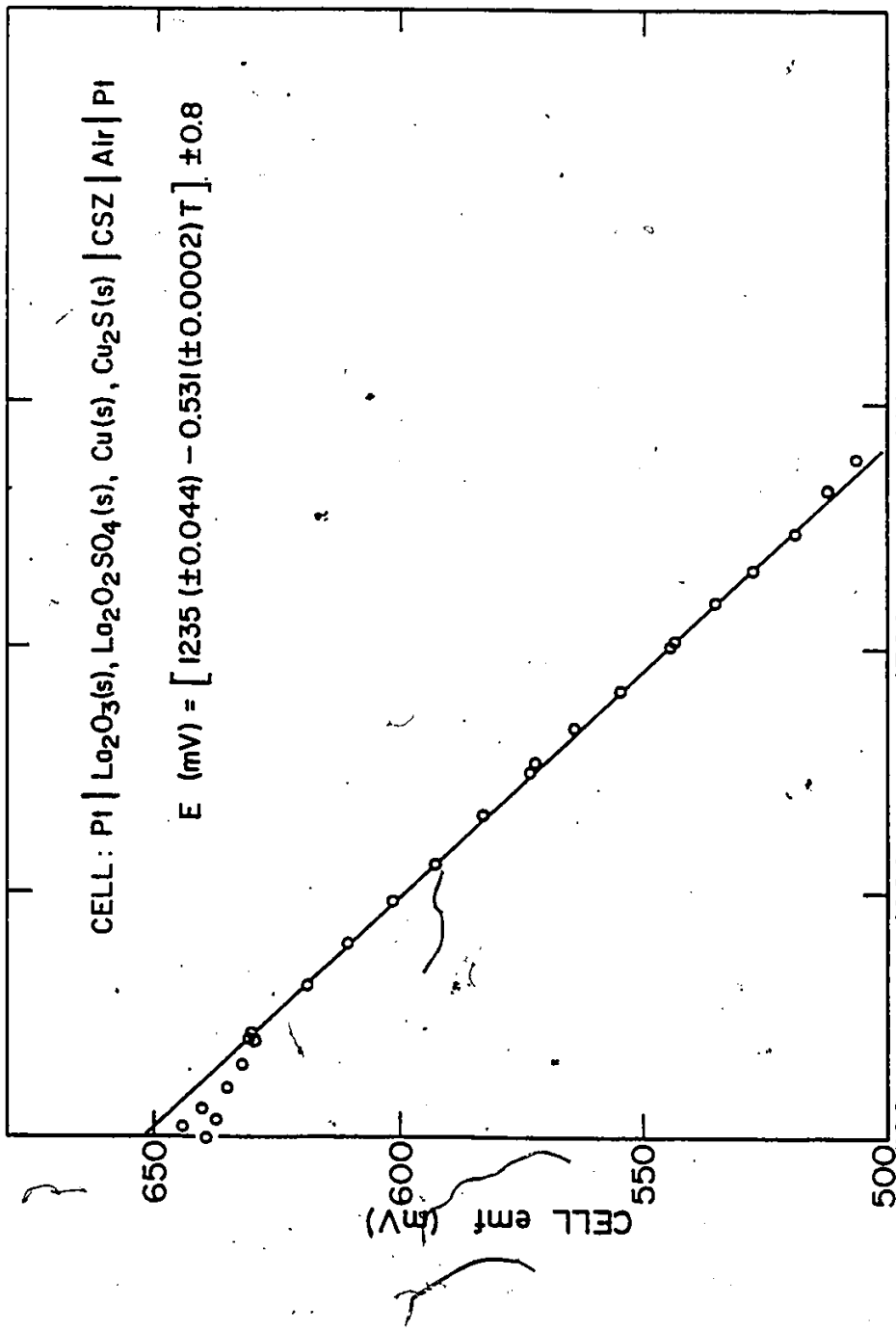

Fig. 5.10(a) The variation of emf with temperature for Cell III(a).

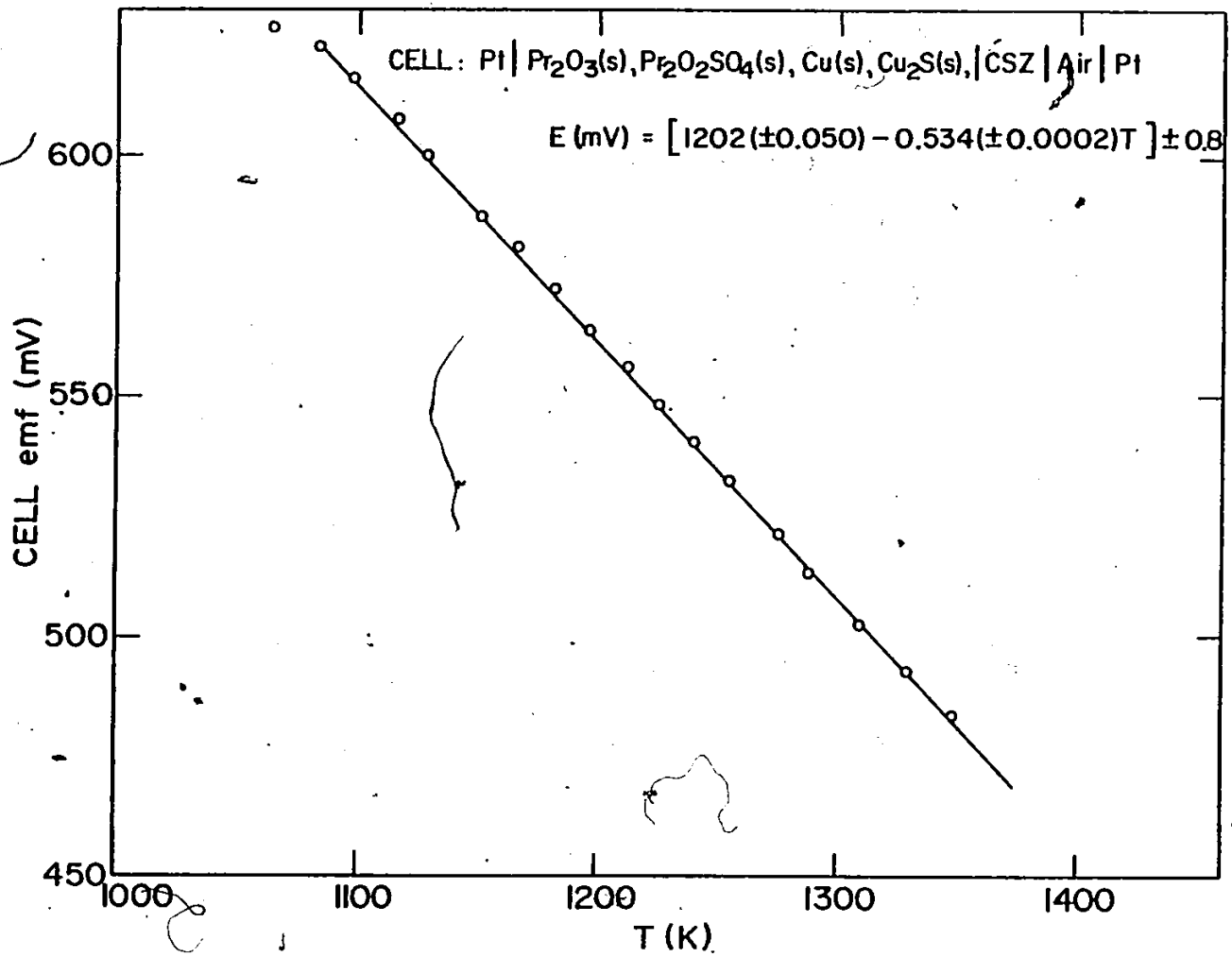

Fig. 5.10(b) The variation of emf with temperature for Cell III(b).

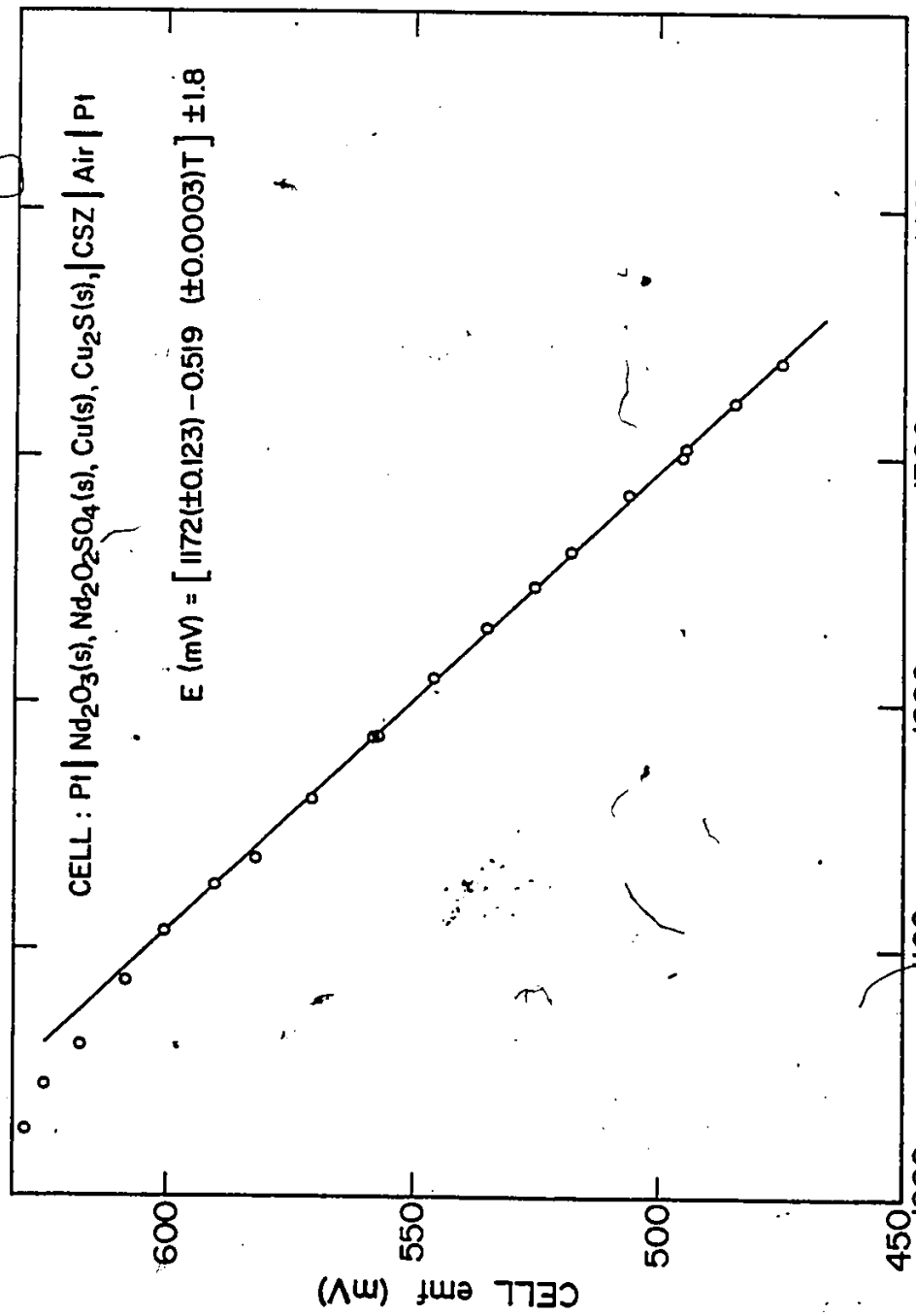

Fig. 5.10(c) The variation of emf with temperature for Cell III(c).

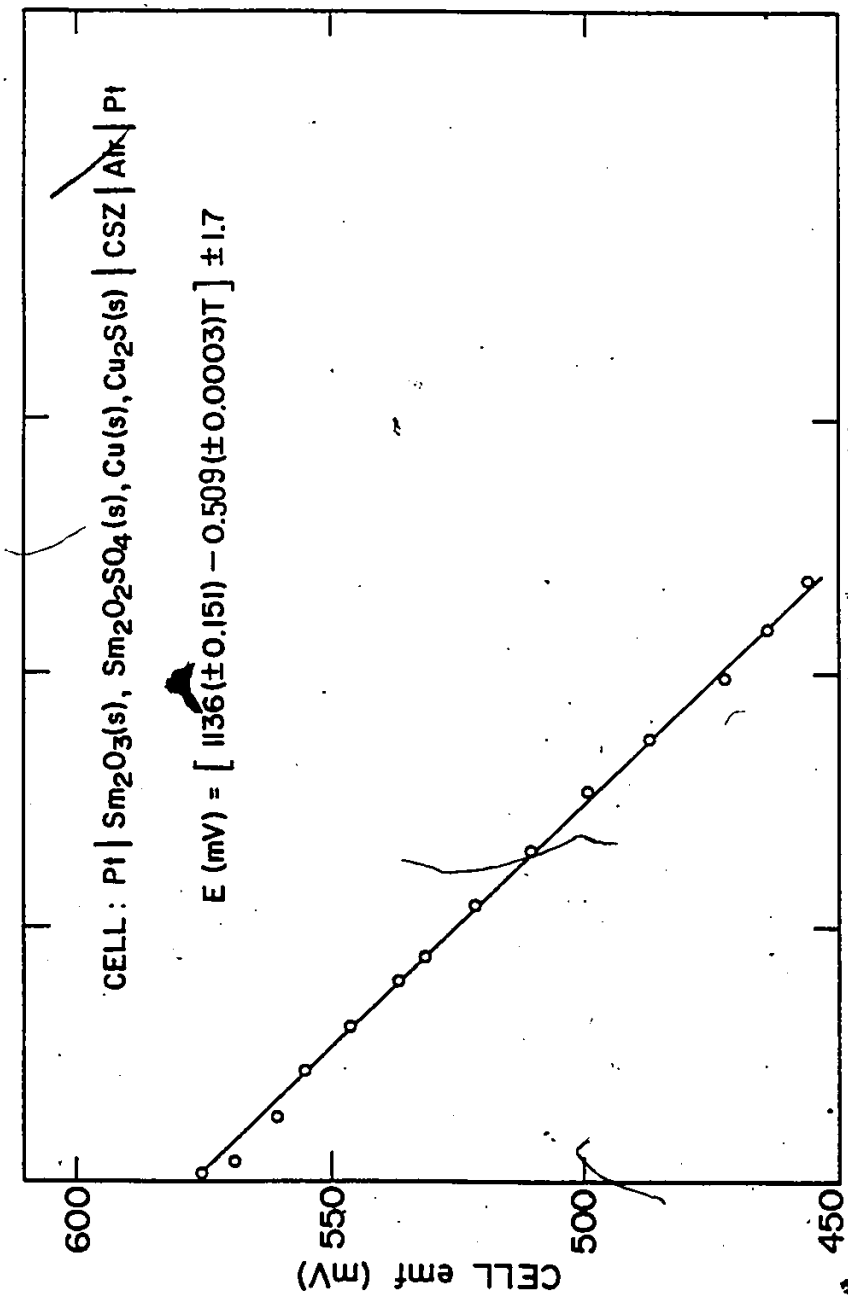

Fig. 5.10(d) The variation of emf with temperature for Cell III(d).

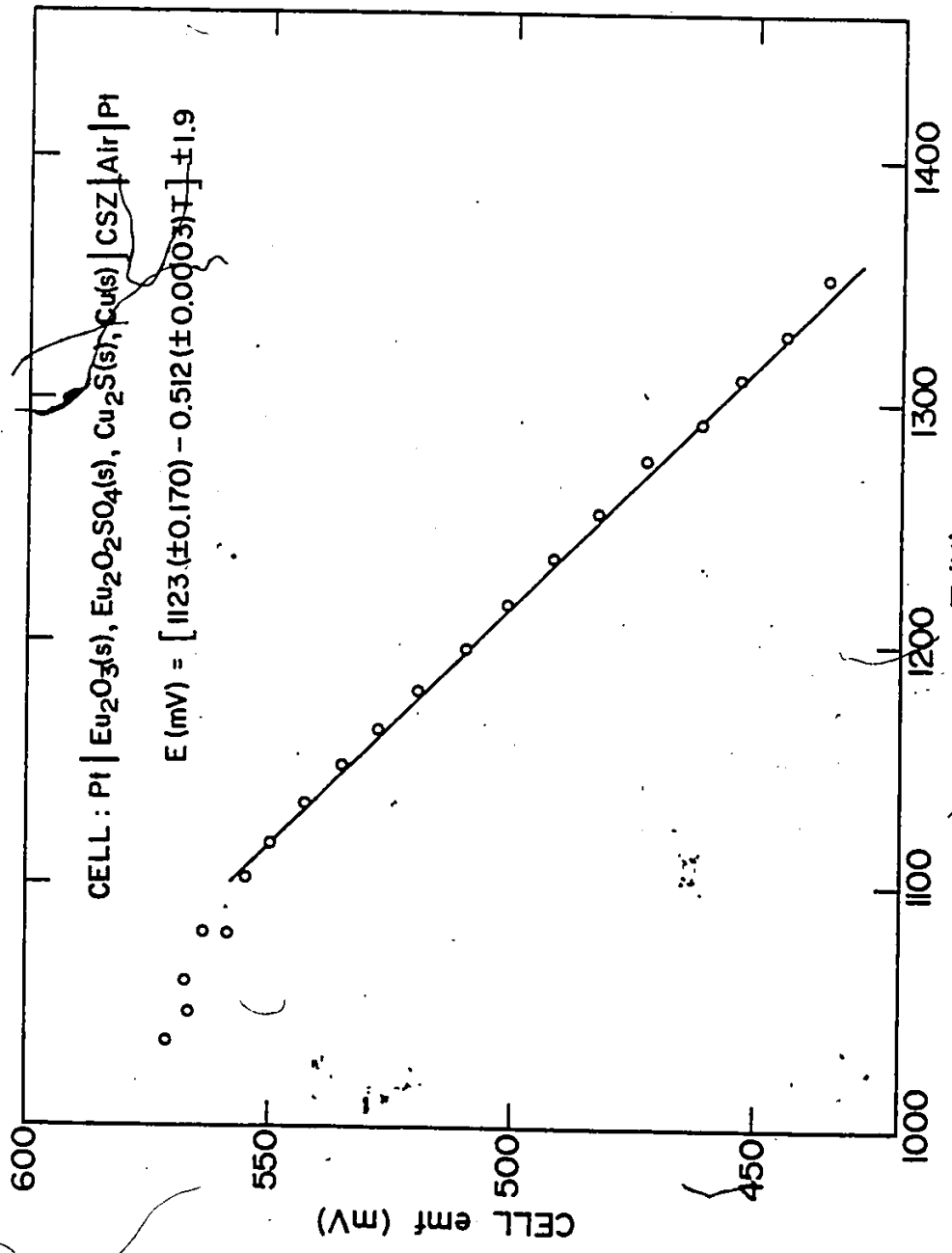

Fig. 5.10(e) The variation of emf with temperature for Cell III(e).

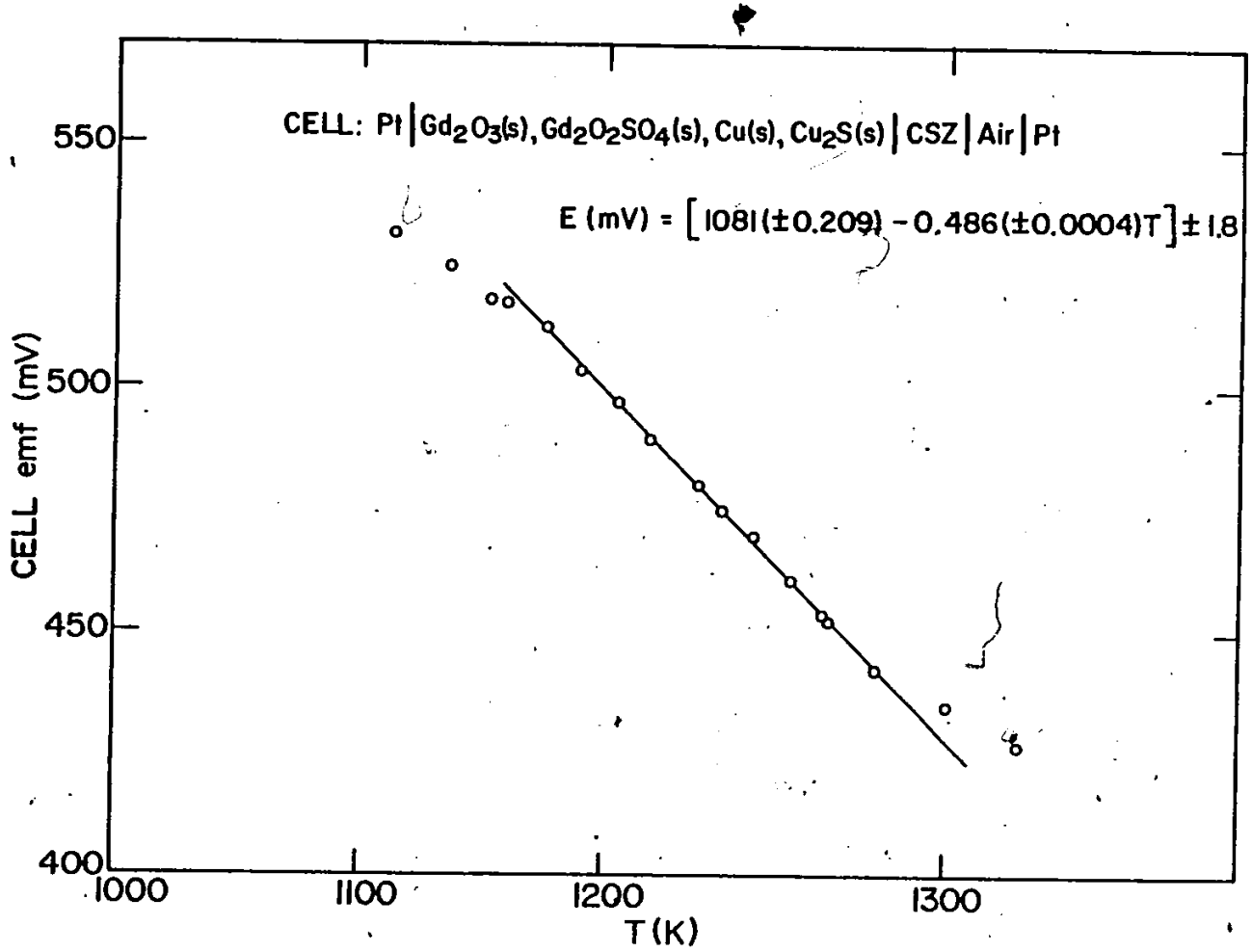

Fig. 5.10(f) The variation of emf with temperature for Cell III(f).

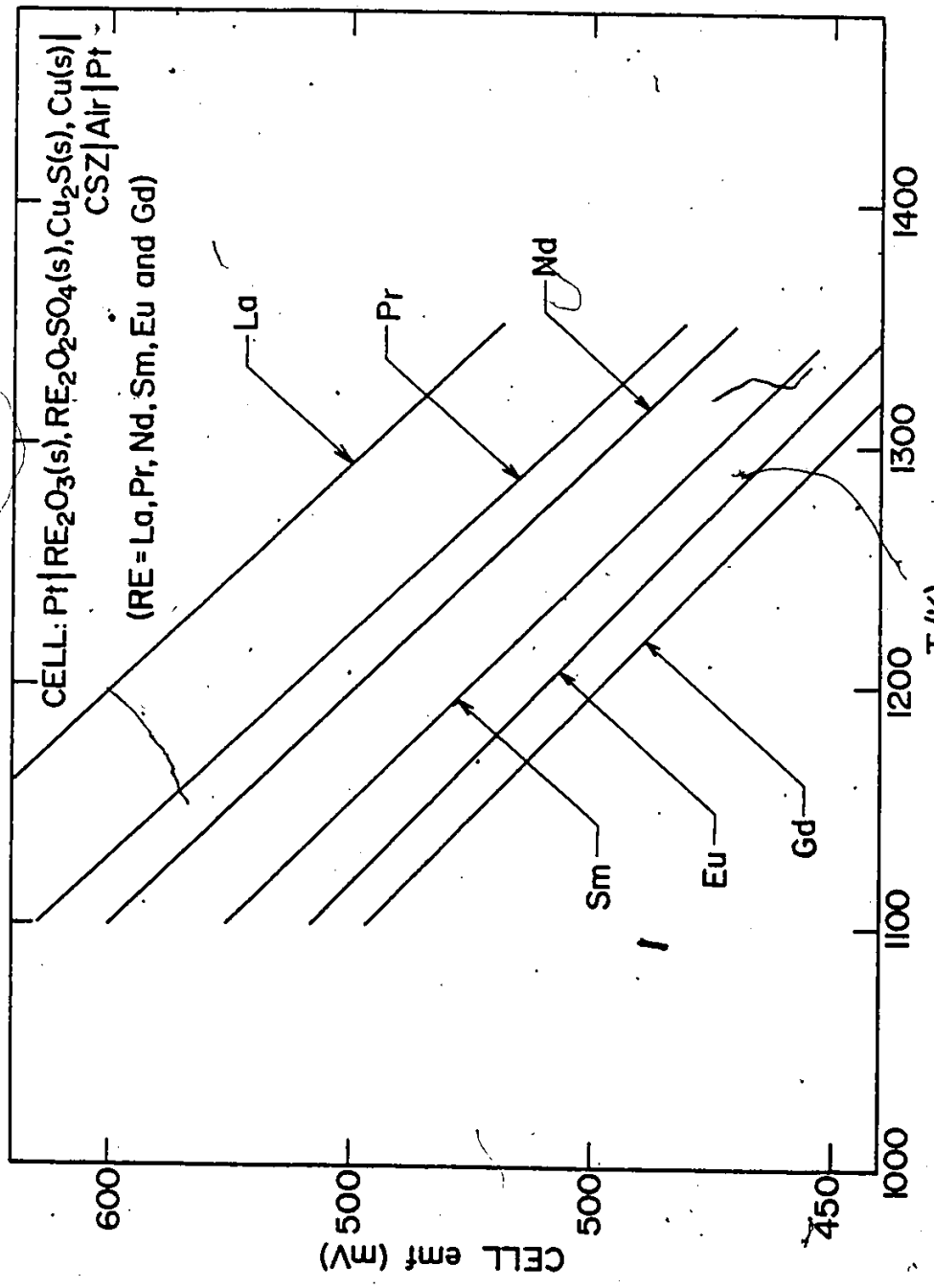

Fig. 5.11 Variation of emf with temperature for cells of Type III.

Section 5.4.6. The linear portion of a cell emf vs. temperature plot was analysed using linear regression analysis. Equations of the best-fit lines are given in Table 5.13.

5.4.2 Analysis of the Anode Products

The products in the anodes of Configuration II could be easily analysed by X-ray diffraction. The results from such analyses are presented in Table 5.14, and indicate that oxides of RE elements coexist with their corresponding oxysulfates at sulfur potentials fixed by the Cu/Cu_2S couple.

The products in the anodes constructed in Configuration III were analysed microscopically. However, it was possible to identify only the Cu-rich and the Cu_2S-rich phase under a microscope, the rare earth phases being too small and too widely dispersed. In some electrodes which were heated above the melting point of Cu_2S, rare earth compounds segregrated into the Cu_2S-rich phase. However, even in these electrodes, different rare earth compounds could not be distinguished by a microprobe because of the small size of the rare earth phases and the strong background of sulfur from Cu_2S. Figure 5.12 shows micrographs of an electrode, which was heated to a temperature above the melting point of Cu_2S, at different magnifications. When the Cu_2S-rich part of such an electrode was examined by X-ray diffraction, the presence of both oxide and oxysulfate, with oxysulfate present in major proportions, was indicated. Thus, during the cell operation, some of the oxide is converted to oxysulfate. Because of problems associated with the

TABLE 5.13

LEAST SQUARE ANALYSIS OF THE EMF DATA FROM THE CELLS OF TYPE III

CELL: $Pt|RE_2O_3(s), RE_2O_2SO_4(s), Cu_2S(s), Cu(s)|CSZ|Air|Pt$

RE (Cell No.)	Temperature Range (K)	$E(mV) = A(\pm S_A) + B(\pm S_B)T$				Standard Deviation (mV)	Correlation Coefficient
		A (mV)	S_A (mV)	B (mV/K)	S_B (mV/K)		
La (III(b))	1140-1340	1235	.044	-0.5306	.0002	0.80	-.9998
Pr (III(b))	1080-1340	1202	.050	-0.5358	.0002	0.80	-.9998
Nd (III(c))	1040-1340	1172	.123	-0.5196	.0003	1.80	-.9992
Sm (III(d))	1100-1300	1136	.151	-0.5091	.0003	1.70	-.9987
Eu (III(e))	1100-1320	1123	.170	-0.5117	.0003	1.90	-.9988
Gd (III(f))	1160-1310	1081	.209	-0.4855	.0004	1.80	-.9978

TABLE 5.14

X-RAY DIFFRACTION ANALYSIS OF THE BOTTOM LAYER OF ANODES CONSTRUCTED IN CONFIGURATION II

RE	Composition of the Bottom Layer Before Operation of the Cell	Composition of the Bottom Layer After Operation of the Cell	Comment
La	$La_2O_3 + La_2O_2SO_4$	$La_2O_3 + La_2O_2SO_4$	Amount of Oxysulfate increases
Pr	$Pr_2O_3 + Pr_2O_2SO_4$	$Pr_2O_3 + Pr_2O_2SO_4$	Same as above
Nd	$Nd_2O_3 + Nd_2O_2SO_4$	$Nd_2O_3 + Nd_2O_2SO_4$	Same as above
Sm	Sm_2O_3 (B type) + $Sm_2O_2SO_4$	Sm_2O_3 (B type) + $Sm_2O_2SO_4$	Same as above
Eu	Eu_2O_3 (B type) + $Eu_2O_2SO_4$	Eu_2O_3 (B type) + $Eu_2O_2SO_4$	Same as above
Gd	Gd_2O_3 (C type) + $Gd_2O_2SO_4$	Gd_2O_3 (C type) + $Gd_2O_2SO_4$	Same as above

Fig. 5.12 Micrographs of the electrode mixture consisting of La_2O_3, $La_2O_2SO_4$, Cu_2S, Cu in the molar ratio 1:1:2:4 after use at a temperature above the melting point of Cu_2S at two different magnifications. In both micrographs , the bright phase is Cu; the darker phase is Cu_2S; the darkest area consist of the rare earth compounds.

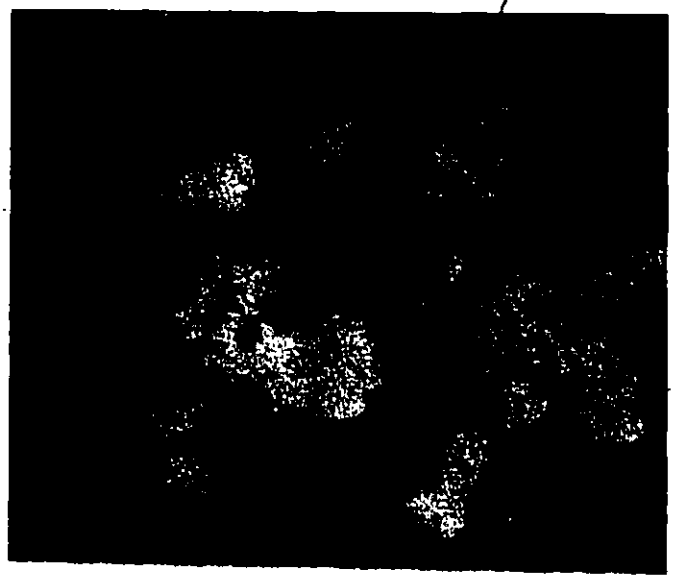

X200

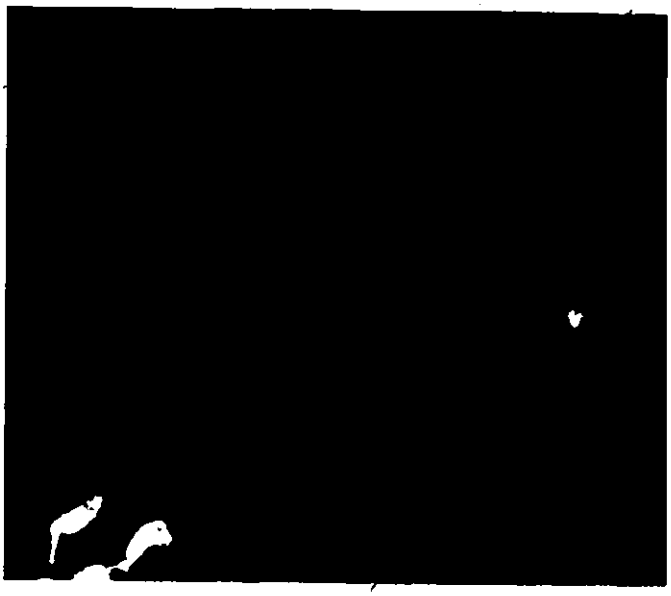

X900

analysis of the products in an anode constructed in Configuration III, more than 50% of the studies were done using anodes in Configuration II, in which case products could easily be identified by X-ray diffraction techniques.

5.4.3 Standard Free Energy Changes for the Virtual Cell Reaction:

$$\frac{2}{3}\,RE_2O_3(s) + \frac{2}{3}\,Cu_2S(s) + O_2(g) = \frac{2}{3}\,RE_2O_2SO_4 + \frac{4}{3}\,Cu(s)$$

The cells of Type II can be represented as:

$$Pt \mid RE_2O_3(s),\ RE_2O_2SO_4(s),\ Cu_2S(s),\ Cu(s) \mid CSZ \mid Air \mid Pt$$

and two electrode reactions can be represented as follows:

Anode: $\frac{2}{3}\,RE_2O_3(s) + \frac{2}{3}\,Cu_2S(s) + 2O^{=} = \frac{2}{3}\,RE_2O_2SO_4(s) + \frac{4}{3}\,Cu(s) + 4e$

Cathode: $4e + O_2(.21\ atm) = 2O^{=}$

Thus, the virtual cell reaction can be represented by:

$$\frac{2}{3}\,RE_2O_3(s) + \frac{2}{3}\,Cu_2S(s) + O_2(.21\ atm) = \frac{2}{3}\,RE_2O_2SO_4(s) + \frac{4}{3}\,Cu(s) \quad (5.8)$$

The partial pressure of oxygen at the anode can be calculated using Eqn. (5.5), and by a treatment similar to that discussed in Section 5.2.3, the standard free energy change for the reaction:

$$\frac{2}{3}\,RE_2O_3(s) + \frac{2}{3}\,Cu_2S(s) + O_2(g) = \frac{2}{3}\,RE_2O_2SO_4(s) + \frac{4}{3}\,Cu(s) \quad (5.9)$$

can be expressed as:

$$\Delta G^{\circ}_{5.9} = 2.303 \log(P_{O_2}(.21 \text{ atm})) - 4FE \qquad (5.10)$$

Values of the partial pressures of oxygen in the anode and $\Delta G^{\circ}_{5.9}$ are listed in Tables 5.15 and 5.16, respectively.

5.4.4 Standard Entropy Change for the Reaction:

$$\frac{2}{3} Re_2O_3(s) + Cu_2S + O_2 = \frac{2}{3} RE_2O_2SO_4 + \frac{4}{3} Cu$$

Following the discussion in Section 5.2.5, the value of -B from Table 5.16 can be equated to the standard entropy change, $\Delta S^{\circ}_{5.9}$, for Reaction 5.9. $S^{\circ}_{5.9}$ for systems involving light rare earths is about -45 cal /mole O_2.K, $\Delta S^{\circ}_{5.9}$ can also be written as:

$$\Delta S^{\circ}_{5.9} = \frac{2}{3} S^{\circ}_{RE_2O_2SO_4} + \frac{4}{3} S^{\circ}_{Cu} - \frac{2}{3} S^{\circ}_{Cu_2S} - \frac{2}{3} S^{\circ}_{RE_2O_3} - S^{\circ}_{O_2}.$$

Rearranging,

$$\Delta S^{\circ}_{5.9} = \frac{4}{3}\left(\frac{1}{2} S^{\circ}_{RE_2O_2SO_4} - \frac{1}{2} S^{\circ}_{RE_2O_3} - S^{\circ}_{O_2}\right) + \frac{4}{3} S^{\circ}_{Cu} - \frac{2}{3} S^{\circ}_{Cu_2S} + \frac{1}{3} S^{\circ}_{O_2}$$

Hence, assuming $S^{\circ}_{RE_2O_3} \simeq S^{\circ}_{RE_2O_2S}$, the term inside the brackets can be replaced by $\Delta S^{\circ}_{5.6} = -39$ cal /mole O_2.K (Section 5.2.5). Thus,

$$\Delta S^{\circ}_{5.9} = -52 + \frac{4}{3} S^{\circ}_{Cu} - \frac{2}{3} S^{\circ}_{Cu_2S} + \frac{1}{3} S^{\circ}_{O_2} \qquad (5.11)$$

Taking the values of S°_{Cu}, $S^{\circ}_{Cu_2S}$ and $S^{\circ}_{O_2}$ from the literature (60), $\Delta S^{\circ}_{5.9}$ is estimated to be about -48 cal /mole O_2.K in the temperature range under consideration. This value is in good agreement

TABLE 5.15

PARTIAL PRESSURE OF OXYGEN AT THE ANODE OF CELLS OF TYPE III

RE	Temperature Range (K)	$\log (P_{O_2}) = A + B/T$ (P_{O_2} in atms.)	
		A	B
La	1140–1340	10.01	-24910
Pr	1080–1340	10.08	-24240
Nd	1040–1340	9.79	-23640
Sm	1100–1300	9.59	-22900
Eu	1100–1320	9.64	-22640
Gd	1160–1310	9.11	-21790

TABLE 5.16

STANDARD FREE ENERGY CHANGE FOR THE REACTION:

$$\frac{2}{3} RE_2O_3(s) + \frac{2}{3} Cu_2S(s) + O_2(g) = \frac{2}{3} RE_2O_2SO_4(s) + \frac{4}{3} Cu(s)$$

RE	Temperature Range (K)	ΔG^o = A + BT (cal /mole O_2)		Standard Deviation about the Fitted Line (cal /mole O_2)	95% Conf. Interval for A (cal /mole O_2)	95% Conf. Interval for B (cal /mole O_2·K)
		A (cal /mole O_2)	B (cal /mole O_2·K)			
La	1140-1340	-113990	45.83	±70	±37	±.029
Pr	1080-1340	-110930	46.13	±70	±41	±.033
Nd	1040-1340	-108180	44.84	±170	±96	±.079
Sm	1100-1300	-104820	43.87	±160	±106	±.089
Eu	1100-1320	-103590	44.11	±170	±106	±.087
Gd	1160-1310	-99710	41.69	±170	±104	±.108

with the values of $\Delta S^{o}_{5.9}$ (i.e. -B in Table 5.16) obtained from the second law analysis of $\Delta G^{o}_{5.9}$.

5.4.5 Error in the Standard Free Energy Changes of the Reaction:

$$\frac{2}{3} RE_2O_3(s) + \frac{2}{3} Cu_2S(s) + O_2(g) = \frac{2}{3} RE_2O_2SO_4(s) + \frac{4}{3} Cu(s)$$

In view of the discussion in Section 5.2.6, the experimental errors introduced in $\Delta G^{o}_{5.9}$ are estimated to be $\pm$180 cal . In addition, there are statistical errors (see Appendix A for details) which have been listed in Table 5.16.

5.4.6 Possibility of Secondary Reactions in the Anode Compartment: Limitations of Type III Cells

From the discussion in Section 5.1.5, it can be concluded that no reaction occurs between Cu_2S and the rare earth compounds. Also, there is no possibility of a reaction between Cu metal and the rare earth compounds.

The lower limit of the temperature range in which cells of Type III are operable is determined by the kinetics of the attainment of equilibrium between the phases present in the anode. It was found that most cells gave steady and reproducible emf above 1100K.

The upper limit of the temperature range in which cells of Type III are operable is determined by the liquidus temperature of the Cu-rich phase. Once the Cu-rich phase melts, it combines with the Pt contact lead, establishing an indefinite Cu activity at the anode which

in turn sets up an indefinite activity of oxygen.

The Cu-rich phase, saturated with sulfur containing a negligible amount of oxygen (well below the saturation level), melts at 1340K(96). This temperature forms an absolute upper limit to the temperature range in which Type III cells can be operated. For a cell where no significant reaction between the Pt and Cu-rich phase took place, such as the one involving lanthanum compounds (Fig. 5.10(a)), the change in slope of the cell emf vs. temperature plot is caused by

(1) the melting of the Cu-phase and

(2) a change in the activity of Cu due to the increased solubility of sulfur in the Cu-rich liquid (the solubility of sulfur in the Cu-rich liquid is 1.653 at. % at 1340K and increases to 1.860 at. % at 1378K, compared to its solubility in solid Cu which is around .014 at. % (96)).

Calculations show that the change in slope in the emf vs. temperature plot (Figs. 5.10), due to the melting of Cu, is about .05mV/K. Also, assuming the sulfur content of the Cu-rich liquid to be 1.653 at. %, the change in slope of the cell emf vs. temperature plot due to the change in the activity of Cu (caused by the increased solubility of sulfur in liquid Cu), is calculated to be less than .01mV/K. Thus, the combined change in slope is around .06mV/K. This is in good agreement with the observed change in slope of the cell emf vs. temperature plot for the lanthanum system (Fig. 5.10 (a)).

Since the cells involving the compounds of praseodymium, neodymium and samarium were not operated at high enough temperatures,

the aforementioned change in slope due to the melting of Cu rich phase could not be observed.

If the solubilities of oxygen and sulfur in the Cu-rich Cu-O-S melt are taken as their respective solubilities in the Cu-O and Cu-S binaries, then the calculations show that no significant change in Cu activity in the melt will occur. Thus, an unusually large change in slope of the cell emf vs. temperature plot for gadolinium can not be attributed to an increased oxygen content of the Cu-rich liquid in the anode only. A more likely reason could be the change in Cu activity because of its alloying with the Pt lead contact on melting of the Cu-rich liquid in the anode. Also, as Figure 5.13 shows, the oxygen partial pressures prevailing in the anode of a cell of Type III are at least 2 orders of magnitude lower than the oxygen partial pressures corresponding to the Cu/Cu_2O equilibrium. Thus, no formation of Cu_2O can be expected within the cell.

The cells involving europium (Fig. 5.10 (e)) showed a behaviour similar to that observed for cells involving lanthanum compounds. However, in this case the temperature, at which the change in slope of the cell emf vs. temperature plot occurred, dropped to about 1325K. This drop may be solely due to the increased oxygen content of the Cu-rich phase in the anode involving europium compounds compared to that involving lanthanum compounds. No data on the changes in liquidus temperature or the oxygen content of sulfur saturated Cu with oxygen partial pressure is available. However, following the treatment of Yazawa and Azakami (97), it can be said that the oxygen content of the

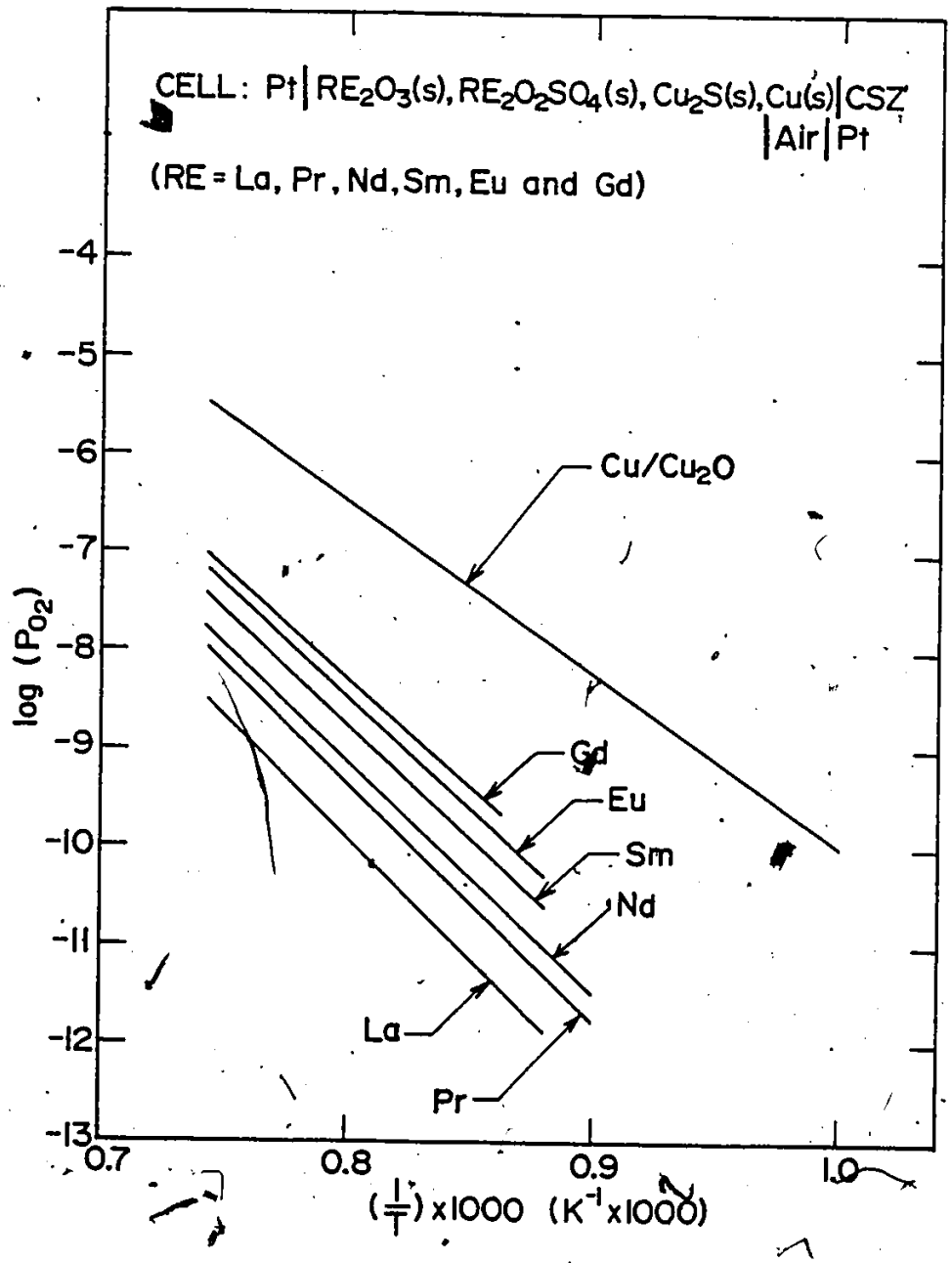

Fig. 5.13 Variation of the anode oxygen partial pressure with temperature for cells of Type III. The higher oxygen partial pressures for Cu/Cu_2O equilibria indicate that the formation of Cu_2O is unlikely.

Cu-rich liquid could be about 2 orders of magnitude higher in the anode involving europium compounds as compared to the one involving lanthanum compounds. As an extreme case, the oxygen content of the Cu-rich phase in the anode involving gadolinium compounds will be quite high. Thus, the Cu_2O activity in a cell involving gadolinium compounds could be significant, especially at high temperatures. A smaller value of B (in Table 5.16) for the cell involving gadolinium compounds could arise from the increased activity of Cu_2O within the cell.

5.4.7 Possibility of formation of RE_2O_2S in the Anode

In a cell of Type III, RE_2O_3 and $RE_2O_2SO_4$ coexist at a sulfur partial pressure corresponding to the Cu/Cu_2S equilibrium, in the temperature range investigated. Thus, in the phase stability diagram shown in Fig. 3.6, the Cu/Cu_2S line intersects the phase boundary between RE_2O_3 and $RE_2O_2SO_4$. If the P_{S_2}, corresponding to the Cu/Cu_2S equilibrium, increases faster than that corresponding to the coexistence between oxide, oxysulfide and oxysulfate, as the temperature is increased, then at a certain temperature, the Cu/Cu_2S line will intersect the $RE_2O_2S/RE_2O_2SO_4$ phase boundary. At this temperature, RE_2O_3 will be eliminated and RE_2O_2S will form.

In order to examine the formation of oxysulfide, the $\log(P_{S_2})$ corresponding to the Cu/Cu_2S equilibrium and that corresponding to the univariant equilibrium between oxide, oxysulfide and oxysulfate, is plotted against 1/T (as shown in Fig. 5.14 for the lanthanum compounds). Since the two lines diverge at high temperatures, there is

Fig. 5.14 Equilibrium sulfur partial pressures corresponding to La_2O_3-La_2O_2S-$La_2O_2SO_4$ equilibria as a function of temperature. Partial pressures corresponding to Cu/Cu_2S equilibria are also plotted in the same plot. The divergence of the two lines at high temperatures indicate that the conversion of oxide to oxysulfide is not likely in a cell of Type III.

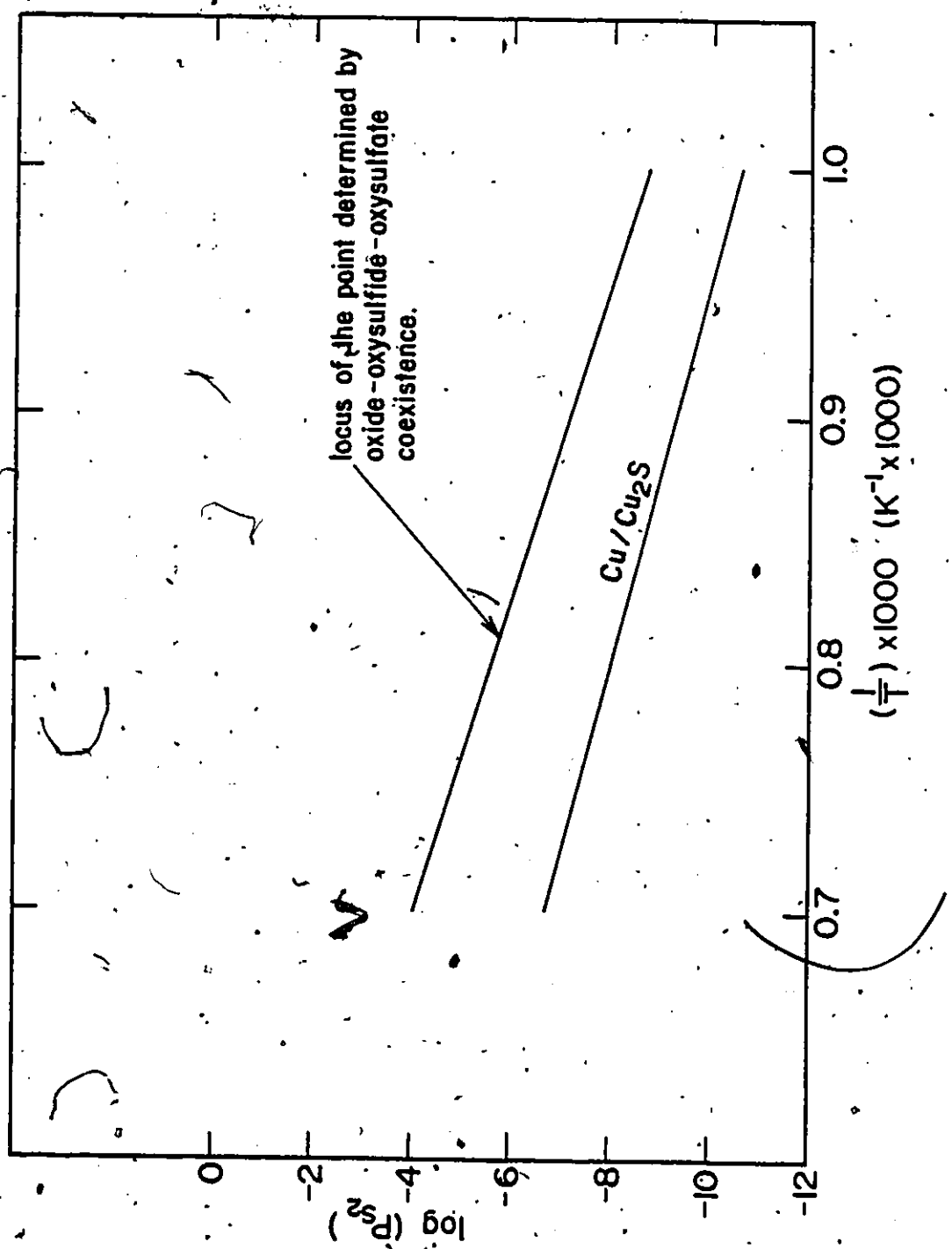
locus of the point determined by oxide-oxysulfide-oxysulfate coexistence.
Cu/Cu2S
log (PS2)
0
-2
-4
-6
-8
-10
-12
0.7
0.8
0.9
1.0
(1/T) x1000 (K-1x1000)

no possibility of oxysulfide formation.

5.4.8 Applicability of Cells of Type III to Study Oxide/Oxysulfide Equilibria

As demonstrated earlier in this section, cells of Type III can be successfully used to study oxide/oxysulfate equilibria. From the nature of the phase stability diagram (Fig. 3.6), it was expected that these cells would also be applicable to study oxide/oxysulfide equilibria. Therefore, a cell of the type:

$Pt|La_2O_3(s), La_2O_2S(s), Cu(s), Cu_2S(s)|CSZ|Air|Pt$ (Type V)

was constructed and operated in a manner similar to that used for the cells of Type III.

No steady emf could be obtained for this cell. At a constant temperature, the cell emf continuously decreased with time, coming to a steady value which was very close to emf of the cell:

$|La_2O_3(s), La_2O_2SO_4(s), Cu(s), Cu_2S(s)|CSZ|Air|Pt.$

Thereafter, the cell operated exactly like Cell III(a). X-ray analysis of the anode products showed that the La_2O_2S present in the original cell had completely converted to $La_2O_2SO_4$.

Since the difference between the oxygen partial pressure at the anode and that at the cathode is about 17 order of magnitude, one could expect a strong diffusional flux of oxygen due to partial electronic conduction in the CSZ. The oxygen could combine with the oxysulfide to form oxysulfate. For this reason, Type V cells will not be suitable to study systems involving Pr, Nd, Sm, Eu and Gd, because the oxygen

partial pressures at the anodes are expected to be even lower than that obtained for the cell involving lanthanum compounds.

The cell:

$Pt|Y_2O_3(s), Y_2O_2S(s), Cu(s), Cu_2S(s)|CSZ|Air|Pt$

was also studied, but it polarized very quickly and the cell emf continuously decreased with time to zero. Since the partial pressure corresponding to the transient emf of this cell was well beyond the electrolytic domain of calcia stabilized zirconia, electronic conduction is again expected to play a significant role in the polarization of this cell. For this reason, a cell of Type V could not be used to study the Ce-O-S system.

5.5 Results from Type IV Cells

5.5.1 Study of the Y-O-S system Using a Cell of Type IV

The cell

$Pt|Y_2O_3(s), Y_2O_2S(s), Ag(s), Ag_2S(s)|CSZ|Air|Pt$

was studied in a very limited temperature range. The upper limit was determined by the melting point of the Ag-saturated Ag_2S, and was 1077K(100). In order for CSZ to conduct ionically, the temperature of the cell should be greater than 1070K. The above two factors result in a very narrow temperature range in which the cell is operable. Inspite of these restrictions, the cell was operated up to about 1179K, the melting point of sulfur-saturated silver. Table 5.17 gives the results from this cell.

TABLE 5.17

EMF DATA FOR THE CELL:

$Pt|Y_2O_3(s), Y_2O_2S(s), Ag(s), Ag_2S(s)|CSZ|Air|Pt$

Temperature (K)	Cell emf (V)
1068	.813
1036	.818
1065	.811
1085	.809

An emf reading for the above cell was taken after a long equilibration time of around 20 hours. The reading at 1068K was expected to be most reliable and thus was used for the calculations. The above data, when combined with the standard free energy of formation of Ag_2s (Ref. 60) and Y_2O_3 (Ref. 3), yields:

$\Delta G_f^o(Y_2O_2S)$ at 1068 K = -354300 cal /mole

This compares very well with the value of -357000 cal /mole estimated by Gschneidner et al.(3). for ΔG_f^o (Y_2O_2S) at 1068K.

5.5.2 Study of the Ce-O-S System Using a Cell of Type IV

The cell:

$Pt|CeO_x(s), Ce_2O_2S(s), Ag(s), Ag_2S(s)|CSZ|Air|Pt$

was studied in a very limited temperature range due to the reasons outlined in the previous section. Only two reading of the cell emf were taken after about 40 hours of equilibration for each reading. These values are listed in Table 5.18.

TABLE 5.18

EMF DATA FOR THE CELL:

$Pt|CeO_x(s), Ce_2O_2S(s), Ag(s), Ag_2S(s)|CSZ|Air|Pt$

Temperature (K)	Cell emf (V)
1040	.906
1072	.894

In view of the considerations outlined in the previous section, the value at 1072K is expected to be the more reliable. From the data of Bevan and Kordis(33), the composition of CeO_x at the prevailing oxygen partial pressure of about 10^{-18} at 1072K, is expected to be very close to CeO_2. Thus, assuming $CeO_2(s)$ to be the oxide in equilibrium with $Ce_2O_2S(s)$ in the prevailing experimental conditions, $\Delta G_f^o(Ce_2O_2S)$ can be calculated. Combining the cell emf data at 1072K with the standard free energy of formation of CeO_2 at 1072K, we obtain

$\Delta G_f^o(Ce_2O_2S)$ at 1072 K = -340100 cal /mole.

This value is in excellent agreement with the value of -340200(±15000) cal /mole, estimated by Gschneidner et al.(3) and the value, -338000 (±4500) cal /mole, determined by Fruehan(38). The error in the present value of ΔG^{o}_{f} (Ce_2O_2S) is estimated to be less than ±3000 cal /mole.

CHAPTER VI

GENERAL DISCUSSION

6.1 Standard Free Energy Changes for the Reaction $\frac{1}{2} RE_2O_2S(s) + O_2(g) = \frac{1}{2} RE_2O_2SO_4(s)$: Extrapolation of the Results

Figure 6.1 shows a plot of the standard free energy changes for Reaction 5.6 against the atomic number of the relevant rare earth element at different temperatures. Some of the data used in this plot are obtained on extrapolating the data of Table 5.7 to temperatures not covered in the experimental range. It is clear from this plot that the relative stability of an oxysulfate with respect to oxysulfide decreases as the atomic number of the rare earth element increases. It is also clear from this plot that $\Delta G^{o}_{5.6}$ decreases quite sharply up to neodymium and more gradually thereafter. The latter portion of this plot is linearly extrapolated to heavier rare earths. The extrapolated results are presented in Table 6.1 along with experimental results obtained in this study.

The error limits given in Table 6.1 are a combination of both the experimental errors of about ±200 cal and the statistical error arising from the linear fit of the data.

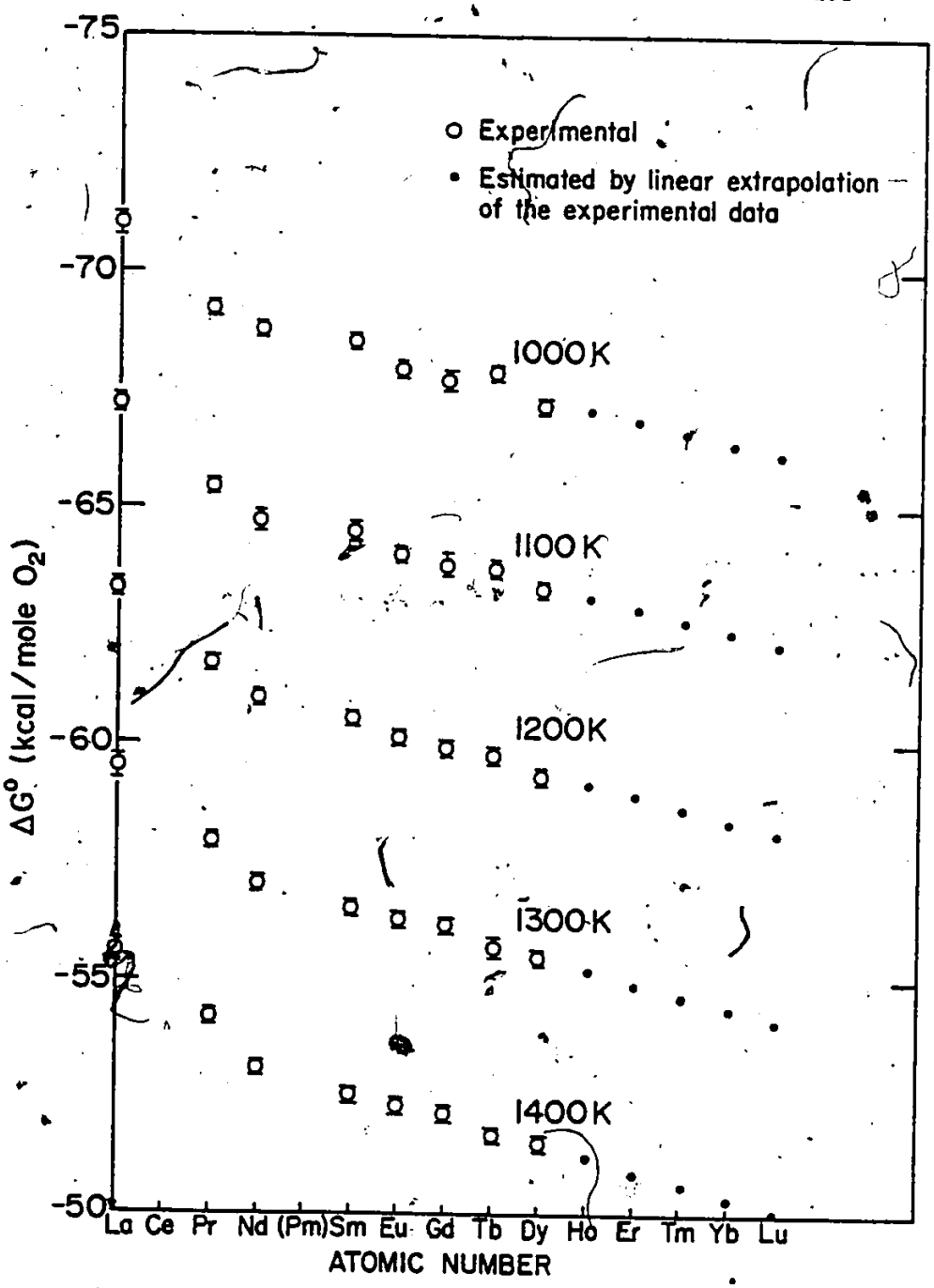

Fig. 6.1 Variation of the standard free energy changes with temperature for the reaction: $1/2\ RE_2O_2S + 2\ O_2 = 1/2\ RE_2O_2SO_4$.

TABLE 6.1

STANDARD FREE ENERGY CHANGES FOR THE REACTION

$$\frac{1}{2} RE_2O_2S(s) + O_2(g) = \frac{1}{2} RE_2O_2SO_4(s)$$

RE	Temperature Range (K)	ΔG° = A + BT (cal /mole O_2) A (cal /mole O_2)	B (cal /mole O_2·K)	Error in ΔG° (cal /mole O_2)
La	1100–1500	-109930	38.91	±320
Pr	1100–1400	-106890	37.67	±360
Nd	1100–1430	-108000	39.21	±320
Sm	1050–1370	-108400	39.92	±490
Eu	1020–1320	-106860	38.95	±360
Gd	1000–1280	-106520	38.88	±270
Tb	1020–1200	-108410	40.56	±460
Dy	1040–1180	-106560	39.39	±270
Ho*	1000–1400	-106840	39.75	--
Er*	1000–1400	-106660	39.82	--
Tm*	1000–1400	-106480	39.89	--
Yb*	1000–1400	-106300	39.96	--
Lu*	1000–1400	-106120	40.03	--

* Estimated

6.2 Standard Free Energies of Formation of Rare Earth Oxysulfates from their Respective Oxides

The standard free energy change for the reaction:

$$\frac{2}{3}\,RE_2O_3(s) + \frac{2}{3}\,Cu_2S(s) + O_2(g) = \frac{2}{3}\,RE_2O_2SO_4(s) + \frac{4}{3}\,Cu(s), \quad (6.1)$$

given in Table 5.16 were combined with the standard free energy of formation of $Cu_2S(s)$*, $\Delta G^{o}_{f,Cu_2S}$, given by:

$$\Delta G^{o}_{f,Cu_2S}(1000\text{-}1300\ K) = [-29872 + 5.503T] \pm 300\ cal/mole,$$

to yield the standard free energies of formation of rare earth oxysulfates from their respective oxides. These values along with the error associated with them are presented in Table 6.2.

The error limits listed in Table 6.2 are due to a combination of experimental and statistical errors and errors in the standard free energy of formation of $Cu_2S(s)$.

6.3 Standard Free Energies of Formation of Rare Earth Oxysulfates

The standard free energies of formation of oxysulfates from their respective oxides, given in Table 6.2, can be combined with the standard free energies of formation of rare earth oxides, compiled by Gschneidner et al. (3) (Table 2.2), to yield the standard free energies of formation of rare earth oxysulfates from their constituent elements. These calculated values of the standard free energies of formation of rare earth

* The data used to evaluate $\Delta G^{o}_{f,Cu_2S}$ has been taken from Mills (42) for $Cu_2S(s)$; and Kubaschewski et al. (87) for Cu(s).

TABLE 6.2

STANDARD FREE ENERGIES OF FORMATION OF RARE EARTH OXYSULFATES FROM THE OXIDES

REACTION: $RE_2O_3(s) + \frac{1}{2} S_2(g) + \frac{3}{2} O_2(g) = RE_2O_2SO_4(s)$

RE	Temperature Range (K)	ΔG° = A + BT (cals/mole)		Error in ΔG° (cal /mole)
		A (cal /mole)	B (cal /mole·K)	
La	1140–1340	-200850	74.24	±580
Pr	1080–1340	-196260	74.69	±580
Nd	1040–1340	-192140	72.76	±730
Sm	1100–1300	-187110	71.30	±720
Eu	1100–1320	-185260	71.66	±730
Gd	1160–1300	-179440	68.03	±730

oxysulfates, $\Delta G^{\circ}_{f,RE_2O_2SO_4}$, are listed in the Table 6.3 along with the associated errors. The same results are plotted in Fig. 6.2.

Figure 6.2 shows that the stability of rare earth oxysulfates decreases as the atomic number of the constituent rare earth increases, $Eu_2O_2SO_4$ being a notable exception, the standard free energy of formation being significantly lower in this case. The lower standard free energy of formation of europium oxysulfate is due to relative stability of the bivalent as compared to trivalent state (3). However, the trend of decreasing stability of the oxysulfates with atomic number is opposite to that observed for oxides and oxysulfides where the stability increased with an increase in atomic number.

Figure 6.2 also shows the $\Delta G^{\circ}_{f,La_2O_2SO_4}$ determined by Grizik et al. (58). This value differs significantly from the value determined in the present study. The reason of this could be found in the approximate nature of the determination made by Grizik et al. (58), as discussed in Section 2.3.2.

6.4 Standard Free Energies of Formation of Rare Earth Oxysulfides

The standard free energies of formation of rare earth oxysulfates, listed in the Table 6.3, can be combined with the standard free energy changes for the reaction:

$$\frac{1}{2}\ RE_2O_2S(s) + O_2(g) = \frac{1}{2}\ RE_2O_2SO_4(s)$$

to yield the standard free energies of formation of the rare earth

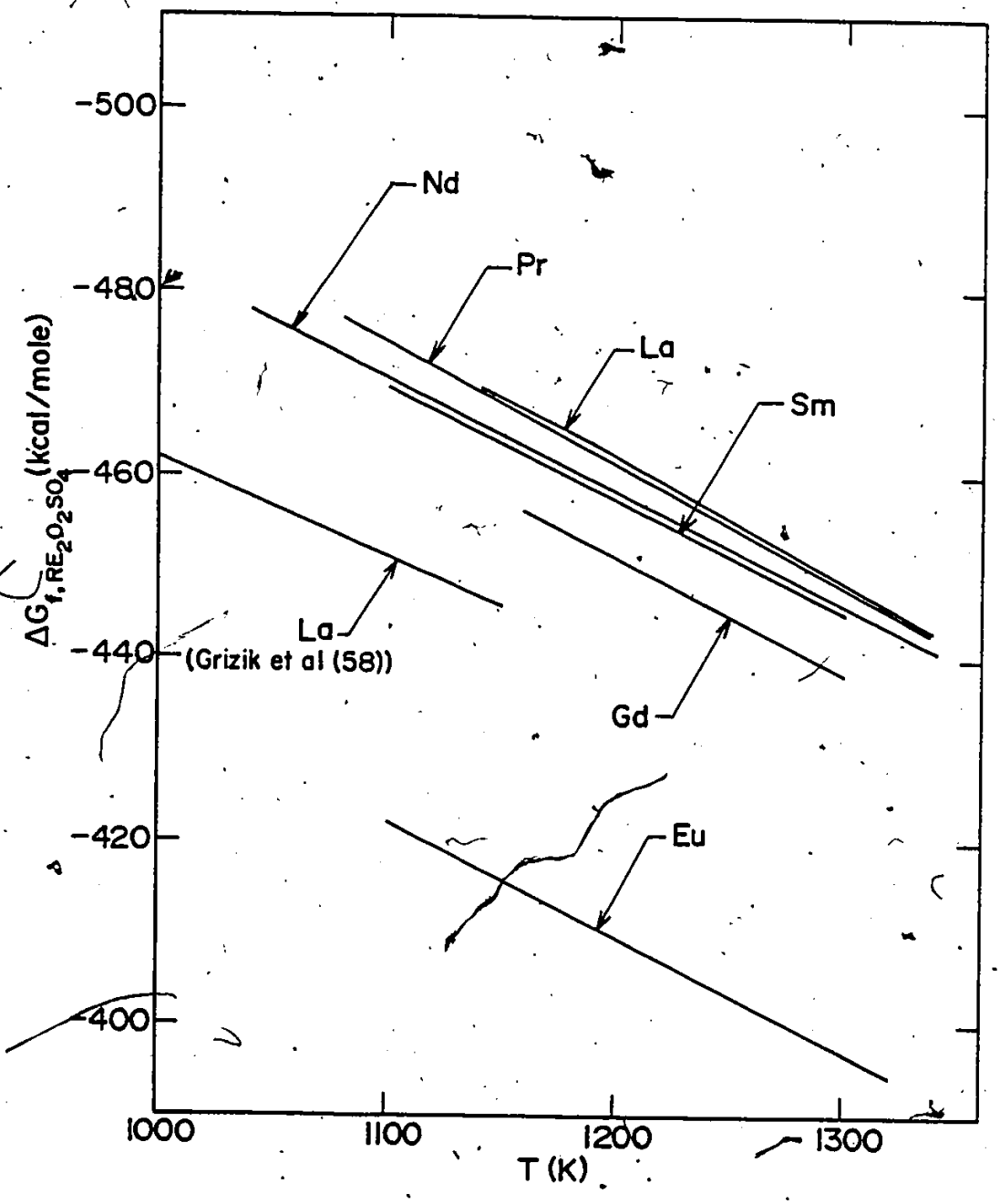

Fig. 6.2 Variation of the standard free energies of formation of rare earth oxysulfates with temperature.

TABLE 6.3

STANDARD FREE ENERGIES OF FORMATION OF RARE EARTH OXYSULFATES

RE	Reaction	Temperature Range (K)	$\Delta G_f^o = A + BT$ (cal /mole) A (cal./mole)	B (cal./mole·K)	Error in ΔG_f^o (cal./mole)
La	$2\,La(\gamma) + 3O_2(g) + \frac{1}{2}\,S_2(g) = La_2O_2SO_4(s)$	1140–1193	-628000	140.7	±3200
La	$2\,La(\ell) + 3O_2(g) + \frac{1}{2}\,S_2(g) = La_2O_2SO_4(s)$	1193–1340	-629700	142.2	±3200
Pr	$2\,Pr(\beta) + 3O_2(g) + \frac{1}{2}\,S_2(g) = Pr_2O_2SO_4(s)$	1080–1204	-629500	141.1	±4300
Pr	$2\,Pr(\ell) + 3O_2(g) + \frac{1}{2}\,S_2(g) = Pr_2O_2SO_4(s)$	1204–1340	-631000	142.4	±4300
Nd	$2\,Nd(\alpha) + 3O_2(g) + \frac{1}{2}\,S_2(g) = Nd_2O_2SO_4(s)$	1040–1128	-622900	150.0	±2900
Nd	$2\,Nd(\beta) + 3O_2(g) + \frac{1}{2}\,S_2(g) = Nd_2O_2SO_4(s)$	1128–1289	-622700	139.7	±2900
Nd	$2\,Nd(\ell) + 3O_2(g) + \frac{1}{2}\,S_2(g) = Nd_2O_2SO_4(s)$	1289–1340	-625900	142.1	±2900
Sm	$2\,Sm(\alpha) + 3O_2(g) + \frac{1}{2}\,S_2(g) = Sm_2O_2SO_4(s)$	1100–1190	-621800	139.6	±3100
Sm	$2\,Sm(\beta) + 3O_2(g) + \frac{1}{2}\,S_2(g) = Sm_2O_2SO_4(s)$	1190–1300	-624300	141.7	±3100
Eu	$2\,Eu(\ell) + 3O_2(g) + \frac{1}{2}\,S_2(g) = Eu_2O_2SO_4(s)$	1100–1320	-577600	142.4	±3500
Gd	$2\,Gd(\alpha) + 3O_2(g) + \frac{1}{2}\,S_2(g) = Gd_2O_2SO_4(s)$	1160–1300	-611100	133.3	±3600

oxysulfides from their constituent elements. These values are listed in Table 6.4 along with associated errors. The same values are plotted in Fig. 6.3. In this Figure, it can be clearly seen that the values of $\Delta G^{\circ}_{f,RE_2O_2S}$ of all rare earth oxysulfides, but that of Eu, lie in a close band. Thus, any regular change in $\Delta G^{\circ}_{f,RE_2O_2S}$ with the atomic number, if present, is not clear due to the large errors associated with these values. Figure 6.3 also shows the values of $\Delta G^{\circ}_{f,Ce_2O_2S}$, determined by Fruehan (38) and the values of $\Delta G^{\circ}_{f,Ce_2O_2S}$ and $\Delta G^{\circ}_{f,La_2O_2S}$ estimated by Gschneidner et al.(3). As already pointed out in Section 5.5.2, the values of $\Delta G^{\circ}_{f,Ce_2O_2S}$ reported by Fruehan and Gschneidner et al. are in excellent agreement with the values, obtained in the present study. Also, the value of $\Delta G^{\circ}_{f,La_2O_2S}$, reported by Gschneidner et al.(3), is in good agreement with that obtained in the present work, within the error limits of $\pm$15000 cal specified by Gschneidner et al.

Gschneidner et al. (3) have estimated the values of $\Delta G^{\circ}_{f,RE_2O_2S}$ for all oxysulfides at 1100 K. A comparison between these values and those obtained in the present investigation (Table 6.5) shows a good agreement in all cases.

TABLE 6.4

STANDARD FREE ENERGIES OF FORMATION OF RARE EARTH OXYSULFIDES

RE	Reaction	Temperature Range (K)	ΔG_f^o = A + BT (cal /mole)		Error in ΔG_f^o (cal /mole)
			A (cal /mole)	B (cal /mole·K)	
La	$2\ La(\gamma) + O_2(g) + \frac{1}{2}\ S_2(g) = La_2O_2S(s)$	1140-1193	-408100	62.9	±3500
La	$2\ La(\ell) + O_2(g) + \frac{1}{2}\ S_2(g) = La_2O_2S(s)$	1193-1340	-409800	64.4	±3500
Pr	$2\ Pr(\beta) + O_2(g) + \frac{1}{2}\ S_2(g) = Pr_2O_2S(s)$	1080-1204	-415700	65.7	±4600
Pr	$2\ Pr(\ell) + O_2(g) + \frac{1}{2}\ S_2(g) = Pr_2O_2S(s)$	1204-1340	-417200	67.1	±4600
Nd	$2\ Nd(\alpha) + O_2(g) + \frac{1}{2}\ S_2(g) = Nd_2O_2S(s)$	1040-1128	-406900	61.6	±3200
Nd	$2\ Nd(\beta) + O_2(g) + \frac{1}{2}\ S_2(g) = Nd_2O_2S(s)$	1128-1289	-406700	61.3	±3200
Nd	$2\ Nd(\ell) + O_2(g) + \frac{1}{2}\ S_2(g) = Nd_2O_2S(s)$	1289-1340	-409900	63.7	±3200
Sm	$2\ Sm(\alpha) + O_2(g) + \frac{1}{2}\ S_2(g) = Sm_2O_2S(s)$	1100-1190	-405000	59.7	±3800
Sm	$2\ Sm(\beta) + O_2(g) + \frac{1}{2}\ S_2(g) = Sm_2O_2S(s)$	1190-1195	-407300	61.9	±3800
Eu	$2\ Eu(\ell) + O_2(g) + \frac{1}{2}\ S_2(g) = Eu_2O_2S(s)$	1100-1320	-363900	64.5	±4000
Gd	$2\ Gd(\alpha) + O_2(g) + \frac{1}{2}\ S_2(g) = Gd_2O_2S(s)$	1160-1300	-398000	55.5	±3800
Ce	$2\ Ce(\ell) + O_2(g) + \frac{1}{2}\ S_2(g) = Ce_2O_2S(s)$	1072	ΔG_f^o = -340100		±3000
Y	$2\ Y(s) + O_2(g) + \frac{1}{2}\ S_2(g) = Y_2O_2S(s)$	1068	ΔG_f^o = -354300		±3000

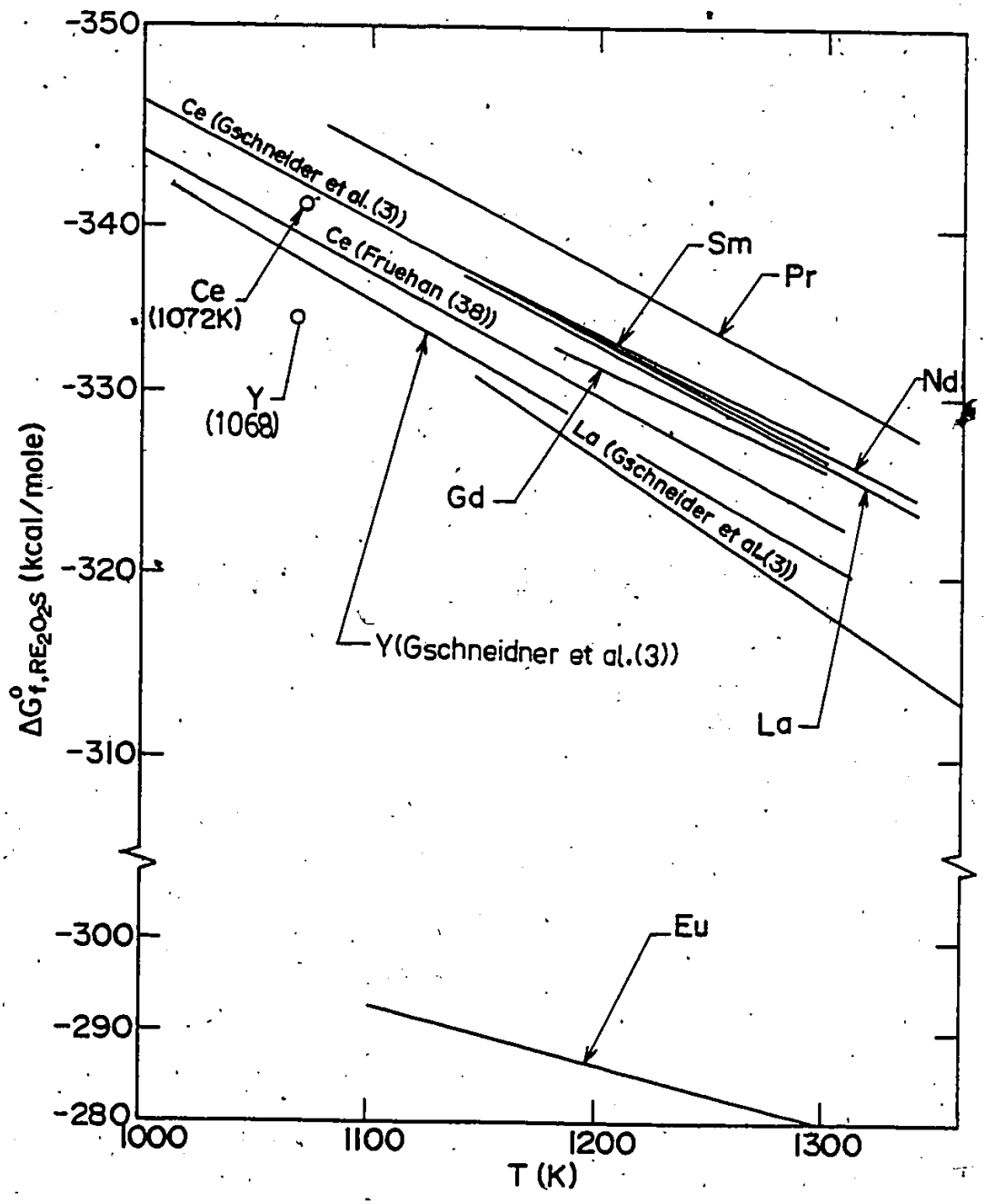

Fig. 6.3 Variation of the standard free energies of formation of rare earth oxysulfides with temperature.

TABLE 6.5

STANDARD FREE ENERGY OF FORMATION OF OXYSULFIDES AT 1100 K

RE	$\Delta G^{o}_{f,RE_2O_2S}$ at 1100 K (cal /mole)	
	Present Work	Gschneidner et al. (3)*
La	-338900 (± 3500)	-337000 (± 15000)
Pr	-343400 (± 4600)	-340000 (± 15000)
Nd	-339300 (± 3200)	-341000 (± 15000)
Sm	-339300 (± 3800)	-343000 (± 15000)
Eu	-293000 (± 4000)	-299000 (± 15000)
Gd	-337000 (± 3800)	-346000 (± 15000)

* Estimated

6.5 Phase Stability Diagrams (PSD) of RE-O-S Systems

Phase stability diagrams are very useful in making predictions about the stability of RE-O-S phase under given conditions of temperature and partial pressures of oxygen and sulfur. Phase stability diagrams for RE-O-S systems can be constructed utilizing the experimentally determined values of $\Delta G^{o}_{f,RE_2O_2S}$ and $\Delta G^{o}_{f,RE_2O_2SO_4}$, and the data from literature on thermodynamics of oxides, sulfides and sulfates.

All the diagrams have common general features, however, they differ in some important aspects from each other. These differences are highlighted in the vicinity of the point, defined by the oxide-oxysulfide-oxysulfate co-existence. This region is most important from the viewpoint of the present study. The various RE-O-S phase stability diagrams would differ from each other in the following important aspects:

1. Some rare earths, such as cerium, do not form an oxysulfate and form oxides having a wide range of compositions.
2. Some rare earths, such as praseodymium and terbium, form stable oxysulfates even though they form oxides with a wide range of compositions.
3. Europium and ytterbium have a stable valence of less than +3 in some of their oxides, but europium forms an oxysulfate stable at high temperatures, whereas ytterbium does not.
4. The stability of an oxysulfate, relative to the oxysulfide and oxide, continuously decreases as the atomic number of the constituent rare earth increases.

These aspects are highlighted by constructing the phase stability diagrams of the La-O-S, Ce-O-S and Gd-O-S systems.

Figure 6.4 shows the phase stability diagram of the La-O-S system at 1100 K. The data used in construction of this diagram were taken from the present work for La_2O_2S and $La_2O_2SO_4$; from Grunzweig (70) for the $La_2(SO_4)_3/La_2O_2SO_4$ equilibrium; from Gschneidner et al. (3) for La_2O_3; from Mills (42) for LaS and La_2S_3; and from Vasileva et al. (98) for LaS_2. The data for La_3S_4 are not known. Thus for the present construction, $\Delta G^o_{f,La_3S_4}$ is taken equal to the $\Delta G^o_{f,Ce_3S_4}$. Because of the large errors associated with the standard free energies of formation of some of the compounds, the data are inconsistent with each other. Thus, the phase stability diagram is constructed so as to make various data consistent with each other and not to violate the phase rule.

Additional complications are introduced, in the phase stability diagram of the Ce-O-S system by the existence of non-stoichiometry in the oxides of cerium. Figure 6.5 shows the phase stability diagram for the Ce-O-S system at 1100 K. The data used in the construction of this diagram has been taken from Gschneidner and Kippenhan (99) for sulfides; from Gschneidner et al. (3) and Fruehan (48) for the oxysulfide; from Bevan and Kordis (33) for oxides; and from Barin et al. (60) for $Ce_2(SO_4)_3$. This diagram is drawn by making the available data self-consistent at the low oxygen and sulfur partial pressures. However, when this is done, various phase boundaries become inconsistent with each other at high oxygen and sulfur partial pressures. Furthermore, when Fruehan's (48) data, instead of the Gschneidner's

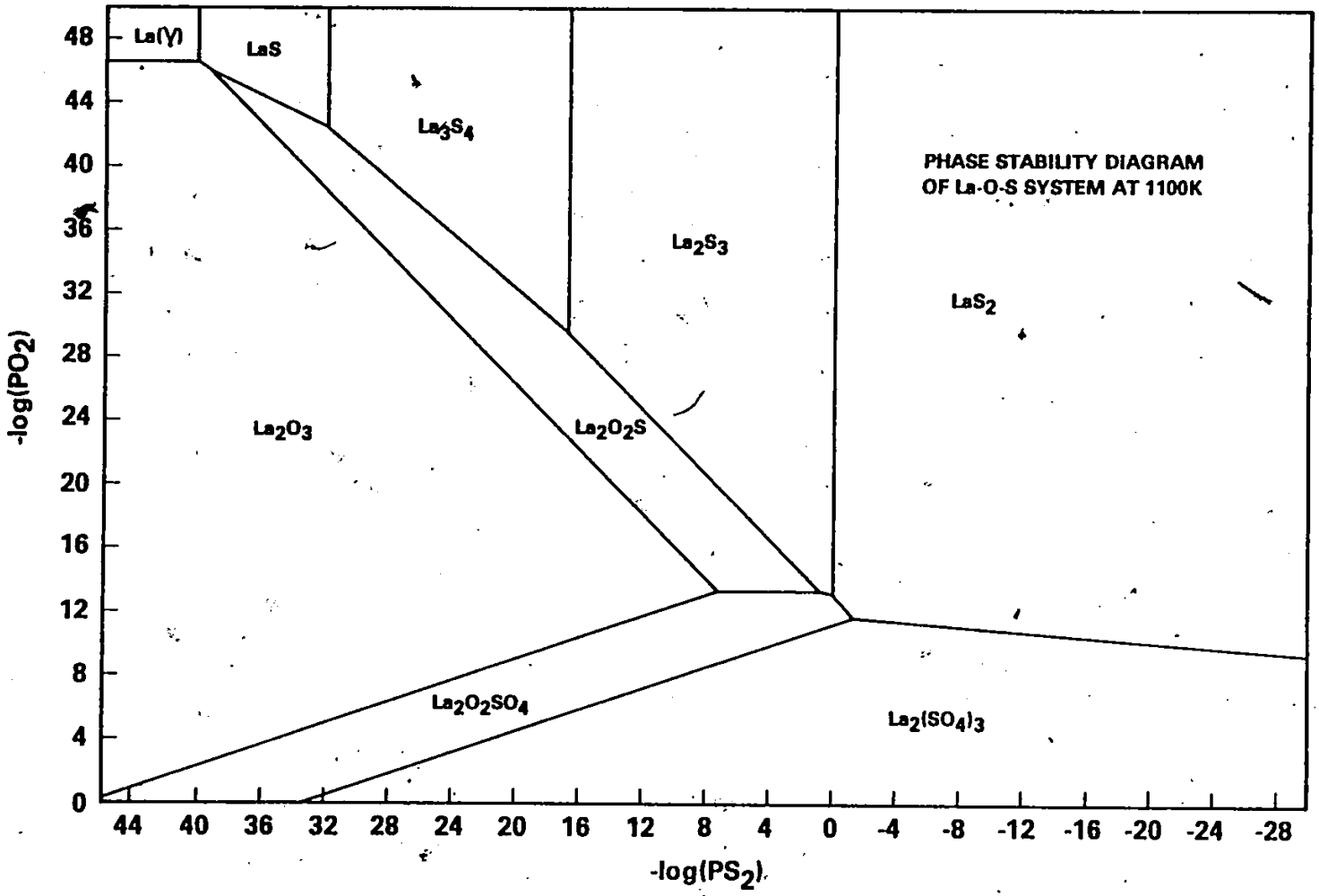
PHASE STABILITY DIAGRAM
OF La-O-S SYSTEM AT 1100K
La(γ)
LaS
La3S4
La2S3
LaS2
La2O3
La2O2S
La2O2SO4
La2(SO4)3
-log(PO2)
-log(PS2)
48
44
40
36
32
28
24
20
16
12
8
4
0
44
40
36
32
28
24
20
16
12
8
4
0
-4
-8
-12
-16
-20
-24
-28

Fig. 6.4

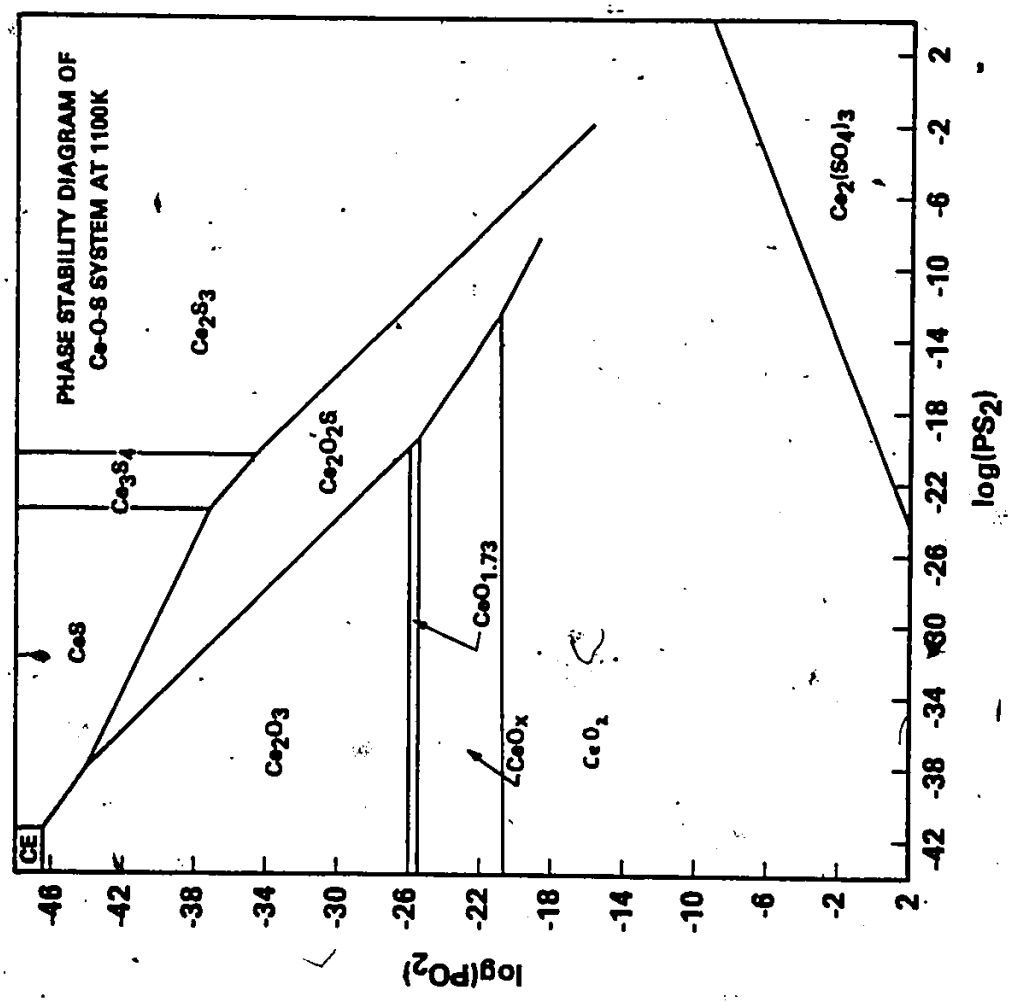
PHASE STABILITY DIAGRAM OF
Ce-O-S SYSTEM AT 1100K
CE
CeS
Ce_3S_4
Ce_2S_3
Ce_2O_2S
Ce_2O_3
$CeO_{1.73}$
CeO_x
CeO_2
$Ce_2(SO_4)_3$
log(PO_2)
log(PS_2)
-46
-42
-38
-34
-30
-26
-22
-18
-14
-10
-6
-2
2

Fig. 6.5

estimates, are used for $\Delta G^{o}_{f,Ce_2O_2S}$, in constructing the phase stability diagram, the Ce_2O_2S phase field becomes very small. This is in contradiction with practice in that Ce_2O_2S is observed over a wide range of oxygen and sulfur partial pressures. Thus, if Fruehan's data is taken to be accurate then the thermodynamic data on sulfides need to be significantly modified in order to maintain a large Ce_2O_2S phase field. However, at this point no judgement can be passed on the accuracy of the data reported in the above two works. The only reason for using the $\Delta G^{o}_{f,Ce_2O_2S_2}$ from Gschneidner et al. (3) in the present construction is because it gives a phase stability diagram that is more consistent with practical observations.

The phase stability diagram of Gd-O-S system is very similar to that of the La-O-S system. However, the point, determined by oxide-oxysulfide-oxysulfate coexistence, shifts to higher values of oxygen and sulfur partial pressures. This is illustrated in Fig. 6.6 where the Gd-O-S phase stability diagram (drawn with solid lines) is superimposed on the La-O-S phase stability diagram (dashed lines). The phase stability diagram of Gd-O-S system is constructed using the data from Mills (42) for sulfides; from Gschneidner et al.(3) for the oxide; from the present work for the oxysulfide and the oxysulfate; and from Grunzweig (70) for oxysulfate/sulfate equilibria.

As temperature increases the point, corresponding to the oxide-oxysulfide-oxysulfate coexistence, moves to lower oxygen and sulfur partial pressures. This is illustrated in the Fig. 6.7 drawn for the Gd-O-S system.

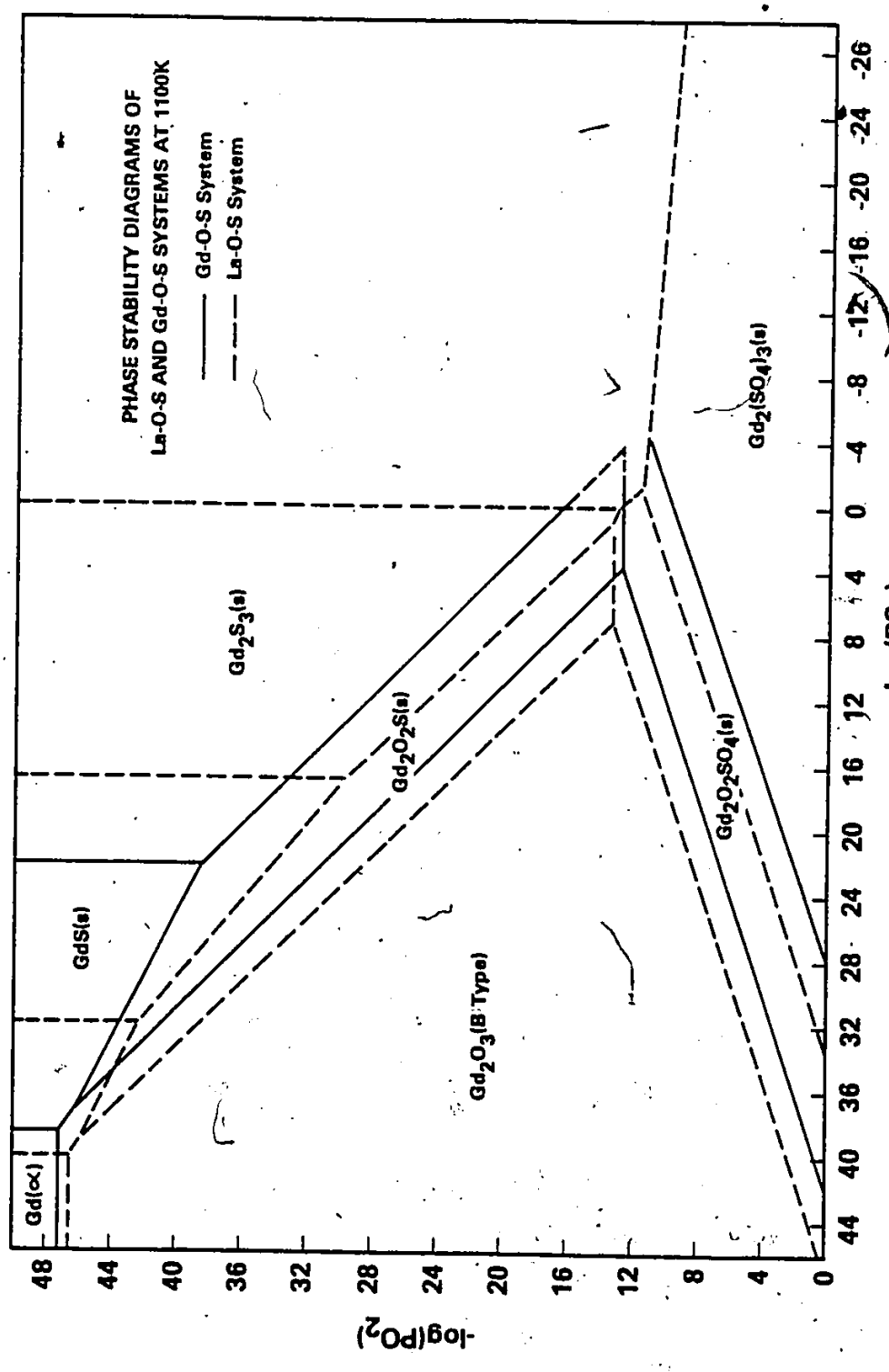
PHASE STABILITY DIAGRAMS OF
La-O-S AND Gd-O-S SYSTEMS AT 1100K
Gd-O-S System
La-O-S System
Gd(α)
GdS(s)
Gd2S3(s)
Gd2O2S(s)
Gd2O3(B Type)
Gd2O2SO4(s)
Gd2(SO4)3(s)
-log(PO2)
-log(PS2)
48
44
40
36
32
28
24
20
16
12
8
4
0
44
40
36
32
28
24
20
16
12
8
4
0
-4
-8
-12
-16
-20
-24
-26

Fig. 6.6

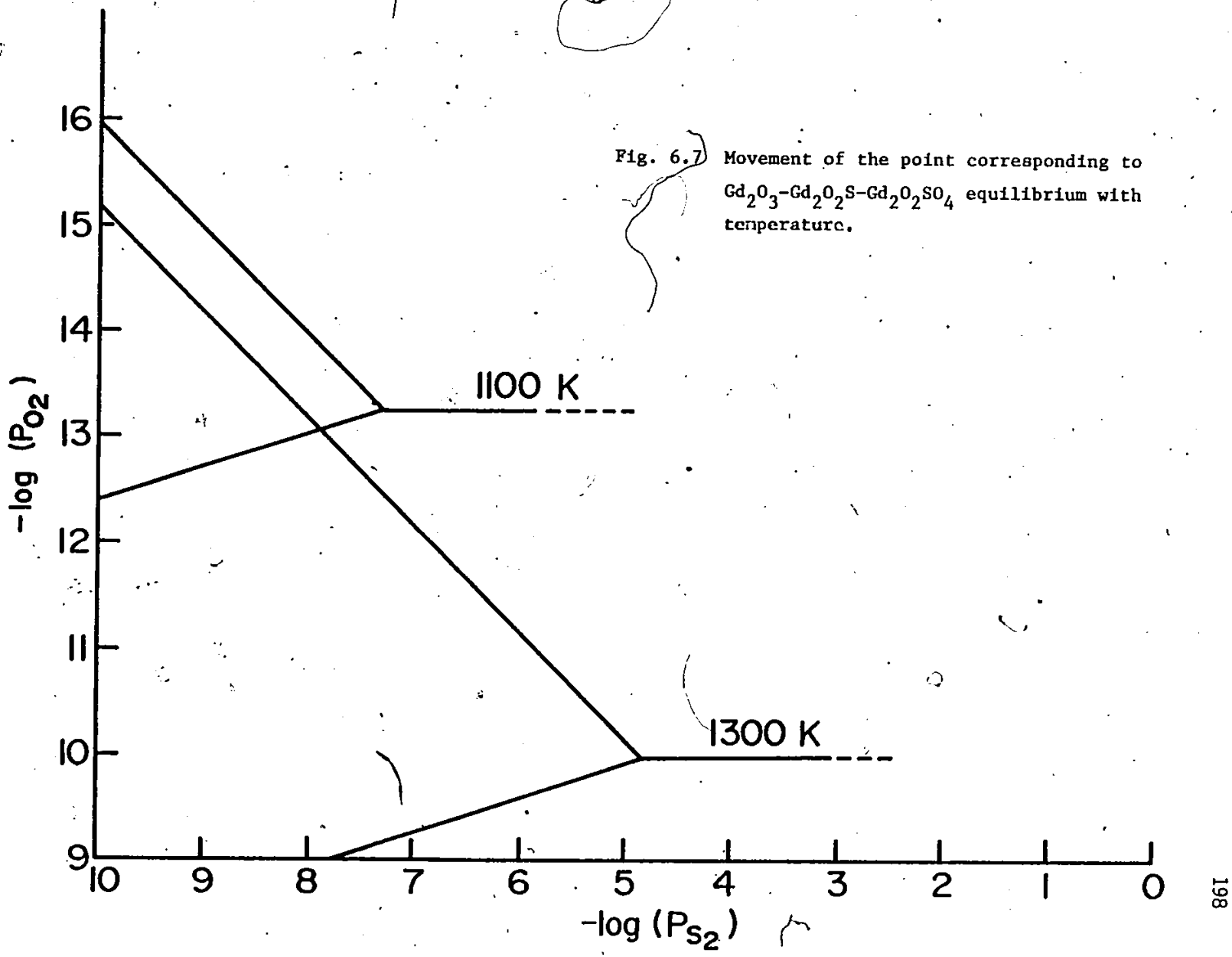

Fig. 6.7 Movement of the point corresponding to Gd_2O_3-Gd_2O_2S-$Gd_2O_2SO_4$ equilibrium with temperature.

CHAPTER VII

CONCLUSION AND SUMMARY

(1) Thermodynamic data on oxygen-sulfur compounds of rare earths are quite scarce in spite of their importance from an industrial viewpoint.

(2) Oxygen concentration cells, using calcia stabilized zirconia, can be successfully used to study ternary rare earth-oxygen-sulfur systems at high temperatures. The cells:

Pt	$RE_2O_2S(s)$, $RE_2O_2SO_4(s)$ in presence of $RE_2O_3(s)$	CSZ	Air	Pt	(Type I)
Pt	$RE_2O_2S(s)$, $RE_2O_2SO_4(s)$ in presence of Ag/Ag_2S	CSZ	Air	Pt	(Type II)
Pt	$RE_2O_3(s)$, $RE_2O_2SO_4(s)$ $Cu(s)$, $Cu_2S(s)$	CSZ	Air	Pt	(Type III)

and

Pt	$RE_2O_3(s)$, $RE_2O_2SO_4(s)$ $Ag(s)$, $Ag_2S(s)$	CSZ	Air	Pt	(Type IV)

were used to study the rare earth-oxygen-sulfur systems at high temperatures.

(3) Cells of Type I were used to study the oxide-oxysulfide-oxysulfate univariant equilibria at high temperatures. These cells could be used to study systems involving rare earths up to dysprosium, cerium system being the only exception. The results obtained using the cells of Type I are summarized in Table 5.2. The results of the least square analysis of the emf data from Type I cells are presented in Table 5.4 and the standard free energies of oxidation of oxysulfides calculated therefrom are presented in Table 5.7.

(4) The lower limit of the temperature range in which a cell of Type I could be operated was set by the kinetics of electrode reactions and the resistance polarization of CSZ at low temperatures. Thus, cells of Type I could not be operated below 1000K.

(5) The upper limit of the temperature range in which a cell of Type I could be operated was determined by the decomposition of oxysulfate to oxide. The temperature of decomposition varied with the system. Thus, a Type I cell involving lanthanum compounds could be operated up to 1500K while that involving dysprosium compounds could be operated only up to 1180K.

(6) The temperature at which an oxysulfate decomposes to the respective oxide decreases as the atomic number of the constituent rare earth element increases. These results are in agreement with those reported by the previous workers (64–68).

(7) The standard free energy change for the reaction:

$$\frac{1}{2}\ RE_2O_2S(s) + O_2(g) = \frac{1}{2}\ RE_2O_2SO_4(s)$$

increases as the atomic number of the constituent rare earth element increases. Fig. 6.1 summarizes this conclusion.

(8) The results from a cell of Type II are found to be identical to the corresponding cell of Type I, indicating that the phase boundaries between oxysulfides and oxysulfates in the relevant Phase Stability Diagrams (PSD) are parallel to the $\log(P_{S_2})$ axis.

(9) Results from the cells of Type II and those from the coexistence studies, summarized in Table 5.1, indicate that (LaO)AgS type compounds do not form in the temperature range examined. These compounds have been reported by Palazzi et al.(90) at lower temperatures.

(10) The cells of Type III were used to study the phase boundary between oxide and oxysulfate in a rare earth system. The results obtained from the cells of Type III are given in Table 5.12. The least square analysis on these results is performed in Table 5.13 and the standard free energy changes for the reaction

$$\frac{2}{3}\ RE_2O_3(s) + \frac{2}{3}\ Cu_2S(s) + O_2(g) = \frac{2}{3}\ RE_2O_2SO_4(s)\ \frac{4}{3}\ Cu(s)$$

obtained therefrom are presented in Table 5.16.

(11) The cells of Type III could be used to study the systems involving rare earths upto gadolinium, cerium system being the only exception. The criteria that should be met by a system in order to be studied utilizing cells of Type III are discussed in Sections 3.4, 3.5 and 3.6.

(12) The lower limit of the temperature range in which a cell of Type III can be operated was determined by the kinetics of electrode reactions and the resistance polarization of the cell, the former being the more important factor. Thus no cell of Type III could be operated below 1040K.

(13) The upper limit of the temperature range in which a cell of Type III could be operated was determined by the temperature at which Cu-rich liquid phase formed. This temperature depended upon the oxygen and sulfur contents of the Cu-rich phase which in turn was determined by the oxygen and sulfur partial pressures in the electrode. Thus, the temperature at which Cu-rich liquid formed depended upon the rare earth system. For this reason, the cells of Type III involving lanthanum compounds could be operated right upto the melting point of pure copper, while those involving compounds of gadolinium could be studied only up to 1210K.

(14) The oxygen partial pressure prevailing in the anode compartment of a cell of Type III increased as the atomic number of the constituent rare earth increased. However, only systems giving oxygen partial pressures which were at least two orders of magnitude lower than those established by the Cu/Cu_2O equilibrium could be studied, so as to avoid the establishment of a mixed potential in the cell.

(15) Coexistence studies, reported in Tables 5.1 and 5.14, indicated that no chemical reaction takes place in the anode of cells of Type III.

(16) The cells of the type:

$$Pt \mid RE_2O_3(s), RE_2O_2S(s), Cu(s), Cu_2S(s) \mid CSZ \mid Air \mid Pt$$

could not be studied because the oxygen partial pressure established at the anode was found to be outside the electrolytic domain of CSZ.

(17) The cells of Type IV could be operated in a very restricted temperature range as discussed in Section 5.5.1. These cells were used to study the phase boundary between oxide and oxysulfide in the cerium-oxygen-sulfur and the yttrium-oxygen-sulfur systems.

(18) The standard free energies of formation of the oxysulfates of lanthanum, praseodymium, neodymium, samarium, europium and gadolinium were determined using the cell data and are listed in Table 6.3. The standard free energies of formation of oxysulfides of lanthanum, praseodymium, neodymium, samarium, europium and gadolinium have also been determined using the cell data and are listed in Table 6.4.

(19) The values of the standard free energies of formation of lanthanum oxysulfate obtained in the present study are found to be in disagreement with those obtained from the data of Grizik et al. (58). However, the values of Grizik et al. (58) are expected to involve large errors because of the approximate nature of the technique used in their study. The values obtained in the present study are expected to be much more reliable.

(20) The standard free energies of formation of oxysulfides at 1100K obtained in the present study are in excellent agreement with those estimated by Gschneidner et al. (3). This comparison is shown in Table 6.5.

(21) The standard free energy of formation of Y_2O_2S at 1068K is found to be -354300 cal /mole. This value compares very well with the value of -357000 (±15000) cal /mole estimated by Gschneidner et al. (3).

(22) The standard free energy of formation of Ce_2O_2S at 1072K is found to be -340100 (±3000) cal /mole. This value is in excellent agreement with the value of -340100 (±15000) cal /mole, estimated by Gschneidner et al. (3), and the value of -338000 (±4500) cal /mole, determined by Ruehan (38).

(23) Phase Stability Diagrams for La-O-S, Gd-O-S and Ce-O-S systems were constructed to illustrate the principles involved in their construction and highlight their utility.

(24) Cells similar to Type IV cells can be utilized to study rare earth-oxygen-halogen systems. One such cell which can be used to study rare earth-oxygen-fluorine system can be represented by

$$Pt \mid RE_2O_3(s), REOF, Ag(s), Ag_2F \mid CSZ \mid Air \mid Pt.$$

Similar cells can be constructed to study other rare earth-oxygen-halogen systems. However, this is only a preliminary proposal and a detailed coexistence study for the components needs to be done before actual experiments can be taken up.

REFERENCES

1. Eyring, L., The Binary Rare Earth Oxides, Handbook on the Physics and Chemistry of Rare Earths, Vol. 3, Eds. Gschneidner, K.A., Jr., and Eyring, L., North-Holland Publising Company, 1979, p. 337.

2. Blasse, S., Handbook on Physics and Chemistry of Rare Earths, Vol. 4, Ed. Gschneidner, K.A., Jr., and Eyring, L., North Holland, 1979, p. 237.

3. Gschneidner, K.A., Jr., Nancy Kippenhanan and McMasters, O.D., Thermochemistry of the Rare Earths, IS-RIC6, Rare Earth Information Center, Institute for Atomic Research, Iowa State University, Iowa.

4. M. Grunzweig, Ph.D. Dissertation, Darmstadt, W. Germany, 1913 (as reported by Kellogg, H.H., Trans. AIME, 230 (1964), p. 1622).

5. Kiukkola, K. and Wagner, K., J. Electrochem. Soc., 104 (1957), p. 308.

6. Kiukkola, K. and Wagner, K., J. Electrochem. Soc., 104 (1957), p. 379.

7. Larson, H.R. and Elliot, J.F., Trans. AIME, 239 (1967), p. 1713.

8. Goldsmith, V.M., Ulrich F. and Barth, T., Mat. Naturv., KI5 (1925).

9. Foex, M. and Traverse, J.P., Rev. Int. Hautes Temp. Refract, 3 (1966), p. 429.

10. Pauling, L., Z. Krystallogr., 69 (1928), p. 415.

11. Cromer, D.T., J. Phys. Chem., 61 (1956), p. 753.

12. Pauling, L. and Shappel, M.D., Z. Krystallogr., 75 (1930), p. 128.

13. Eyring, L. and Holmberg, B., Ordered Phases and Nonstoichiometry in the Rare Earth Oxide Systems, Advances in Chemistry Series 39, Ed. Gould, R.F., Am. Chem. Soc., Washington, D.C., p. 46.

14. Miller, A.E. and Daane, A.H., J. Inorg. Nucle. Chem., 27 (1965), p. 1955.

15. Bedford, R.G. and Catalano, E., J. Solid State Chem., 3 (1971), p. 112.

16. Ackerman, R.J. and Rauh, E.G., J. Chem. Thermodyn., 3 (1971), p. 609.

17. Westrum, E.F., Jr., Developments in Chemical Thermodynamics of Lanthanides, Advances in Chemistry Series 71, Am. Chem. Soc., Washington, D.C., 1967, p. 25.

18. Holley, C.E., Jr., Huber, E.J., Jr. and Baker, F.B., The Enthalpies, Entropies and Gibbs Energies of Formation of Rare Earths Oxides, Progress in Science and Technology of Rare Earths, Vol. 3, Ed. Eyring, L., Pergamon Press, Oxford, p. 343.

19. Stretz, L.A. and Bautista, R.G., J. Chem. Thermodyn., 7 (1975), p. 83.

20. Kuntz, L.K. and Bautista, R.G., Met. Trans., 7B (1976), p. 107.

21. Novikov, I.I. and Mardykin, I.P., Tepl. Vysokikh Temperatur, 13(2) (1975), p. 318.

22. Hultgren, R., Desai, P.D., Hawkins, D.T., Gleiser, M., Kelley, K.K. and Wagman, D.D., Selected Values of the Thermodynamic Properties of the Elements, American Society for Metals, Metals Park, Ohio (1973).

23. Basili, R., El-Sharkawy, A. and Atalla, S., Rev. Int. Hautes Temper. Refract., 16 (1979), p. 331.

24. Eick, H.A., Baenziger, N.C. and Eyring, L., J. Am. chem. Soc., 78 (1956), p. 5147.

25. Fishel, N.A., Haschke, J.M. and Eick, H.A., Inorg. Chem., 9 (1970), p. 413.

26. Haschke, J.M. and Eick, H.A., J. Phys. Chem., 73 (1969), p. 374.

27. Huber, E.J., Jr. and Holley, C.E., Jr., J. Chem. Thermodyn., 1 (1969), p. 301.

28. Huber, E.J., Jr. and Holley, C.E., Jr., J. Chem. Thermodyn., 2 (1970), p. 896.

29. Teany, D.T. and Moruzzi, V.L., Les Elements des Terres Rares, Volume II, Centre National de la Recherche Scientifique, Paris (1970), pp. 131.

30. McMasters, O.D., Gschneidner, K.A., Jr., Kaldis, E. and Sampietro, G., J. Chem. Thermodyn. 6 (1974), p. 845.

31. Rau, R.C., Acta Cryst., 20 (1966), p. 716.

32. McCarthy, G.J., J. Am. Cer. Soc., 57(11) (1974), p. 502.

33. Bevan, D.J.M. and Kordis, J., J. Inorg. Nuclear Chem., 26 (1964), p. 1509.

34. Height, T.M. and Devan, D.J.M., 1976, unpublished work (as quoted in Ref. 1).

35. Iwasaki, B. and Katsura, T., Bull. Chem. Soc. Japan, 44 (1971), p. 1297.

36. Campserveaux, J. and Gernadian, P., J. Chem. Thermodynamics, 6 (1974), p. 795.

37. Sorensen, O. Toft., J. of Solid State Chemistry, 18 (1976), p. 217.

38. Fruehan, R.J., Met. Trans., 10 B (1979), p. 143.

39. Hyde, B.G., Bevan, D.J.M. and Eyring, L., Philosophical Transactions of Royal Society, London, Series A, vol. 259 (1966), p. 583.

40. Turcotte, R.P., Warmkessel, J.M., Tilley, R.J.D. and Eyring, L., J. of Solid State Chemistry, 3 (1971), p. 265.

41. Flahaut, J., Handbook on the Physics and Chemistry of Rare Earths, Vol. 4, Eds. Gschneidner, K.A., Jr., and Eyring, L., North-Holland Publishing Company, N.Y., 1979, p. 1.

42. Mills, K.C., Thermodynamic Data for Inorganic Sulfides, Selenides and Tellurides, Butterworth, London, 1974.

43. Montgomery, R.L., U.S. Bur. of Mines Rpt. Invent., 5468 (1959).

44. Finogenov, A.D., Russian Journal of Physical Chemistry, 46(4) (1972), p. 616.

45. Fenochka, B.V. and Gordienko, S.P., Russian Journal of Physical Chemistry, 47(9), 1973, p. 1384.

46. McMasters, O.D., Gschneidner, K.A., Jr., Kaldis, E., and Sampietro, G., J. Chem. Thermo., 6 (1974), p. 845.

47. Hariharan, A.V. and Eick, H.A., High Temp. Science, 3 (1971), p. 123.

48. Steiger, R.A. and Cater, E.D., High Temperature Science, 7 (1975), p. 204.

49. Gordienko, S.P. and Fenochka, B.V., Russian Journal of Physical Chemistry, 47 (1973), p. 585.

50. Nogteva, V.V. and Paukov, I.E., paper 06, First Int. Conf. on Calorimetry and Thermodynamics, Warsaw, 1969.

51. Gronvold, F. and Westrum, E.F., Jr., Thermodynamics of Nuclear Materials, Proc. Sym. Therm. of Nuclear Matls., Vienna, (1962), p. 3.

52. King E.F. and Weller, W.W., U.S. Bur. Mines Rept. Invest. 5485 (1959).

53. Tikhonov, V.V., Golubkov, A.V. and Smirnov, I.A., Fiz, Tverd. Tela, 8 (1966), p. 3094.

54. Zachariasen, W.H., Acta Cryst., 2 (1949), p. 60.

55. Sochchin, N.P., Izv. Akad. Nauk SSSR, Neorg. Matly., 9(9), 1973, p. 1516.

56. Eick, H.A., J. Am. Chem. Soc., 80 (1958), p. 43.

57. Fahey, J.A., Twelfth Rare Earth Research Conf., Vol. II, Vail, Colorado (1976), p. 762.

58. Grizik, A.A., Abdullina, I.G. and Garifdzhanova, N.M., Russian Journal of Inorganic Chemistry, 19(9) (1974), p. 1412.

59. Kreskov, G.A., Thermochemistry of Compounds of Rare-earth and Actinide Elements, Moskow, Atomizdat, 1972.

60. Barin, I., Knacke, O. and Kubaschewski, O., Thermochemical Properties of Inorganic Substances, Supplement, Springer-Verlag, Berlin, 1976.

61. Rossat-Mignod, J., Quezel, G., Berton, A., and Chaussy, J., Phys. Stat. Solidi, Series B, 49 (1972), p. 147.

62. Rossat-Mignod, J., Quezel, G., Berton A. and Chaussy, J., Phys. Stat. Solidi, Series B, 63 (1974), p. 105.

63. Hulsing, H., Kahle, H.G., Schwab, M. and Schwarzbauer, H.J., Journal of Magnetism and Magnetic Materials, 9 (1978), p. 68.

64. Eick, H.A., J. Am. Chem. Soc., 80 (1958), p. 43.

65. Haynes, J.W. and Brown, J.J., J. Electrochem. Soc., 115 (1968), p. 1060.

66. Hale, W.H., J. Inorg. Nuclear Chem., 33 (1971), p. 1227.

67. Ozawa, L., J. Electrochem. Soc., 124 (1977), p. 413.

68. Leskela, M. and Niinisto, L., J. of Thermal Analysis, 18 (1979), p. 307.

69. Nathans, M.W. and Wendlandt, J. Inorg. Nucl. Chem., 24 (1962), p. 869.

70. Grunzweig, M., Ph.D. Dissertation, Darmstadt, W. Germany (as reported by Kellogg, H.H., in Trans. AIME, 230 (1964), p. 1623).

71. Vahed, A. and Kay, D.A.R., Met. Trans. 7B (1976), p. 375.

72. Ghosh, D., Apte, P. and Kay, D.A.R., Proceedings of Third International Iron and Steel Congress, Chicago, 1978.

73. Electromotive Force Measurements in High Temperature Systems, Proc. Sym. held by Nuffield Research Group, Imperial College, London, Ed. Alcock C.B., American Elsevier Publishing Company, Inc., 1968.

74. Rapp, R.A. and Shores, D.A., Solid Electrolyte Galvanic Cells, in Physicochemical Measurements in Metals Research, Ed. Rapp. R.A., Techniques in Metals Research, Volume IV, Part 2, Ed. Bunshah, R.F., Interscience Publishers, N.Y., 1970, p. 123.

75. Physics of Electrolytes I and II, Ed. Hladik J., Academic Press, London, 1972.

76. Solid Electrolytes, Topics in Applied Physics, vol. 21, Ed. Geller, S., Springer-Verlag, Berlin, 1977.

77. Solid Electrolytes, Ed. Hagenmuller, P. and Van Gool, W., Academic Press, N.Y., 1978.

78. Solid Electrolytes and Their Applications, Ed. Subbarao E.C., Plenum Press, N.Y., 1980.

79. Duwez, P., Odell, F. and Brown, F.H., J. Am. Ceram. Soc., 35 (1952), p. 107.

80. Carter, R.E. and Roth, W.L., Electromotive Force Measurements in High Temperature Systems, Ed. Alcock C.B., American Elsevier Publishing Co., 1968.

81. Patterson, J.W., J. Electrochem. Soc., 118 (1971), p. 1033.

82. Wagner, C., Z. Physik. Chem., B21 (1933), p. 25.

83. Goto, K.S. and Pluschkell, W., Physics of Electrolytes, Vol. II, Ed. Hladik, J., Academic Press, London, 1972, p. 539.

84. Steele, B.C.H., Electromotive Force Measurements in High Temperature Systems, Ed. Alcock, C.B., American Elsevier Publishing Company, 1968, p. 3.

85. Ramanarayanan, T.A., Solid Electrolytes and their Applications, Ed. Subbarao, E.C., Plenum Press, 1980.

86. Espelund, A.W. and Flengas, S.N., Canadian Journal of Chemistry, 49 (1971), p. 1545.

87. Kubaschewski, O. and Alcock, C.B., Metallurgical Thermochemistry, Pergamon Press, London, 1979.

88. Inorganic Index to Powder Diffraction File, Joint Committee on Powder Diffraction Standards, 1977.

89. Chaudhary Nabendu, S., J. Electrochem. Soc., 120 (1973), p. 1663.

90. Palazzi, M., Carcaly, C., Laruelle, P. and Flahaut, J., Fifteenth Rare Earth Res. Conf., Rolla, MO, 1981.

91. Azizov, T. Kh., Abbasov, A.S., Mustafaev, F.A. and Aliev I. Ya., Vses. Konf. Kalorim. (Rasshiv. Tezisy. Dokl.), 7th, 1977, p. 30-32 (Akad. Nauk SSR In. Khim. Fiz., Moscow, USSR).

92. Skeaff, J.M. and Espelund, Canadian Metallurgical Quarterly, 12(4), 1973, p. 445.

93. Charette, G.G. and Flengas, S.J., J. Electrochemical Soc., 115 (1968), p. 796.

94. Elrefai, F., Ph.D. Thesis, McMaster University, 1980.

95. Steele, B.C.H. and Alcock, C.B., Trans. AIME, 233 (1965), p. 1359.

96. Kellogg, H.H., Canadian Metallurgical Quarterly, 8(1), p. 3.

97. Yazawa Akira and Azakami Takeshi, Canadian Metallurgical Quarterly, 8(3), p. 257.

98. Vasileva, I.G., et al., Izv. Akad. Nauk SSSR, Neorg. Mater., 15(8), (1979), p. 1330.

99. Gschneidner, K.A. and Kippenhan, N., Report No. IS-RIC-5, Rare Earth Information Center, Ames, Iowa.

100. Johnson, N.L. and Leone, F.C., Statistics and Experimental Design, Vol. I, John Wiley and Sons, Inc., New York, 1964.

101. Lindgren, B.W., McElrath, G.W. and Berry, D.A., Introduction to Probability and Statistics, Macmillan Publishing Co., Inc., New York, 1978.

APPENDIX A

LINEAR REGRESSION ANALYSIS

This section summarizes the statistical methods used in this investigation to treat the experimental data. These methods are discussed by Johnson and Leone (100) and Lindgren et al. in great detail (101).

In the present work, we are mainly concerned with the linear regression of a dependent variable on a single independent variable x. Such a regresssion is performed by calculating estimates of the two parameters, α and β, in the formula

$$E(y/x) = \alpha + \beta x$$

where $E(y/x)$ is the regression function; α and β are two parameters, representing intercept and slope, respectively.

The following assumptions are made in order to obtain the least square estimates of α and β:

1. The x_i values are controlled and/or observed without error.
2. The regression of y on x is linear, that is,

$$E(y/x) = \alpha + \beta x$$

3. The deviations $y_i - E(y/x_i)$ are mutually independent.
4. These deviations have the same variance, whatever the value of x_i.

5. These deviations are normally distributed.

Using the method of least square, the following estimates of the slope, b, and the intercept, a, can be obtained. Thus for n observations,

$$b = \frac{n \Sigma x_i y_i - \Sigma x_i \Sigma y_i}{n \Sigma x_i^2 - (\Sigma x_i)^2}$$

$$a = \bar{y} - b\bar{x}$$

where Σ represents the sum from i=1 to n; $\bar{y}$ is the mean value of y, given by $\Sigma y_i/n$; and $\bar{x}$ is the mean value of x, given by $\Sigma x_i/n$.

The goodness of linear fit of the data points to the regression line is measured by the standard deviation, S^*, about the fitted line, and is given by

$$S^* = (\Sigma (y_i - a - bx_i)^2/(n-2))^{1/2}$$

The least square coefficients, a and b, can be thought of as estimates of the true coefficients in the regression function, $\alpha + \beta x_i$. To see how good they are as estimators, one has to study their distribution, and in order that this be possible, the specification of the regression model must include a distribution for the error component ϵ. This is usually assumed to be normal. The standard errors, s_a and s_b in a and b as estimators of α and β can be obtained (101) as

$$s_a = \pm \sigma^* (1/n + \bar{x}^2/\Sigma (x_2 - \bar{x})^2)]^{1/2}$$

$$s_b \doteq \pm[\sigma^*/(\Sigma (x_i - \bar{x})^2)^{1/2}]$$

where $\sigma^{*\dagger}$ is the standard deviation about the fitted line for the population (S^* is the standard deviation for the sample).

When only S^* is known, the confidence interval for the estimators of α and β can be obtained using t-distribution with (n-2) degrees of freedom. The 100 (1-α) percent confidence interval for the slope and the intercept are given by

$$b - \frac{(t_{n-2,1-\alpha/2} \cdot S^*)}{(\Sigma (x_i - \bar{x})^2)^{1/2}} < \beta < b + \frac{(t_{n-2,1-\alpha/2} \cdot S^*)}{(\Sigma (x_i - \bar{x})^2)^{1/2}}$$

$$a - t_{n-2,1-\alpha/2} \cdot ((1/n + \bar{x}^2/\Sigma (x_i - \bar{x})^2)^{1/2} \cdot S^* < \alpha$$

$$< a + t_{n-2,1-\alpha/2} \cdot ((1/n + \bar{x}^2/\Sigma (x_i - \bar{x})^2)^{1/2}$$

The correlation coefficient, γ, is the measure of the correctness of the model and is given by

$$\gamma = \frac{n \Sigma x_i y_i - \Sigma x_i \cdot \Sigma y_i}{[[n \Sigma x_i^2 - (\Sigma x_i)^2] [n \Sigma y_i^2 - (\Sigma y_i)^2]]^{1/2}}$$

---

† In the results treated in this work $S^* = \sigma^*$, since the number of observations are large.

Although in the present work, there was obviously an error in measurement of temperature, the independent variable, the above analysis is not invalidated. Since any error in the temperature measurement can be considered as an error in the free energy, assuming the temperature was correct. The errors discussed above only represent the statistical errors and do not include any systematic errors.